

SKB

**TECHNICAL
REPORT**

87-02

**Fuel rod D07/B15 from Ringhals 2 PWR:
Source material for corrosion/leach
tests in groundwater
Fuel rod/pellet characterization program
part one**

Roy Forsyth
Studsvik Energiteknik AB, Nyköping

March 1987

FUEL ROD D07/B15 FROM RINGHALS 2 PWR:
SOURCE MATERIAL FOR CORROSION/LEACH TESTS IN
GROUNDWATER

FUEL ROD/PELLET CHARACTERIZATION PROGRAM

Part One

Edited by Roy Forsyth

Studsvik Energiteknik AB

March 1987

This report concerns a study which was conducted for SKB. The conclusions and viewpoints presented in the report are those of the author(s) and do not necessarily coincide with those of the client.

Information on KBS technical reports from 1977-1978 (TR 121), 1979 (TR 79-28), 1980 (TR 80-26), 1981 (TR 81-17), 1982 (TR 82-28), 1983 (TR 83-77), 1984 (TR 85-01), 1985 (TR 85-20) and 1986 (TR 86-31) is available through SKB.

FOREWORD

A joint SKB/STUDSVIK experimental program to determine the corrosion rates and to establish the corrosion mechanisms of spent UO_2 fuel in groundwater under both oxidizing and reducing conditions is in progress in the Hot Cell Laboratory of Studsvik Energiteknik AB.

High burnup fuel of both BWR and PWR type are studied. Characterization of the spent fuel at both rod and pellet level is an important part of the experimental program.

Experiments on PWR fuel have been concentrated so far on specimens from one rod, manufacturer's number 03688, which had occupied position B15 in assembly D07. This assembly had been irradiated for 5 cycles in the Ringhals 2 reactor between 1977 and 1983. The calculated assembly burnup was 41.3 MWd/kg U.


The present report is a collection of separate reports describing those items in the characterization program which have been performed so far. No overall summary of the experimental results is given here, and the report should be viewed as a collection of reference data.

The following reports are included:

<u>Report number</u>	<u>Subject</u>
NF(P)-87/13	Visual inspection of the oxide layer on the fuel rod's external surface.
NF(P)-85/19	Axial gamma scanning.
NF(P)-87/14	Profilometry and eddy-current examination.
NF(P)-87/12	Determination of the residual pellet/clad gap.
NF(P)-87/16	Determination of the fission gas release and the burnup.
NF(P)-87/11	Ceramographic examination of fuel cross-sections. Alpha- and beta-autoradiography.
NF(P)-86/48	Micro-gamma scanning of a fuel cross-section.

Roy Forsyth Studsvik, March 1987.

Studsvik Arbetsrapport - Technical Note

Projekttidentifikation – Project identification	Datum – Date	Rapport nr – Report No.
SKB/STUDSVIK UO ₂ corrosion program	87-03-14	NF(P)-87/13
Titel och författare – Title and author		
Visual inspection of the oxide layer on fuel rod 03688 from Ringhals 2.		
Kjell Pettersson		
Distribution		
<input checked="" type="checkbox"/> Begränsad distribution – Restricted distribution	<input checked="" type="checkbox"/> Rapporten skall ej förhandsviseras – Internal note	
Godkänd av – Approved by	Kontonr – Internal note	Antal ex – No. of copies
	6228A	
SUMMARY		
<p>The oxide layer on fuel rod 03688 from Ringhals 2 has been examined visually by periscope. The observations indicate that the lower part of the rod has not reached transition in the oxidation process, while it is in this stage in a region 150-600 mm from the bottom and has passed transition in oxidation above 600 mm from the bottom. The oxidation close to the spacers is less than in surrounding parts of the rod.</p>		
NF158/BEm		

I:209042/I:209043 (Ej repr) 85-04

CONTENTS

	<u>Page</u>
1. INTRODUCTION	1
2. RESULTS OF THE EXAMINATION	2
3. DISCUSSION	5
REFERENCES	6
Figures 1-2	
Figures 3-4	
Figures 5-6	

1. INTRODUCTION

This investigation is a part of a project with the aim of characterizing PWR-fuel within the SKB program for the permanent disposal of spent nuclear fuel.

2. RESULTS OF THE EXAMINATION

All measurements refer to the distance from the furthest end of the lower end plug. Before examination the rod was cut in two pieces. The cut was performed 2015 mm from the bottom and, according to gamma scanning results, at the position of a spacer. This was also later confirmed by the visual inspection.

The end plug was marked with the punched figures 03688. About 60 mm up the rod the cladding tube had a marking "AI.9.5".

At the lower end of the rod the oxide was even and grey black. About 150 mm from the bottom small irregularities in the oxide layer start as shown in Fig 1. These then increase in size but hardly in density and the oxide surface then has the mottled appearance which is illustrated in Fig 2. At a quick glance, the appearance is reminiscent of BWR-rods with nodular corrosion. However, from what can be seen in the periscope, these patches are not very thick as no level difference can be seen between the white paths and the surrounding dark oxide. Already 525 mm from the bottom (Fig 2) the white oxide has formed a continuous layer of white oxide around the major part of the rod. The rod has the mottled appearance of Fig 2 only in a sector of about 90° .

At the position of the second spacer, about 700 mm from the bottom, the oxide growth diminishes and the rod is sparsely patchy as shown in Fig 3.

Above the spacer, 780 mm, the oxide is again much more compact and from 900 mm nearly con-

tinuous up to the position of the next spacer, 1340-1380 mm from the bottom. Here the oxide is however more compact than at the preceding spacer, (Fig 4) and immediately above the spacer position, the rod is completely white.

When the change from grey black to white oxide is observed, (Figs 2-4), the impression is obtained that the white patches are zirconium oxide. In areas where the rod is completely white, the surface has however such a dull, powderish character that the impression is given that the rods have a coating. Fig 5 is an attempt to show what in the periscope appears to be a mottled oxide under a light-coloured coating, giving the surface a somewhat uneven appearance. With this background, it is interesting to note that the white surface layer has fallen off where the rod was in contact with the rod-feed rollers. on which the rod rests when rotated during the examination (Fig 6).

This observation may seem to support the hypothesis that the white layer is a loose covering, but it can not be excluded that the white layer is a zirconium oxide which is easily removed. To better characterize the white layer a smear test was made. Gamma spectrometric examination showed that the activity of the specimen was dominated by Ce, Cs, Zr/Nb and Co. Ce and Cs are likely to be contamination from the hot cell. With a rough calculation, the ratio between Zr and Co activity suggests that the Co-content should have been 30 ppm of the Zr weight at the start of the irradiation.

Check of a number of charge analyses for Zircaloy-4 shows that the cobalt contents in these have not been larger than 5 ppm. The specifica-

tion limit for Co in Zircaloy is 20 ppm. Consequently, it is likely that the material which falls off is a mixture of ZrO_2 and crud.

Between 1660 and 2015 mm from the bottom the fuel rod was not examined due to limitations of the movement of the periscope table. Observations through the cell window showed however that the rod was completely covered with white oxide in this region.

The upper segment of the rod was completely covered with white oxide, except where the surface had been damaged by our handling of the rod. At the positions for spacers, 2020, 2700 and 3370 mm from the bottom, the surface layer seemed however to be somewhat thinner. It was also apparent that the layer is thinner upstream from the contact point of the spacers. The variation was however too small to be shown in photographs.

3. DISCUSSION

The observations are in good agreement with the standard model for corrosion of Zircaloy in hot water (1). According to this model, Zircaloy first oxidizes with decreasing rate and then, after the so called transition, it oxidizes at constant rate. The transition is assumed to arise due to a change in the oxide layer, which causes the oxide layer to lose its ability to retard oxygen transport. According to one model, this is possible by a phase transformation in the oxide which, due to accompanying volume changes, makes the oxide porous. At the same time the oxide becomes stoichiometric and white.

In laboratory tests it is observed that the edges of the specimens become grey white at the transition and that this grey white oxide spreads all over the specimen with time.

In a fuel rod, sites for nucleation are missing for geometrical reasons, and one can imagine that nucleation starts randomly on the surface. When the white oxide subsequently grows, one obtains the mottled appearance which is observed on the lower part of the rod. Finally, the spots grow together giving a rod completely covered by white oxide.

On this fuel rod all stages are represented, simply due to the temperature distribution in a reactor, with relatively low temperature in the lower part. It is also possible that the relatively low neutron flux in the lower part contributes so that the rod has not even reached the beginning of transition near the bottom end.

The gamma scanning showed that there have been local minima of power at the positions of the spacers. It is likely that this has contributed to less corrosion around the spacers. Garzarolli et al (2) have also stated that turbulence and increased flow velocity contributes to a temperature decrease around the spacers. The visual observations of the PWR-rod from Ringhals in fact agree qualitatively very well with the more extensive examinations of PWR corrosion reported by Garzarolli et al.

REFERENCES

- 1 COX B
Oxidation of Zirconium and its alloys.
I Advances in Corrosion Science and
Technology, ed. M G Fontana and R W
Staehle, vol 5, Plenum Press, New York
1976

- 2 GARZAROLLI F et al
Waterside corrosion of Zircaloy clad
fuel rods in a PWR environment.
Zirconium in the Nuclear Industry:
Fifth Conference, ASTM STP 754, D G
Franklin ed., ASTM 1982, pp 430-449

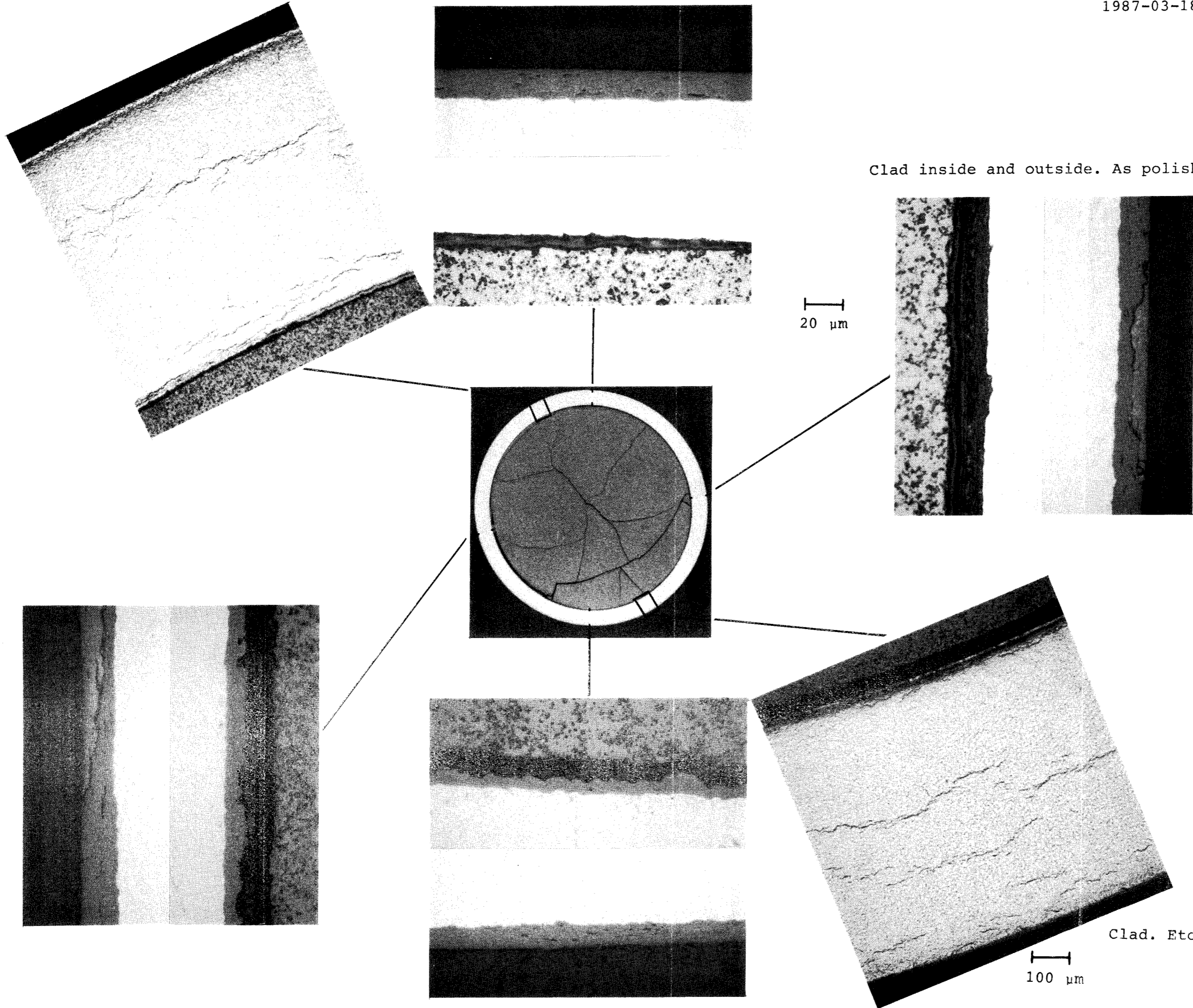
Sample 1265
Clad and gap

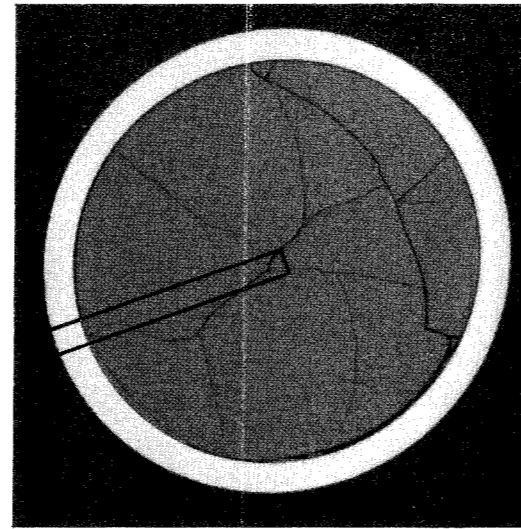
Clad inside and outside. As polished.

20 μm

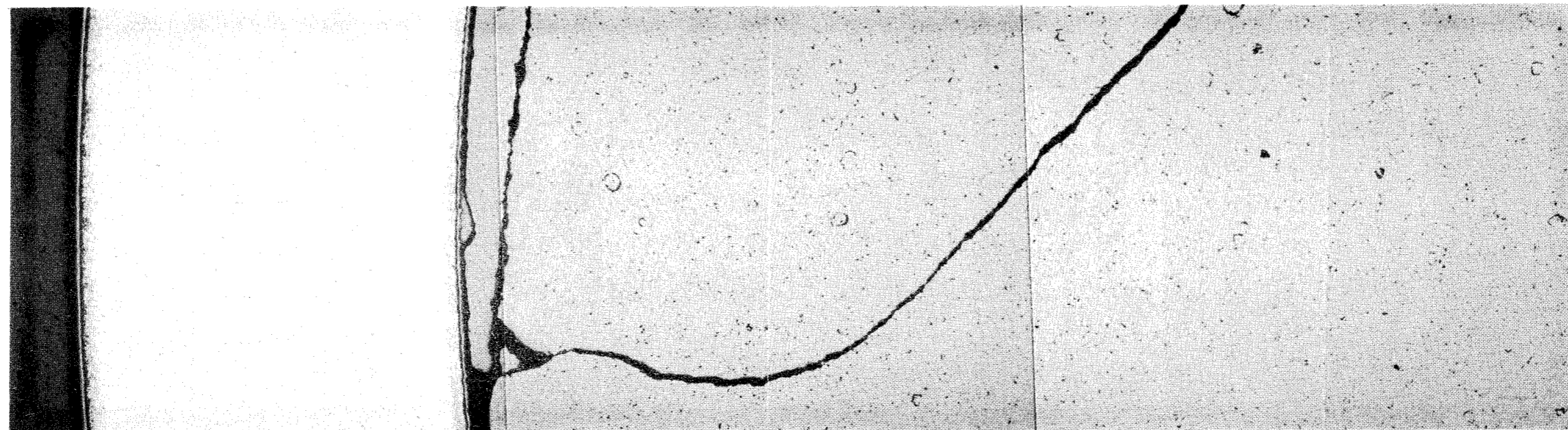
100 μm

Clad. Etched for hydrides.

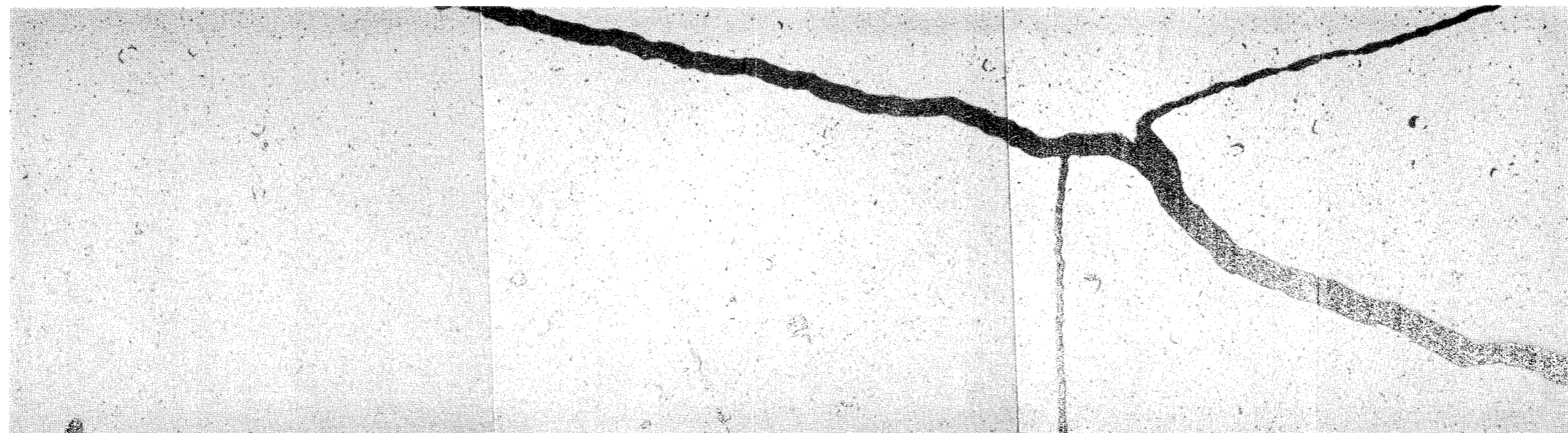




Sample 1265
Radial fuel section.
As polished.

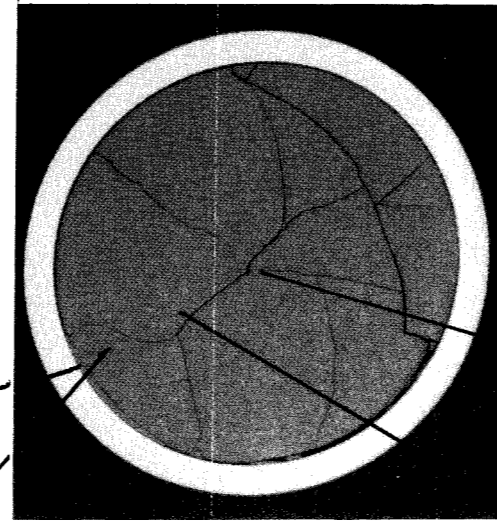


1 mm

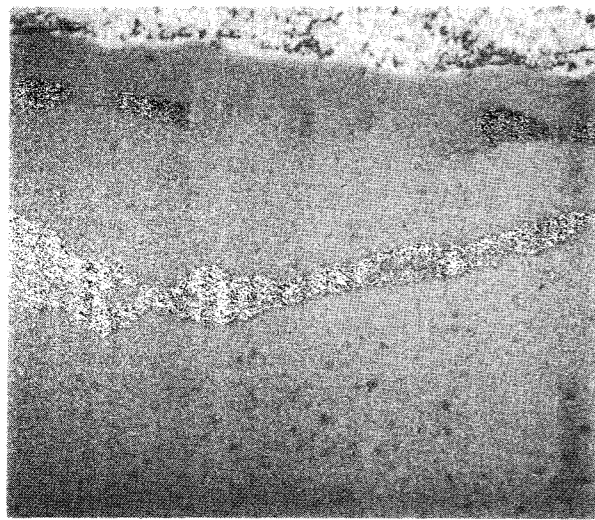


↑
Centre

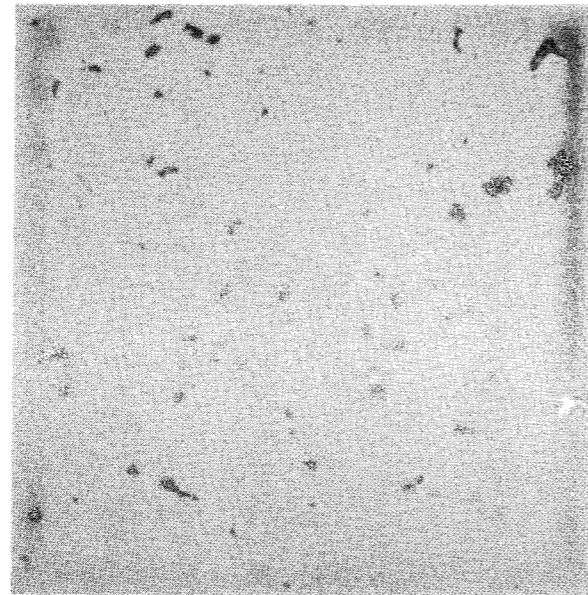
Sample 1265
Fuel detail micrographs.



As polished

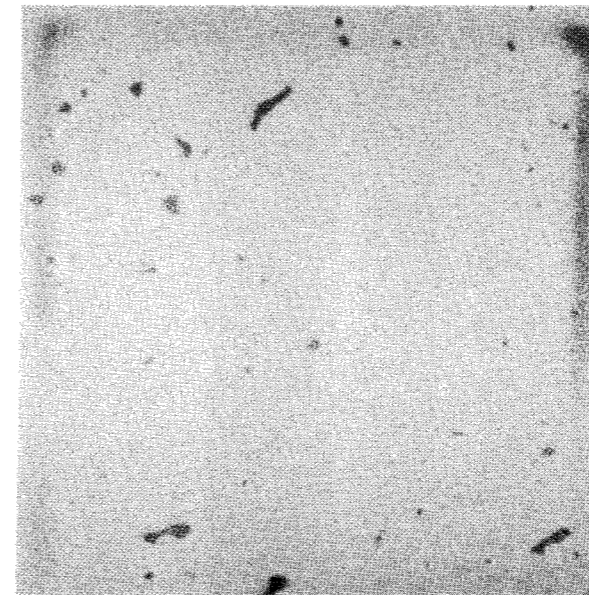


r = 4.5 mm (periphery)

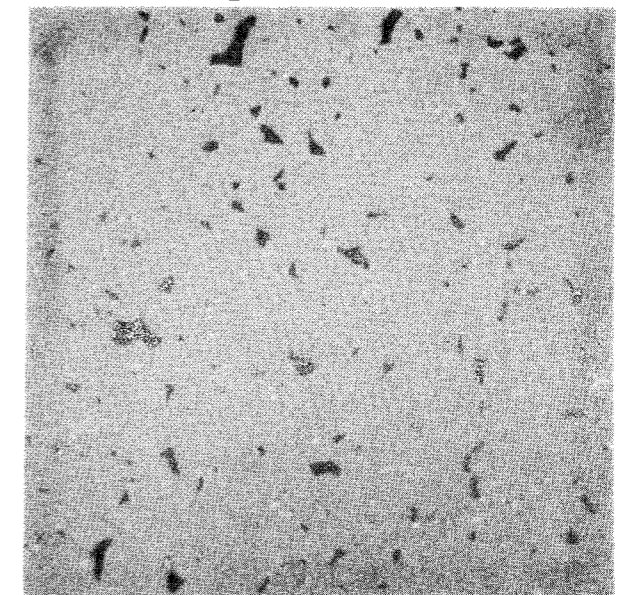


r = 4.0 mm

10 μ m

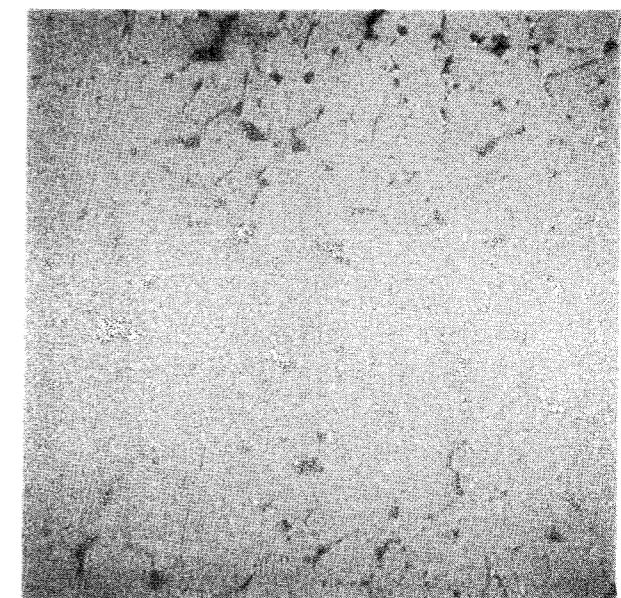
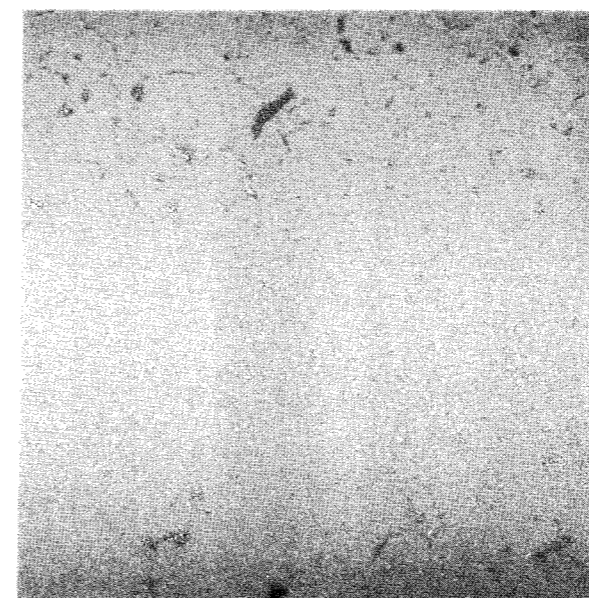
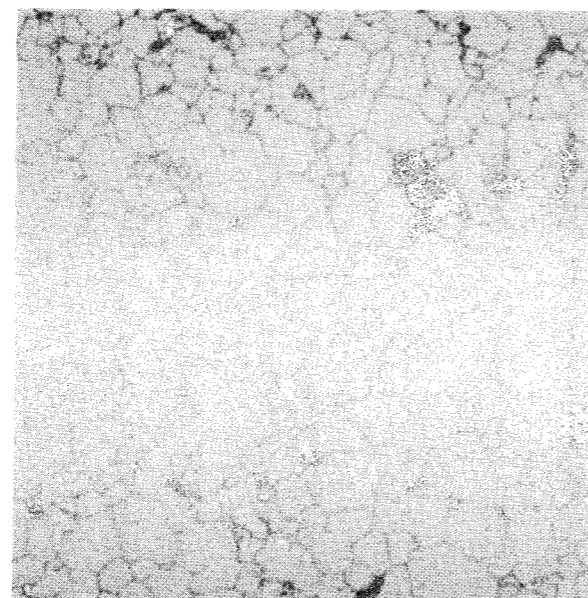
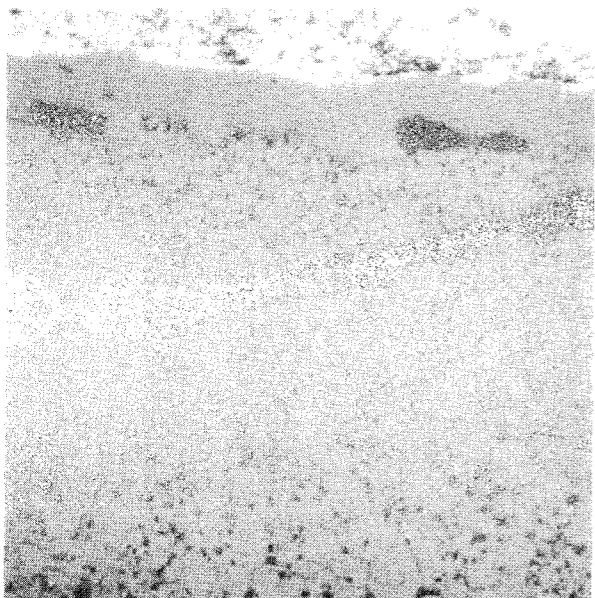


r = 2.0 mm



r = 0 (centre)

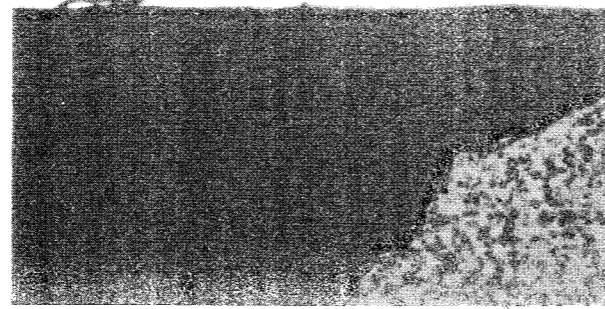
Etched





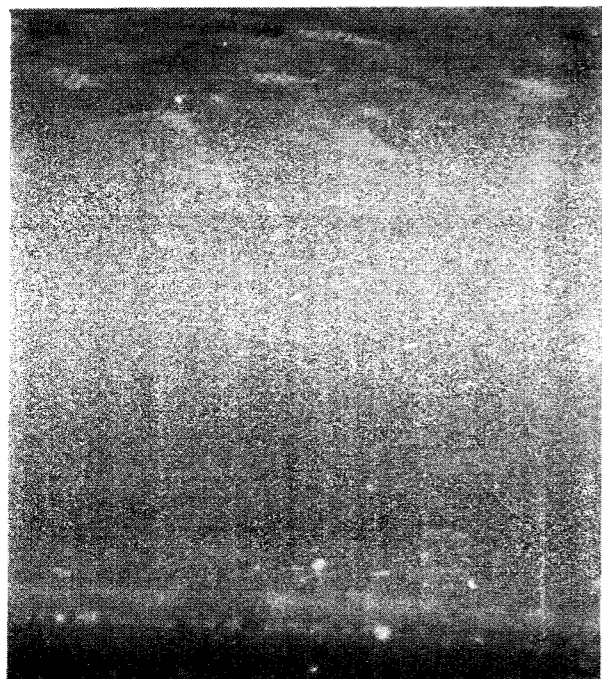
20 µm

Clad inner wall.
Polarised light.



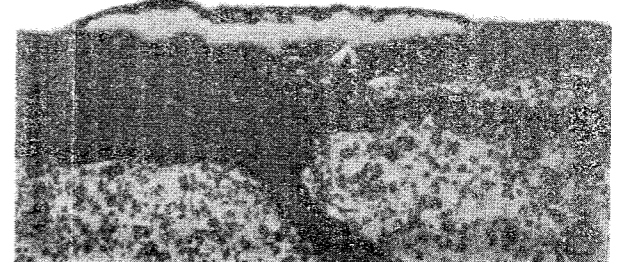
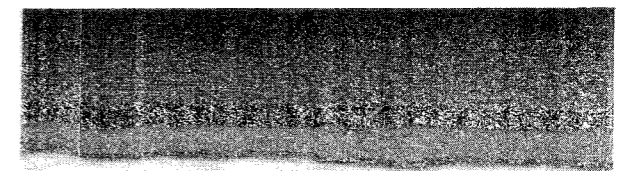
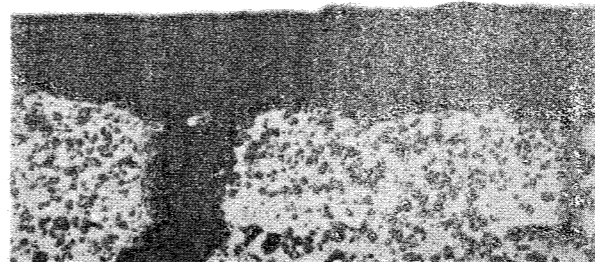
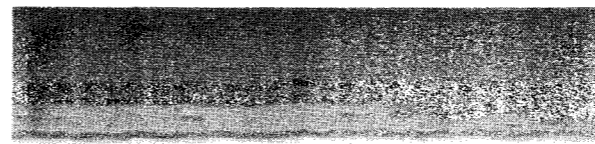
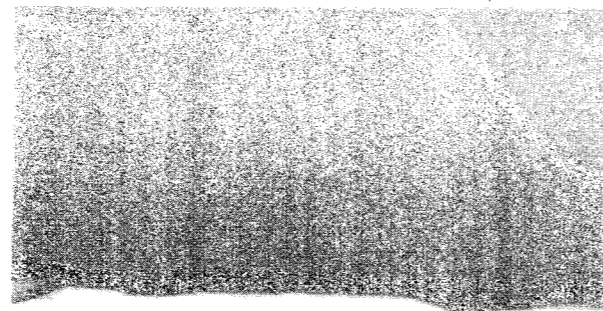
Clad.
Etched for hydrides.

100 µm



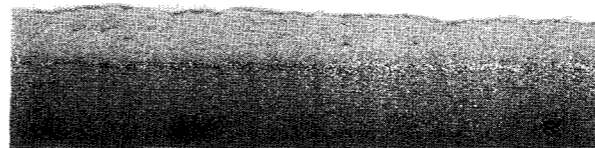
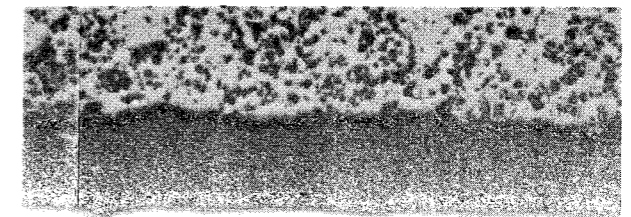
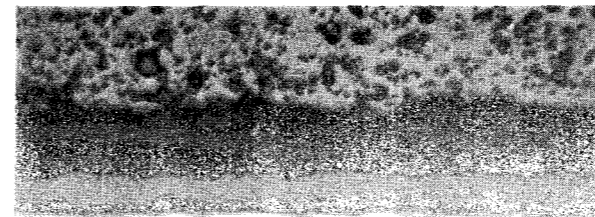
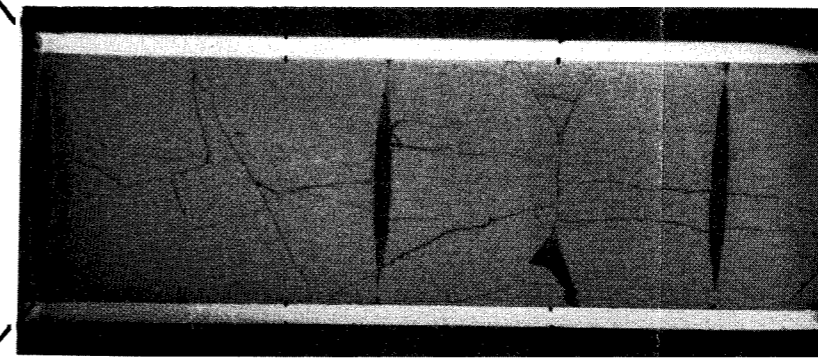
20 µm

Clad outer wall.
Polarised light.



20 µm

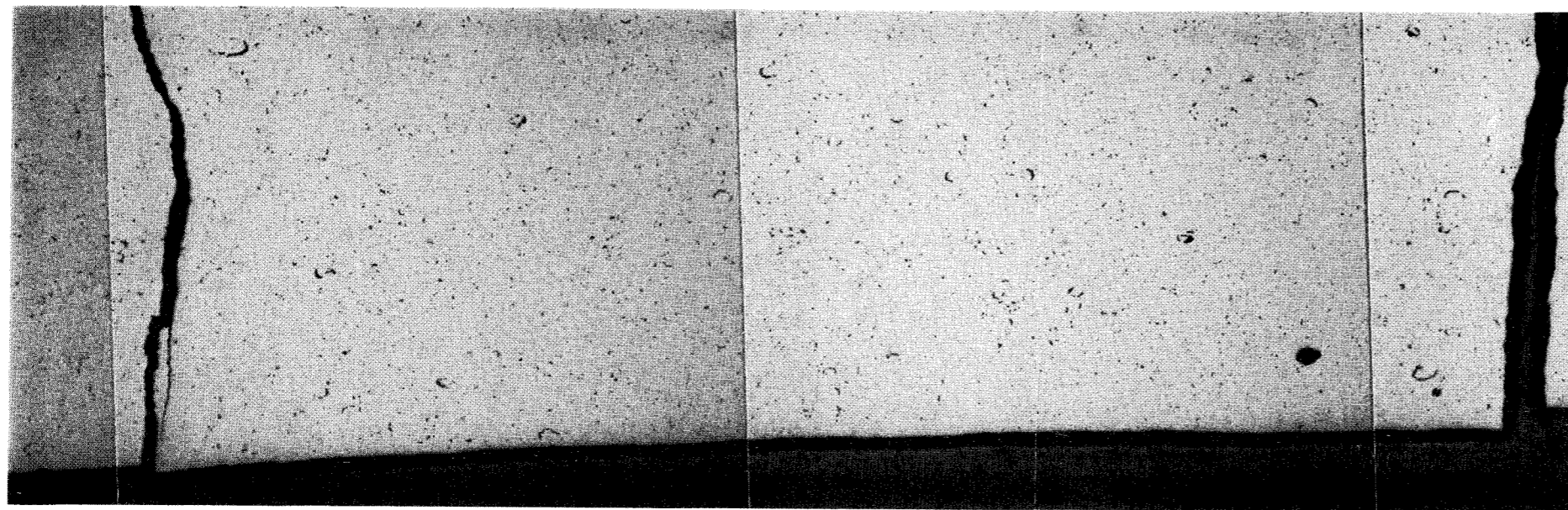
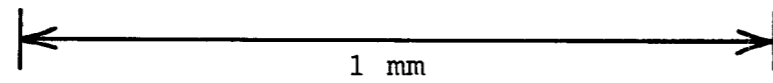
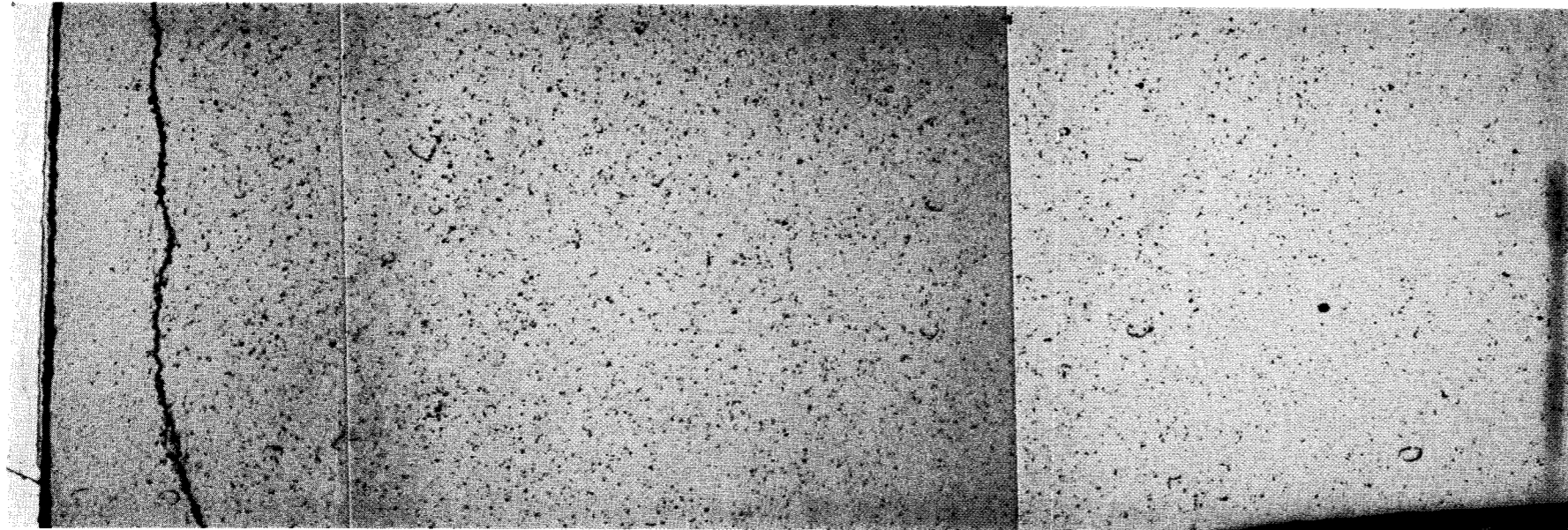
Sample 1266
Clad and gap.



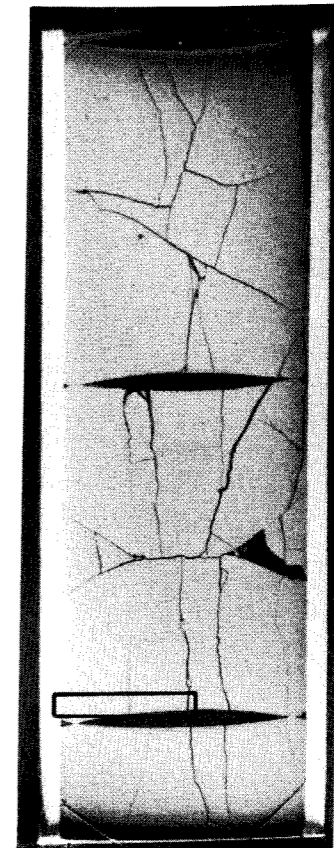
Clad inside and outside.
As polished

Sample 1266

Pellet-end radial fuel section.
As polished.

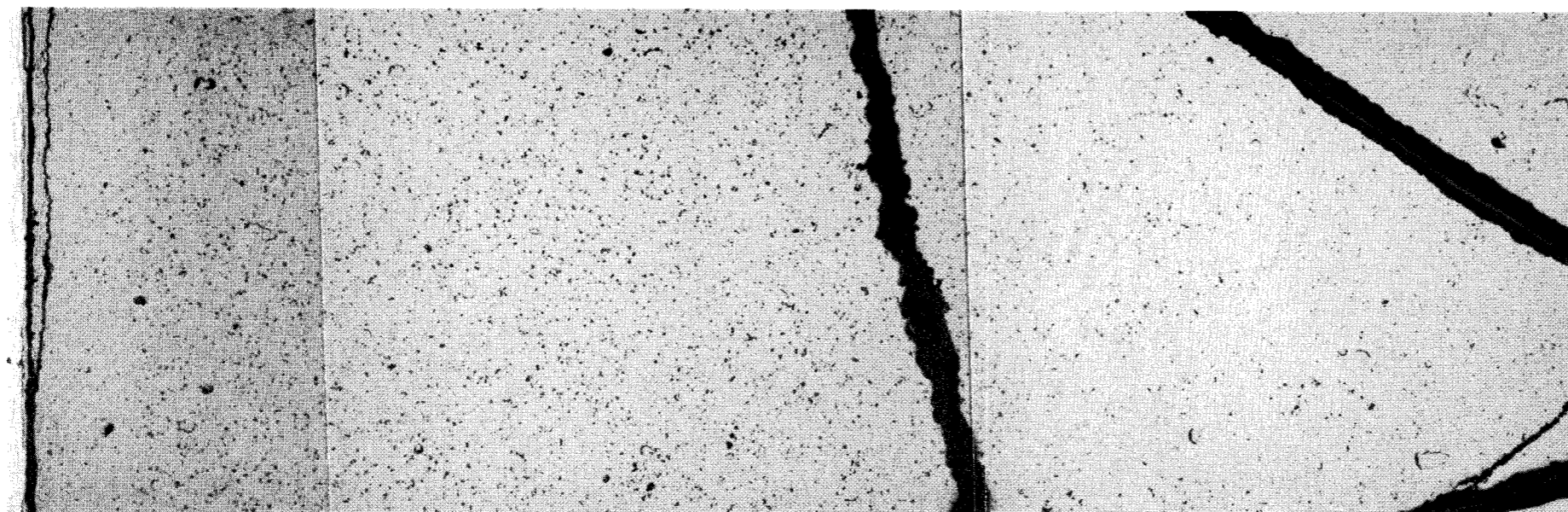


↑
Centre

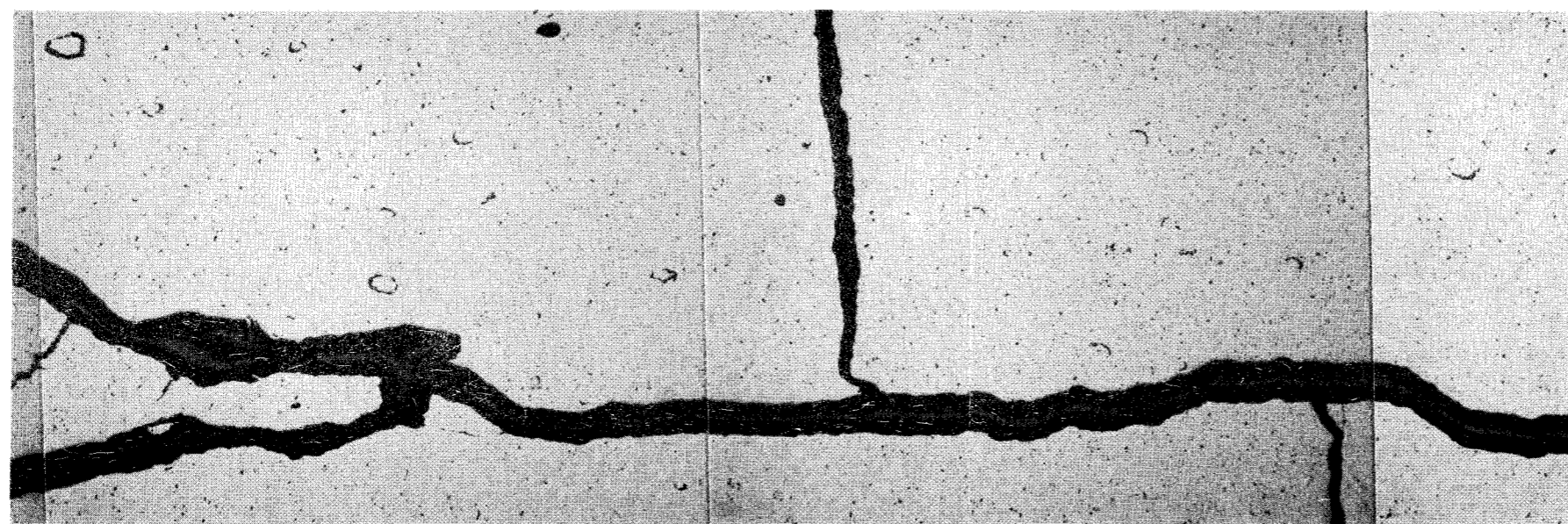


Sample 1266

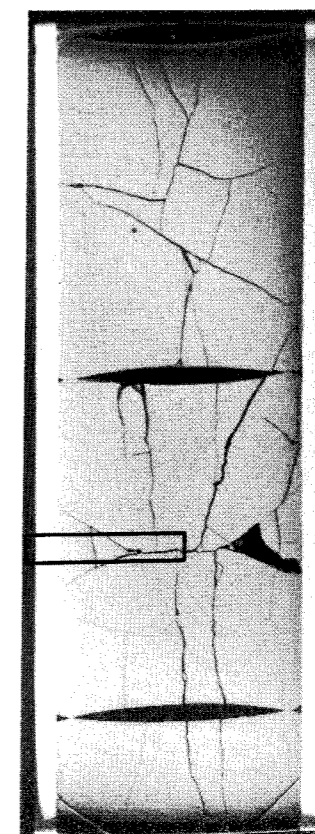
Mid-pellet radial fuel section.
As polished.



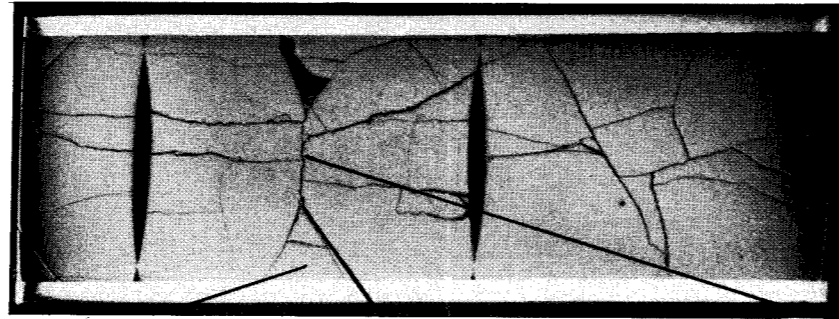
1 mm



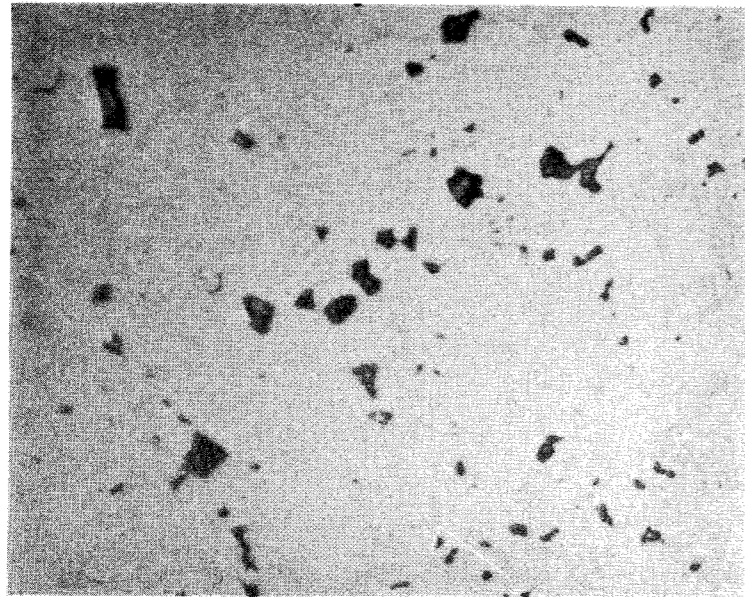
↑
Centre



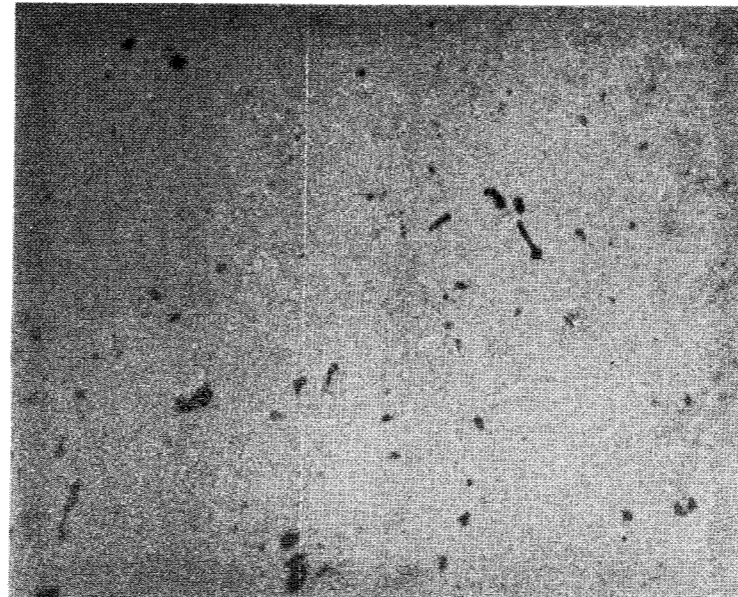
Sample 1266
Fuel detail micrographs.



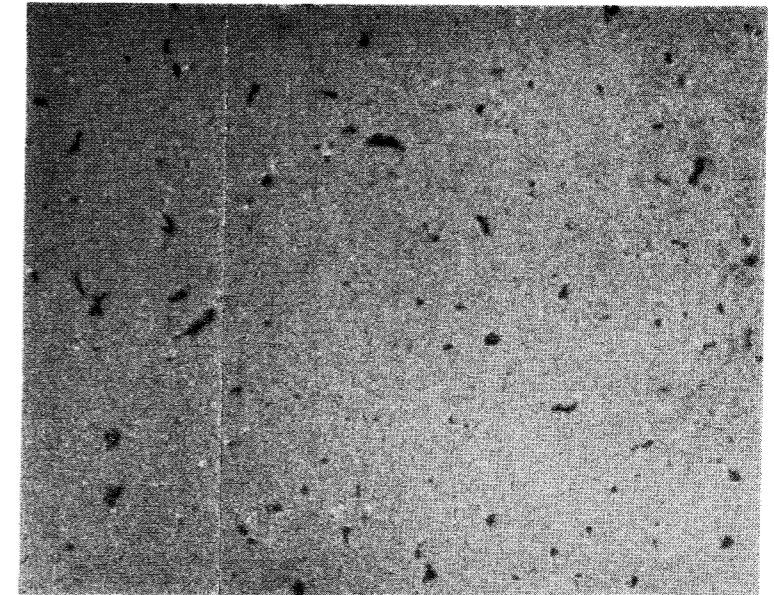
As polished



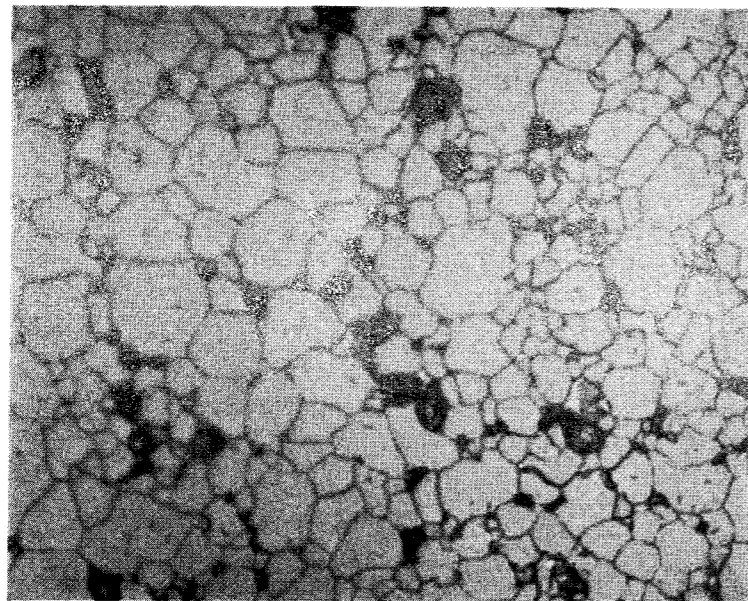
$r = 4.0$ mm



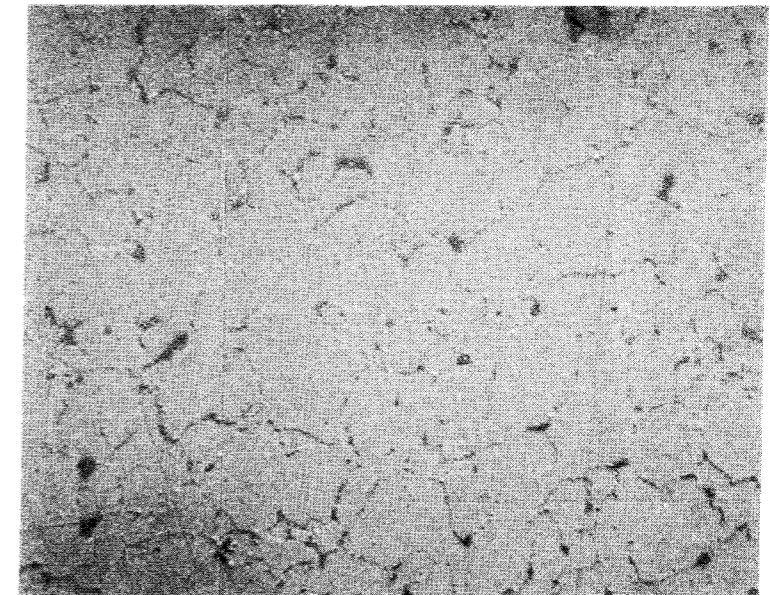
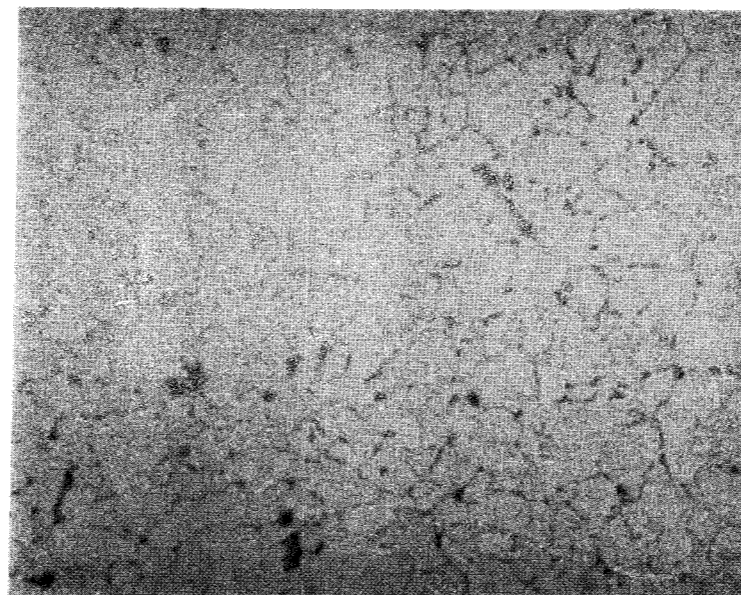
10 μ m
 $r = 2.0$ mm



$r = 0$ (centre)



Etched



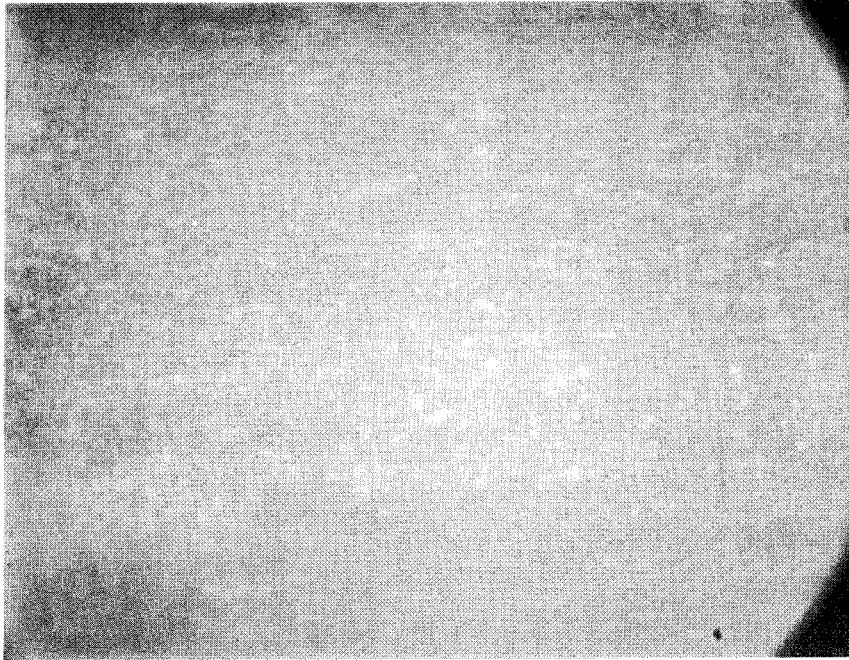


Fig. 1 Small unevennesses in the oxide layer 150 mm from bottom. 15X
All pictures are oriented with the bottom end of the fuel rod to the left.

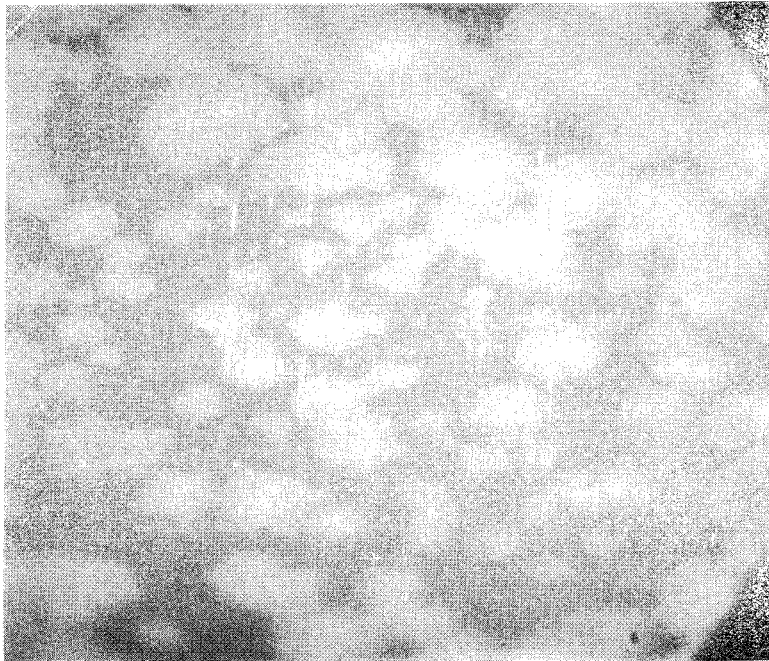


Fig. 2 Mottled oxide. 525 mm from bottom. 15X



Fig. 3 Oxide patch at spacer's con- 15X
tact point. 700 mm from bottom.

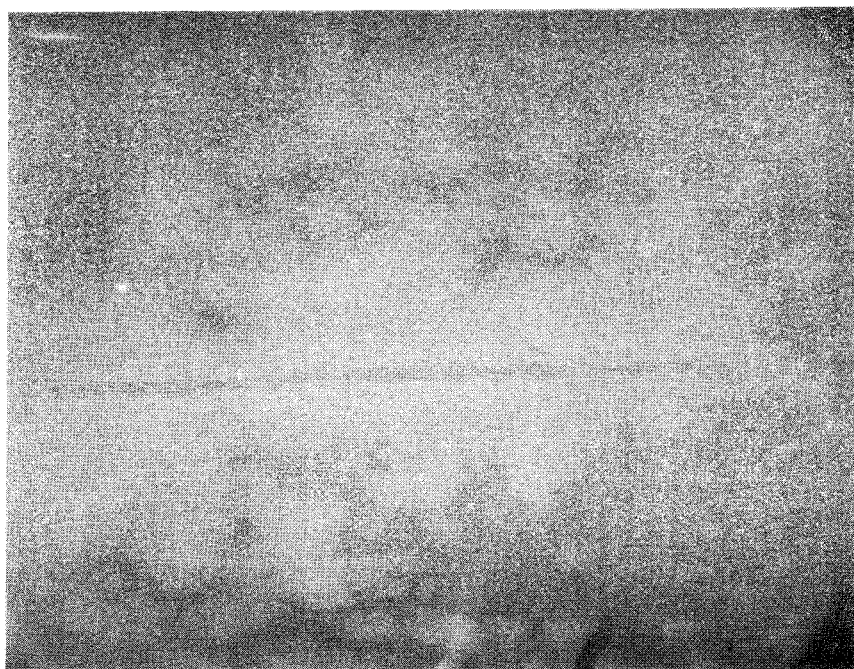


Fig. 4 Oxide at third spacer from 15X
bottom. 1350 mm from bottom.
The white oxide covers more
of the surface here than at
the preceding spacer.

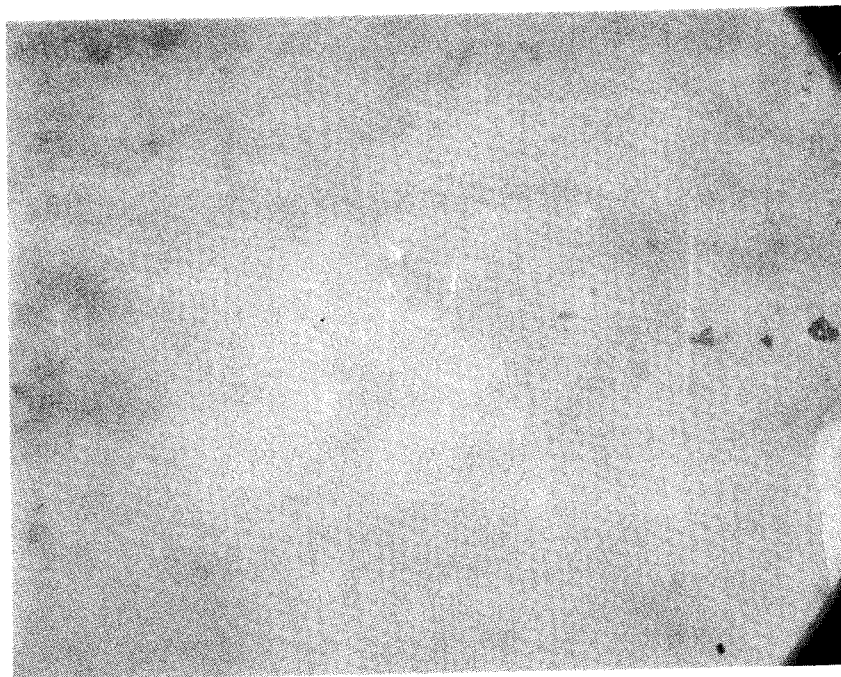


Fig. 5 Uneven oxide, which in the 15X periscope gives the impression of a mottled oxide layer under a light-coloured layer. 1070 mm from bottom.

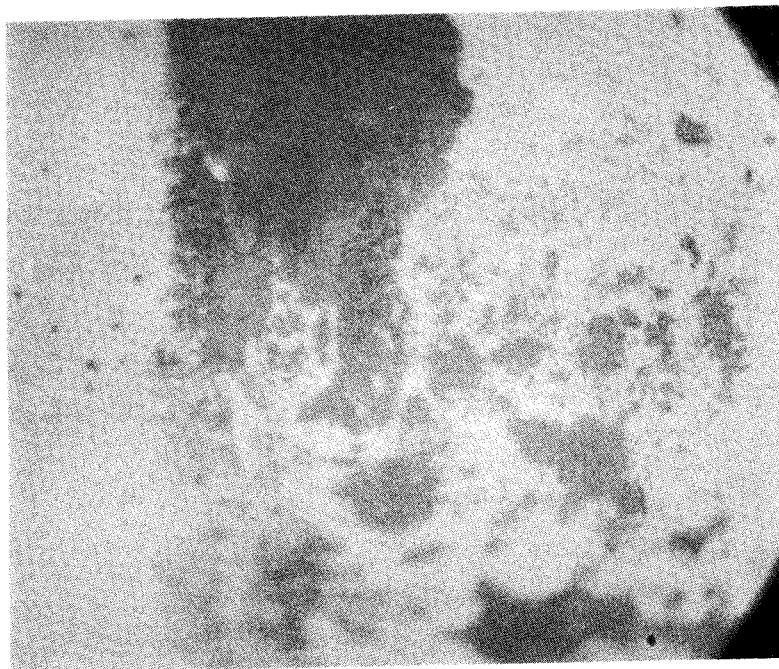


Fig. 6 Coating or white oxide removed by contact with the rod-feed roller during inspection. 15X 2190 mm from bottom.

Studsvik Arbetsrapport - Technical Note

Projektidentifikation – Project identification	Datum – Date	Rapport nr – Report No.
SKB/STUDSVIK UO ₂ CORROSION PROGRAM	85-03-27	NF (P) -85/19
Titel och författare – Title and author		
Axial gamma scanning of PWR fuel rod number 3688 from Ringhals 2 R S Forsyth B Bivered		
Distribution		
Restricted distribution		
<input checked="" type="checkbox"/> Begränsad distribution – Restricted distribution	<input checked="" type="checkbox"/> Rapporten skall ej förhandsviseras – Internal note	
Godkänd av – Approved by	Kontonr – Internal note	Antal ex – No. of copies
<i>RS Forsyth</i>	PN5608D	
ABSTRACT		
As part of the characterization program for a high burnup PWR rod which will be used in leaching experiments and studies on corrosion mechanisms, axial gamma scanning and gamma spectrometric measurements on selected fuel pellets have been performed.		
NF134/BA		

I:209042/1,209043 (Ej reпр) 85-04

1 INTRODUCTION

In the SKB/Studsvik program for the study of the corrosion of spent reactor fuel in granitic groundwater, a series of experiments have been performed where fuel/clad specimens and fragments of fuel from a high burnup BWR fuel rod (42 MWd/kg U) have been contacted with a synthetic groundwater, and the amounts of fission product and actinide species present in the aqueous phase have been determined as a function of contact time (1).

The results so far available indicate that a number of mechanisms can be postulated in order to explain the apparently large differences in behaviour between the various species, including redistribution and segregation during reactor operation, solubility limitations and possible adsorption and precipitation effects, all of which may be related to the microstructure, morphology and stoichiometry of the fuel itself.

These effects will be studied in detail in a new phase of the program where fuel from a high burnup PWR rod (~ 47 MWd/kg U) will be examined in similar leaching experiments. Fuel specimens will be carefully characterized before and after leaching by such techniques as micro-gamma-scanning, ceramography, scanning electron microscopy and EPMA.

As the first stage in fuel characterization, this report presents the results of gamma spectrometric examination of the fuel rod.

2 EXPERIMENTAL

The fuel rod selected for the experiments was number 3688 from position B15 in the Ringhals 2 fuel assembly D07 with a calculated rod-average burnup of about 47 MWd/kg U.

Axial gamma scanning of the rod was performed in the NDE facility for full-length power reactor rods at Studsvik's Hot Cell Laboratory. The nuclide used as the monitor for burnup was Cs-137. The experimental and apparatus settings are given in Table 1.

After the first scan, the rod was rotated through 180° and re-scanned to establish whether or not there had been a significant flux gradient over the fuel diameter.

After the second scan, point measurements were performed on selected fuel pellets at regular intervals along the fuel column to determine the axial variation of fission product inventories. The measurements were performed in pairs, the rod being moved 1 mm past the collimator between measurements, as a check on measurement precision and to avoid inaccuracies due to the presence of localised pellet cracking. The measurement time was 1000 seconds.

3 RESULTS

3.1 Axial gamma scanning

The two axial gamma scanning curves (with 180° rotation between scans) were extremely similar so only the second scan is presented in this report as Fig 1. Although there has been some loss of detail and clarity in the size reduction process, it can be clearly seen from the figure that over the whole fuel column, the interpellet gaps are clearly marked. The flux depressions caused by the spacer grids are also evident. It is also clear that the burnup is very even over more than 2 meters of the fuel pellet stack.

The total fuel pellet stack length as measured from the gamma scan, 3658 mm, agreed exactly with the length measured during manufacture. However, a small fuel densification effect can be inferred from the very clearly marked inter-pellet gaps in the fuel zone between the first and second spacer grids from the top of the assembly.

3.2 Point measurements

The locations of the 18 point measurements are also shown in Fig 1. Because of the long irradiation history of the rod (Fig 2) and the decay time of almost two years, the gamma spectrum was dominated by the photopeaks of Cs-134 and Cs-137, but the spectrum also contained peaks from Ru-106, Ce-144 and Eu-154. These are the main gamma-emitting fission products which will be studied during the leaching experiments, and it is, therefore, essential to determine their inventories as a function of location along the

fuel rod. Photopeak energies and other constants used during evaluation are listed in Table 2.

The counting rates for the photopeaks are given in Table 3. These values were then corrected for relative detector efficiency, escape probability for the particular gamma photon from the fuel/clad segment viewed by the 0.5 mm collimator, and gamma transition abundance.

The corrected values, which represent the specific activities of the various fission products assuming a geometric efficiency of 1, are presented in Table 4. Agreement between the gamma photopeaks of a particular nuclide is generally satisfactory, although it can be seen that the 802 keV peak from Cs-134 gives low results probably due to background subtraction difficulties. The spread in the results for Ru-106, Ce-144 and Eu-154 must be regarded as fairly reasonable for this type of non-destructive measurement.

Comparison between the experimental results and the specific activities calculated by the BEGAFIP code suggests that the geometric efficiency was of the order of 10 %, but this will be checked later when the fission product and actinide inventories are determined by dissolution and analysis of selected fuel specimens removed from the rod.

Fission product activity ratios can be useful monitors of fuel burnup processes. For example, since Cs-134 is formed by a neutron capture reaction in the stable fission product Cs-133, its formation is dependent quadratically on the neutron fluence. Thus, the activity ratio between Cs-134 and Cs-137, which is formed only by

fission, is a measure of the fluence, and hence the burnup. This is illustrated in Fig 3, where ratios of the Cs-134 796 keV peak to the Cs-137 662 keV peak for the measured points is plotted against the Cs-137 activity. The linearity obtained confirms the effect, and also suggests that the axial form factor has not changed appreciably during irradiation.

Another aspect of the burnup process which influences the local fission product and actinide inventories and the fuel stoichiometry is the fact that as burnup proceeds, an increasing fraction of the fission events occur in Pu-239, formed by neutron capture in U-238.

One of the consequences of this, is that the relative production rate of the fission products in the 4d group of the periodic system - Mo, Tc, Ru, Rh, Pd - increases with burnup. Since these elements tend to form metallic inclusions in the fuel and therefore cannot bind oxygen atoms "liberated" during fission of the heavy fissile nuclides, a small increase in fuel stoichiometry is expected. This may have a significant effect on solubility mechanisms and will be studied further during the fuel characterization program.

The effect is illustrated in Fig 4, where the ratio of the Ru-106 512 keV peak to the Ce-144 133 keV peak is plotted against the Cs-137 activity (burnup). The fission yield for Ru-106 is higher for fission in Pu-239 than in U-235, while the reverse is the case for Ce-144. Thus, the ratio is a qualitative indication of the variation of the fraction of fissions occurring in Pu-239 as a function of position in the fuel rod. Due to the long irradiation history, however, the curve reflects mainly the events during the later stages of irradiation.

REFERENCE

- 1 FORSYTH R S, SVANBERG K and WERME L
Symposium on Scientific Basis for
Nuclear Waste Management VII,
Boston (1983)

Table 1 Axial gamma scan: experimental data.

Nuclide	Cs-137
Energy channel width	656-668 keV
Collimator (slit type)	Width 0.5 mm
Detector	Ge/Li No 178
Cps range	300 full scale
Time constant	3.3 sec
Scan speed	6 mm/min
Chart speed	1.5 mm/min

Table 2 Point measurements: correction factors.

Nuclide	Energy (keV)	Det. Efficiency (%) (30 cm geometry)	Escape Probability	Abundance (%)
Cs-137	662	3.44 E-04	0.61	84.6
Cs-134	563	4.09 E-04	0.54	8.82
	569	4.00 E-04	0.56	15.8
	604	3.97 E-04	0.58	98.0
	796	2.45 E-04	0.65	89.0
	802	2.40 E-04	0.66	9.5
Ru-106	512	5.32 E-04	0.51	20.6
	622	3.80 E-04	0.59	9.9
Ce-144	133	5.40 E-03	0.028	10.8
	696	3.13 E-04	0.62	1.47
Eu-154	723	2.60 E-04	0.63	19.1
	873	1.88 E-04	0.68	11.3
	1274	1.37 E-04	0.75	33.6

POINT	Cs-137		Cs-134				Ru-106		Ce-144		Eu-154		
	662	563	569	604	796	802	512	622	133	696	723	873	1274
1	134.5	6.50	11.5	68.1	42.6	2.72	31.9	11.6	20.2	2.45	1.46	0.80	0.73
2	134.3	5.08	9.3	66.1	43.1	3.87	32.8	11.8	20.3	2.62	1.57	0.71	0.84
3	178.2	10.82	19.2	113.2	74.4	6.84	49.5	17.8	26.4	3.37	2.08	1.16	1.18
4	177.7	10.90	19.2	114.6	75.0	6.95	50.1	17.8	27.8	2.29	2.23	1.25	1.38
5	210.8	14.32	26.2	158.8	104.7	6.53	62.0	22.1	29.4	4.30	2.87	1.97	1.87
6	210.4	15.01	26.5	159.6	103.4	6.29	64.4	22.7	30.1	4.07	2.69	1.56	1.85
7	247.7	20.42	36.1	222.8	144.4	9.02	80.5	29.2	32.9	4.52	2.88	2.31	2.30
8	248.4	21.01	37.1	224.7	146.2	9.25	83.0	29.8	34.2	3.87	3.89	2.34	2.50
9	261.7	23.27	41.4	246.5	162.1	14.71	87.3	31.2	33.8	4.31	3.52	2.30	2.91
10	260.6	23.65	40.0	248.6	163.0	14.49	88.4	31.0	33.9	4.36	3.53	2.39	2.59
11	262.6	24.05	42.4	248.4	165.3	14.79	92.1	32.0	35.5	4.41	3.50	2.18	2.55
12	261.2	23.58	42.2	250.6	164.1	14.82	91.6	32.5	35.5	4.77	3.55	2.39	2.74
13	265.4	23.52	42.4	255.7	167.5	9.87	95.2	33.5	36.0	3.19	3.70	2.45	2.46
14	264.7	24.44	43.4	258.4	165.7	10.07	95.7	33.3	35.8	5.32	3.56	2.24	2.60
15	265.5	23.94	42.6	257.5	166.6	10.31	92.5	33.0	36.0	4.50	3.82	1.52	2.42
16	264.4	24.40	42.0	255.0	166.2	15.09	93.4	32.4	36.4	4.09	3.90	2.27	2.74
17	186.6	11.96	21.8	132.7	84.4	5.47	56.8	21.3	29.1	3.87	2.98	-	1.57
18	186.6	12.52	21.5	131.7	83.4	7.26	56.6	20.7	30.2	3.93	2.40	1.49	1.58

Table 3 Point measurements: Counting rates (cps) for the major gamma photopeaks.

POINT	Cs-137	Cs-134					Ru-106		Ce-144		Eu-154		
	662	563	569	604	796	802	512	622	133	696	723	873	1274
1	2.54 E8	1.07 E8	1.05 E8	0.97 E8	0.97 E8	0.58 E8	1.76 E8	1.61 E8	3.72 E8	2.58 E8	1.56 E7	1.85 E7	0.71 E7
2	2.53	0.84	0.84	0.94	0.98	0.83	1.81	1.63	3.72	2.76	1.68	1.64	0.81
3	3.35	1.79	1.74	1.62	1.69	1.46	2.73	2.47	4.86	3.54	2.21	2.67	1.14
4	3.35	1.80	1.75	1.63	1.70	1.49	2.76	2.47	5.10	2.82	2.38	2.88	1.33
5	3.98	2.37	2.38	2.27	2.38	1.40	3.42	3.08	5.40	4.53	3.06	4.57	1.81
6	3.98	2.48	2.41	2.28	2.35	1.35	3.54	3.14	5.52	4.29	2.87	3.60	1.79
7	4.68	3.38	3.28	3.19	3.28	1.93	4.44	4.07	6.06	4.74	3.07	5.34	2.22
8	4.68	3.48	3.38	3.22	3.31	1.98	4.56	4.13	6.30	4.09	4.15	5.41	2.42
9	4.92	3.83	3.77	3.51	3.67	3.15	4.81	4.31	6.21	4.53	3.74	5.31	2.70
10	4.92	3.89	3.64	3.54	3.70	3.09	4.87	4.26	6.24	4.59	3.77	5.51	2.50
11	4.95	3.96	3.86	3.54	3.77	3.15	5.08	4.44	6.51	4.65	3.74	5.04	2.47
12	4.92	3.89	3.83	3.83	3.73	3.15	5.05	4.50	6.51	5.01	3.81	5.54	2.64
13	5.02	3.89	3.86	3.64	3.80	2.12	5.24	4.65	6.63	3.36	3.94	5.67	2.37
14	4.99	4.02	3.96	3.70	3.77	2.16	5.27	4.62	6.60	5.58	3.81	5.17	2.50
15	5.02	3.96	3.86	3.67	3.80	2.22	5.08	4.59	6.60	4.74	4.07	3.50	2.34
16	4.99	4.02	3.93	3.64	3.77	3.22	5.15	4.50	6.99	4.32	4.17	5.24	2.64
17	3.51	1.98	1.98	1.89	1.92	1.17	3.14	2.96	5.34	4.05	3.18	-	1.52
18	3.51	2.07	1.96	1.88	1.89	1.55	3.11	2.87	5.55	4.14	2.56	3.44	1.53

POINT 10	261	24	40	249	163	14	88	31	34	4.4	3.5	2.4	2.6
δps													

Table 4 Specific activities (Bq/gU) for the major fission products assuming an arbitrary geometry factor of 1. (Reference date 1st April 1985).

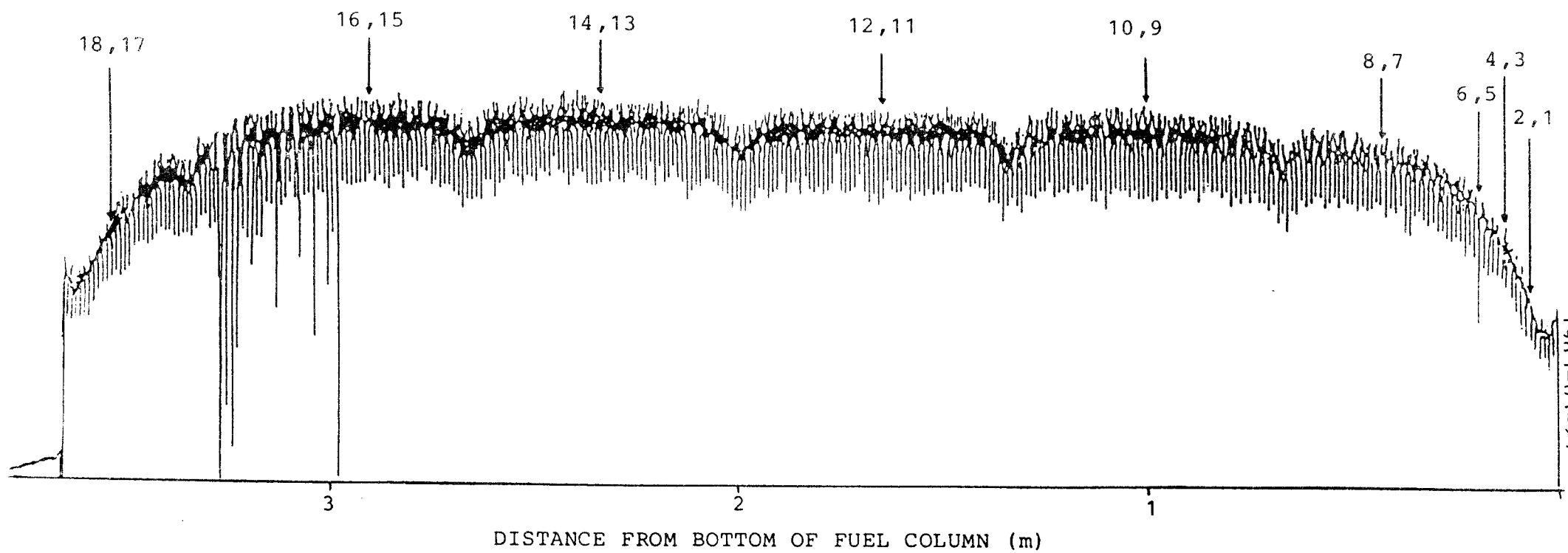


Fig 1. Axial gamma scan (Cs-137) of PWR rod number 03688 from Ringhals 2 assembly D07.

AVERAGE ROD
POWER (kW/m)

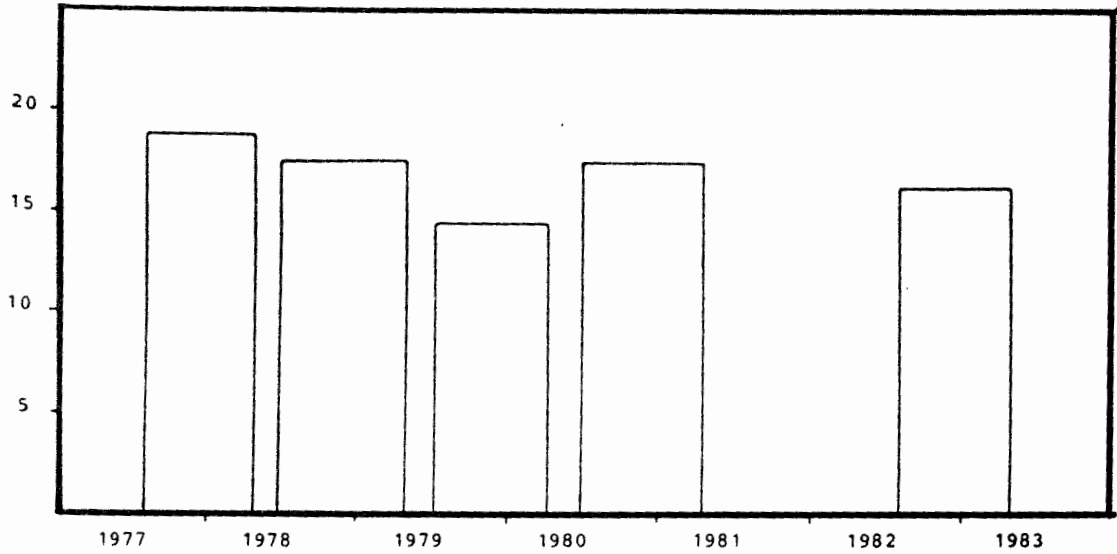


Fig 2. Schematic rod irradiation history

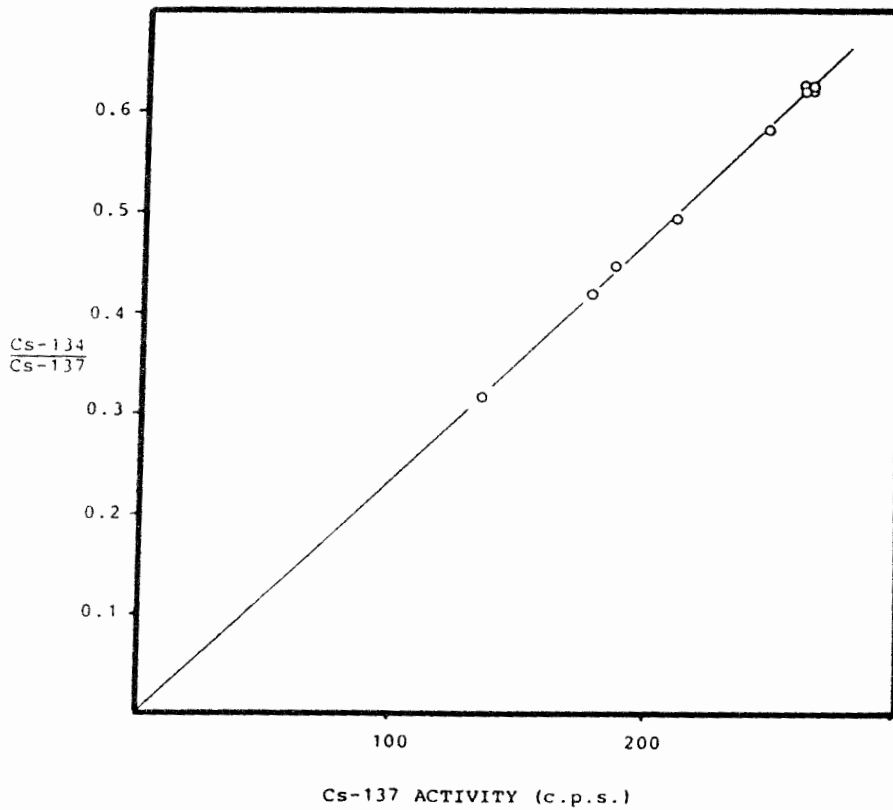


Fig 3. Results of point measurements demonstrating validity of Cs-134/Cs-137 ratio as burnup monitor.

CONTENTS

	<u>Page</u>
1. PROFILOMETRY	
1.1 Method	1
1.2 Results	1
2. EDDY CURRENT	
2.1 Method	2
2.2 Results	2
Figures 1 - 4	

1. PROFILOMETRY

1.1 Method

As the fuel rod was too long for the profilometry rig, the rod was cut in three pieces before the measurements. The length of the pieces were respectively 90 (top), 1759 and 2015 mm (bottom). No marks to indicate the generatrices were made before cutting the rod. The bowing of the fuel rod was consequently not measured.

The two lower pieces of the rod have been measured along their full length with two orientations 0° - 180° and 90° - 270° . The ovality has been measured by spiral profilometry. The measurements have been recorded with the length scale 1:3.

1.2 Results

The nominal outer diameter according to the manufacturer's drawing is 10.75 mm. This diameter is preserved only at the plenum. The diameter has diminished to <10.7 mm for other parts of the cladding. There are apparent ridges and crud from the bottom end plug up to 2800 mm from the bottom.

The bowing of the rod is relatively large and not in only one direction as is usual for BWR-rods. The bowing is S-shaped with distances between the bows corresponding to distances between spacers. The largest measured bowing in a length of 500 mm is 1.25 mm.

The results are shown in Figures 1-2. The length scale is 6 mm/scale division. Curve C shows the diameter with 0.005 mm/scale division. Curves A

and B show the bowing with 0.1 mm/scale division. All measurements start from the weld at the bottom end plug and end about 90 mm below the top end plug except for an interval of about 25 mm at the cutting point.

The orientation of the zero generatrice has been indicated with a small saw cut at the lower end of the rod segments.

2. EDDY CURRENT

2.1 Method

As for the profilometry, the rod was examined after cutting.

The measurements have been performed with a double coil with a diameter of 11.5 mm, and a frequency of 200 kHz. An inactive cladding tube with known defects was used for calibration. Two signals with a phase angle of about 90° were registered on a plotter. The signals were adjusted to be sensitive for defects and dimensional changes (ridges) respectively.

All measurements have been recorded on a plotter and on magnetic tape with the length scale 1:3.

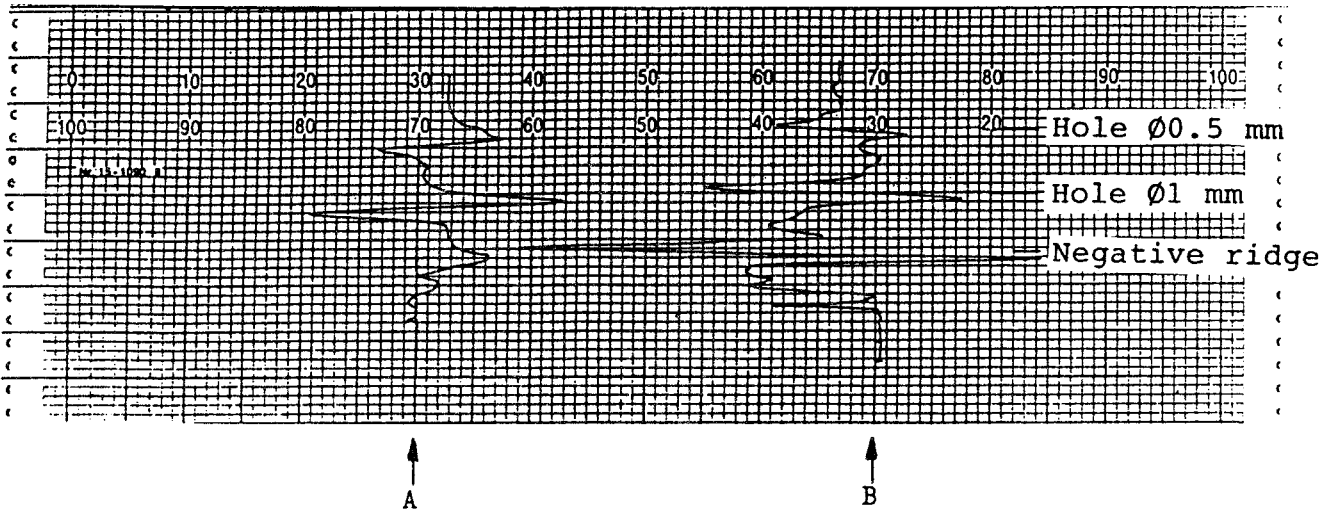
2.2 Results

The results are shown in Figure 3. The length scale is 6 mm/scale division. The left curve (A) is sensitive to defects and the right curve (B) to dimensional changes.

No indications of cladding defects were found.

Calibration of eddy current equipment

Tube reference defects. Diameter 10.25 mm.
Frequency 200 kHz. Double coil diameter 11.5 mm
Sensitivity index 0.10
Oscilloscope 1 V/channel
Plotter 10 V/channel



Curve A. High sensitivity for defects.

Curve B. High sensitivity for defects and
dimensional changes.

Studsvik Arbetsrapport - Technical Note

Projektidentifikation – Project identification		Datum – Date	Rapport nr – Report No.
SKB/STUDSVIK UO ₂ corrosion program		87-03-11	NF(P)-87/12
Titel och författare – Title and author			
Pellet/clad gap measurements of fuel rod 03688 from Ringhals 2.			
Tord Jonsson			
Distribution			
<input checked="" type="checkbox"/> Begränsad distribution – Restricted distribution		<input checked="" type="checkbox"/> Rapporten skall ej förhandsviseras – Internal note	
Godkänd av – Approved by		Kontonr – Internal note	Antal ex – No. of copies
<i>Tord Jonsson</i>		6228A	
SUMMARY			
During irradiation, fuel densification and swelling, and clad creep-down alter the internal volume of the rod. This report describes measurements of the residual pellet/clad gap over a section of the rod adjacent to a section which is used in leaching tests.			
NF158/BEm			

I.209042/1.209043 (Ej repr) 85-04

1. INTRODUCTION

This investigation is a part of a project with the aim of characterizing PWR-fuel before and after contact with ground-water.

2. CLAD TO PELLETT GAP MEASUREMENTS

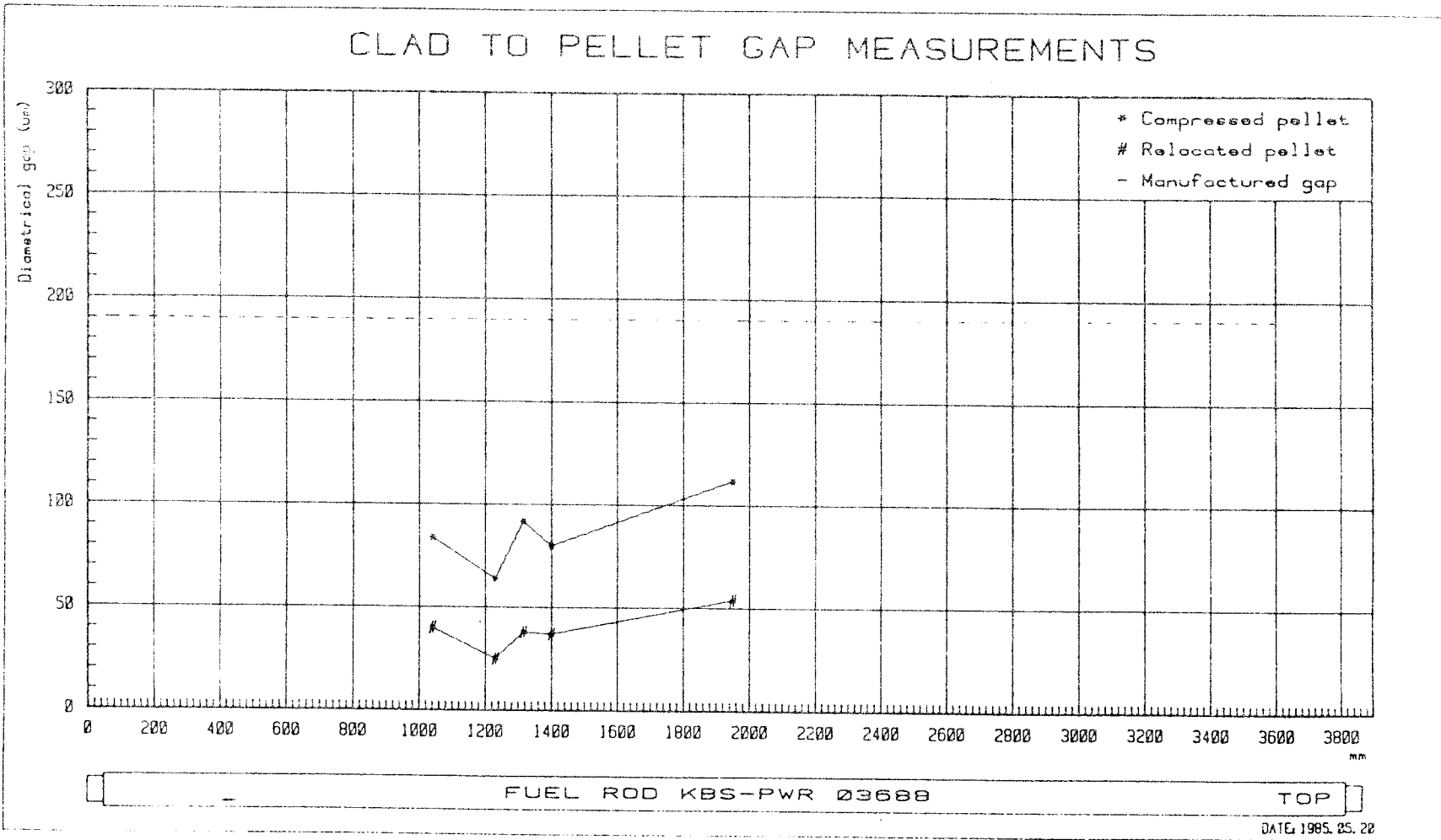
2.1 Method

The rod is compressed transversely between two 10 mm wide flat, edges. The compression force is increased until the total force exceeds the force to deform the cladding by 1000N, and is then decreased back to zero. The relative distance between the edges is measured by a digital gauging probe. The compression force is measured by a load cell as a function of the cladding deformation during the compression and decompression.


For each measurement a deformation/force diagram is plotted. The gap size can be chosen somewhat arbitrarily from the diagrams. We have chosen the deformation when the force on the fuel reaches 50N (first time) during compression as a measure of gap to relocated pellet, and the deformation when the force on the fuel comes down to 50N during decompression as a measure of gap to compressed pellet.

2.2 Results

Gap measurements were performed at a very limited number of axial positions to avoid the need of using the fuel from these positions for other measurements. The results are presented in Figure 1. The gaps have as can be expected diminished during irradiation and are significantly smaller than the nominal fabrication gap, but are still relatively large. The variation between different points seems to be random and, for example, can not easily be correlated to spacer positions: (According to visual examination and drawings of the assembly there are spacers at 1363 and 2026 mm from the bottom of the fuel rod.)



Studsvik Arbetsrapport - Technical Note

Projektidentifikation – Project identification		Datum – Date	Rapport nr – Report No.
SKB/STUDSVIK UO ₂ corrosion program		87-03-16	NF(P)-87/16
Titel och författare – Title and author			
Fuel rod 03688 from Ringhals 2: Measurement of fission gas release and burnup. U-B Eklund and R Forsyth.			
Distribution			
<input checked="" type="checkbox"/> Begränsad distribution – Restricted distribution		<input checked="" type="checkbox"/> Rapporten skall ej förhandsviseras – Internal note	
Godkänd av – Approved by		Kontonr – Internal note	Antal ex – No. of copies
		6228A	
<p>SUMMARY</p> <p>Measurement of the burnup (stable Nd-148 method) of two fuel samples taken from a high burnup section of the rod used for characterization studies and leaching tests gave values of 44.6 and 42.7 MWd/kg U respectively.</p> <p>Use of the mean of these values together with the rod's axial burnup profile as determined by gamma scanning, gave a rod average burnup of 39.9 MWd/kg U, which is somewhat less than the calculated value.</p> <p>The fission gas release from the fuel column during operation, determined by puncturing, gas collection and mass-spectrometric analysis, was 1.06 % (1.05 % Kr: 1.07 % Xe).</p>			
NF160/BEm			

I.209042/I.209043 (E) reпр 85-04

CONTENTS

	<u>Page</u>
1. INTRODUCTION	1
2. FISSION GAS RELEASE DETERMINATION	
2.1 Method	2
2.2 Results	3
3. BURNUP DETERMINATION	
3.1 Dissolution and separation	4
3.2 Instrument	4
3.3 Burnup results	5
3.4 Isotopic composition	5

1. INTRODUCTION

Fuel samples from rod 03688 are being used in an extensive program to determine corrosion rates and mechanisms of the fuel in groundwater. Characterization of the fuel both before and after corrosion testing is an important part of the program.

The burnup of the fuel has been determined experimentally, to check the value calculated at the reactor station, and to serve as input to codes used for the calculation of fission product and actinide inventories. These values, in turn, can be compared with experimentally determined values.

Determination of the fission gas release from the fuel during operation is also a part of rod characterization. The percentage release of Kr and Xe gaseous fission products to the internal free volume of the rod is a good indicator of the percentage release to the fuel/clad gap and fuel cracks of other mobile fission products such as Cs and I. This redistributed fraction of the inventory gives rise to the so-called instant release fraction when the fuel is contacted with groundwater.

2. FISSION GAS RELEASE DETERMINATION

2.1 Method

The method used was Studsvik's standard procedure, involving puncturing the rod, collecting its gaseous contents in a standard volume and measuring the pressure. Mass spectrometric analysis of an aliquot of the gas then enables determination of the total krypton and xenon in the rods' free volume.

The instrument used was a Baltzers quadro-pole instrument - mass-range 1-300, with a Faraday cup collector.

2.2 Results

The measurements and results are summarized below.

ROD 03688Measured release

Meas. temp.	24.2°C
Gas system vol	2076 cm ³
Pressure	198 torr
Rod free vol	22.2 cm ³

Kr/He	0.0056
Xe/He	0.055
Ar/He	0.0042
N ₂ /He	0.049

Vol: He	451 cm ³
Kr	2.53
Xe	24.8
Ar	1.9
N ₂	22.0
Total	<u>502.2</u>

Release Kr	1.05 %
Xe	1.07 %

Rod internal pressure (0°C)	2.29 MPa
-----------------------------	----------

Calculated quantities

Fuel wt. (U)	2122 g
Burnup	39.9 MWd/kg U
MeV/fission	204
Yield Kr	0.0289
Xe	0.277

Vol Generated	
Kr	241 cm ³
Xe	2310

3. BURNUP DETERMINATION

3.1 Dissolution and separation

Two whole pellets, with clad, were cut out from the high burnup section of the rod from which the specimens for corrosion testing were taken. After weighing, the samples were dissolved in cold 7 M HNO_3 . After dissolution, the Zircaloy-4 hulls were removed, dried and weighed.

(Note: Small amounts of a fine, black sediment were present in the solutions after dissolution. These were filtered off through glass sinters, dried and weighed. Since no significant quantities of U, Pu or Nd were found in the sediments, the results of the burnup analysis are unaffected.)

The sediments themselves, however, are of interest for defining the source terms for various fission products. They also arise in the dissolver vessels of reprocessing plants and have been shown to consist mainly of the 4d noble metal fission products Mo, Tc, Ru, Rh and Pd. Further work is being performed to quantify the amounts and composition of the sediments, and will be reported separately.)

The chemical separation and purification steps for U, Pu and Nd were those given in ASTM-E321.

3.2 Instrument

The measurements of isotopic composition were performed with a Varian TH-5 mass spectrometer, with thermal ion source and a Farady cup detector system. The purified fractions were evaporated on a Re filament.

3.3 Burnup results

Values of 44.6 and 42.7 MWd/kg U were obtained for the two near-duplicate specimens.


In conjunction with the burnup profile along the rod as determined by gamma scanning, this gives a rod average burnup of 39.9 MWd/kg U.

3.4 Isotopic composition

The determined isotopic compositions of the separated U and Pu fractions were as below.

	a/o
U-235	0.65
-236	0.49
-238	98.85
Pu-238	2.7
-239	51.3
-240	26.6
-241	12.0
-242	7.4

Studsvik Arbetsrapport - Technical Note

Projektidifikation -- Project identification SKB/STUDSVIK UO ₂ corrosion program	Datum -- Date 87-03-18	Rapport nr -- Report No. NF(P)-87/11
Titel och författare -- Title and author Ceramographic examination of PWR rod 03688. D Schrire, O Mattsson and B-Å Nilsson		
Distribution		
<input checked="" type="checkbox"/> Begränsad distribution -- Restricted distribution	<input checked="" type="checkbox"/> Rapporten skall ej förhandsviseras -- Internal note	
Godkänd av -- Approved by 	Kontonr -- Internal note 6228A	Antal ex -- No. of copies
ABSTRACT This report presents the results of the optical microscopy of an axial and a diametral cross-section of rod 03688. The ceramography includes grain size and pore size distributions at a number of radial locations.		
NF158/BEm		

1.209042/1.209043 (EJ regyr) 85-04

CONTENTS

	<u>Page</u>
1. INTRODUCTION	1
2. CLADDING	2
3. FUEL	
3.1 Ceramography and quantitative microscopy methods	3
3.2 Sample 1265	4
3.3 Sample 1266	5
4. ALPHA AND BETA-GAMMA AUTORADIOGRAPHY	8
5. REFERENCES	9
Table 1 Metallic fission product particles	
Figures 1 - 13	

1. INTRODUCTION

Two adjacent samples were cut from rod 03688 and prepared for optical microscopy. Sample 1265 (the transverse section) had its viewing section 1782 mm from the bottom of the rod. Sample 1266 was an axial section extending from 1461 to 1488 mm from the bottom of the rod.

The samples were prepared for optical microscopy by impregnating and mounting in epoxy resin, grinding (3 stages), diamond polishing (3 stages) and finally attack polishing. Sample 1265 was prepared as a 2 mm thick section, and all grinding and diamond polishing were carried out using white spirit as lubricant. Alpha and beta-gamma autoradiography, as well as micro-gamma scanning, were carried out on the sample after diamond polishing.

2. CLADDING

The hydride structure is shown in Figure 1 (transverse section) and Figure 4 (axial section). The grain structure at the inside and outside of the cladding are shown with polarized light in Figure 4. Note that the hydrides appear white in these photographs.

The outside of the cladding was covered with a uniform oxide layer, ranging in thickness from about 6 to 20 μm . The oxide on the cladding inside was irregular, ranging from no visible oxide to more than 10 μm thick. The presence and thickness of the oxide was strongly related to the proximity of the fuel. Oxide was usually absent opposite fuel pellet interfaces (chamfers), or where the local fuel-clad gap was large, and conversely the thickest oxide layers were mostly found where the gap was smaller (Figures 3, 4). Exceptions to this trend may be due to a difference between the relative local gap size at power and in the cold state. The density of hydrides near the clad inner wall appear to follow the same trend (Figure 1).

There were also extensive areas of fuel-clad bonding, always associated with a relatively thick oxide layer on the clad inner surface (Figure 3).

3. FUEL

3.1 Ceramography and quantitative microscopy methods

After the metallography, the fuel was prepared for microscopy by a two-stage attack polishing technique, followed by chemical etching. 16 photographs were taken at each of 5 radial positions in sample 1266, in the attack polished condition for the porosity analysis, and after etching for grain size measurements (4 radial positions). 1000X magnification micrographs were used for both the porosity analysis and the grain size measurement.

The average intercept length (AIL) grain size was determined by applying circular test lines to the micrographs. The pore size distributions and total porosity fractions were measured on an IBAS (Kontron Messgeräte GmbH) automatic image analysis system at the Swedish Institute for Metals Research. Pores in the size range $0.3 \mu\text{m}^2$ to $100 \mu\text{m}^2$ were measured. No pores larger than $100 \mu\text{m}^2$ were detected. A number of pores smaller than $0.3 \mu\text{m}^2$ were detected; however, these were below the true resolution of the microscope, so no useful information on their size distribution could be obtained.

In addition, the size distribution of metallic fission product particles was also measured in the central regions of the fuel. However, a large fraction of the detected particles were smaller than $0.3 \mu\text{m}^2$, and no reliable information of their true size distribution could be obtained. These data have therefore been summarised, and presented as the number density of all the detected particles, the number density

of those larger than $0.3 \mu\text{m}^2$, and the total volume fraction of the particles.

3.2 Sample 1265

The fuel microstructure along a radial section is shown in Figure 2. The fuel macrocracks do not show any unusual features, apart from the extensive circumferential crack very close to the pellet periphery. This may have been caused during cooling, as a result of the fuel-clad bonding in this region (Figure 3).

The fuel microstructure at different radial positions is shown in Figure 3. The most important observations are the major microstructural and compositional changes at the periphery, the fuel densification at the mid-radius, and the formation and growth of fission gas bubbles and metallic fission product particles towards the pellet centre.

The fuel periphery is characterised by extensive fuel clad bonding (possibly incorporating a caesium-rich phase as well as ZrO_2 and UO_2). The fuel within 0.1 mm of the periphery contains a large amount of very fine porosity, and appears less susceptible to chemical etching than the fuel 0.5 mm from the fuel periphery (Figure 3). This is probably due to the extremely high local burnup at the pellet surface, caused by the fuel self-shielding effect, and the buildup of plutonium. These assumptions are supported by the radial micro-gamma scanning results (1), which show marked increases in the Ru-106, Cs-134 and Cs-137 concentrations at the pellet periphery.

The fuel microstructural changes towards the centre of the pellet are qualitatively consistent with the quantitative microscopy results of sample 1266.

3.3 Sample 1266

The fuel microstructure along a radial section at a pellet end is shown in Figure 5, and at a mid-pellet position in Figure 6. The mid-pellet section is dominated by a large radial crack, but otherwise the macrocracking is similar in both sections.

The fuel microstructure at different radial positions is very similar to that in sample 1265 (Figures 7 and 3). A more detailed, quantitative description of the fuel microstructure is presented in the quantitative microscopy results (Table 1 and Figures 8-12).

At a radius of 4 mm (0.5 mm from the pellet periphery) the fuel microstructure is fairly similar to the as-fabricated fuel as regards the pore size distribution and grain size (Figure 8). There is, however, some reduction in the overall porosity, as well as solid fission product swelling in the fuel matrix. The as-fabricated density (design data) was 10.36 g/cm^3 , corresponding to 5.5 % porosity.

At a radius of 3 mm there is further densification, with the removal of a significant fraction of the pores between about $0.5 \mu\text{m}^2$ and $3 \mu\text{m}^2$, relative to the radial position of 4 mm (Figure 9). The grain growth at this position is still insignificant. Metallic fission product particles are just detectable at this radius (Table 1).

At a radius of 2 mm the densification is almost complete, with the removal of almost all the initial porosity (Figure 10). In addition to the removal of pores, there is also a shift towards smaller pore sizes as the larger pores shrink. The remaining pores may be stabilised by their internal pressures, with fission gas reaching the pores as fast as gas atoms are removed from them. At this radius new fission gas bubbles are just becoming visible, and there is an increase in the number of metallic fission products detected (Table 1).

At a radius of 1 mm there is a marked increase in the number of pores in all the measured size classes, compared to the previous radial position (Figure 11). The greatest increases occur in the smallest class sizes, corresponding to small grain-face fission gas bubbles. The total number and volume fraction of detected metallic fission product particles increase significantly relative to the radial position of 2 mm. The grain size has increased by about 25 % relative to the pellet periphery.

At the pellet centre there are further changes relative to the previous radial position, though not very large. The pore size distribution shows a slight shift towards larger sizes, with a small overall increase in porosity. This reflects the growth and coalescence of intergranular fission gas bubbles. Similarly the metallic fission product particles grow in size, though not in total number, and there is a further slight increase in the grain size (Table 1 and Figure 12). The appearance of the fuel at the pellet centre would indicate a certain amount of interlinkage of grain-edge porosity, with subsequent fission gas release.

Note that an average intercept length grain size of 4.3 μm corresponds to a grain boundary surface per unit volume (S/V) of $4.7 \times 10^5 \text{ m}^2/\text{m}^3$, and a grain size of 5.7 μm to an S/V value of $3.5 \times 10^5 \text{ m}^2/\text{m}^3$, from the relationship (2)

$$S/V = .2/AIL$$

4. ALPHA AND BETA-GAMMA AUTORADIOGRAPHY

Alpha and beta-gamma autoradiography were carried out on sample 1265 after polishing to 1 μm diamond (Figure 13). The alpha-autoradiograph shows the halo at the fuel periphery due to the buildup of transuranium isotopes, typical for fuel with relatively high burnup. This corresponds to the peripheral fuel zone seen in Figure 3.

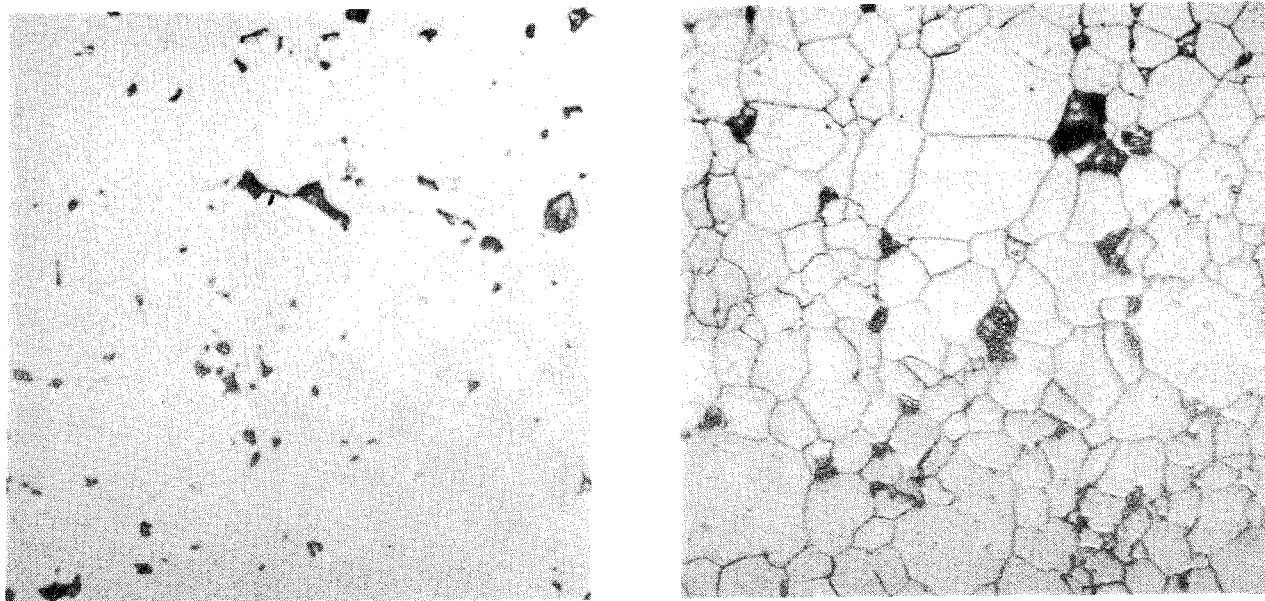
The beta-gamma autoradiograph does not show any major redistribution or local buildup of activity. The lighter patches which can be seen at various locations are an artefact of the specimen preparation procedure.

5. REFERENCES

1. LYSELL, G.,
Studsvik Report NF(P)-86/48,
1986-11-26.
2. UNDERWOOD, E. E.,
"Quantitative Stereology",
Addison-Wesley, Reading,
Mass. (1970).

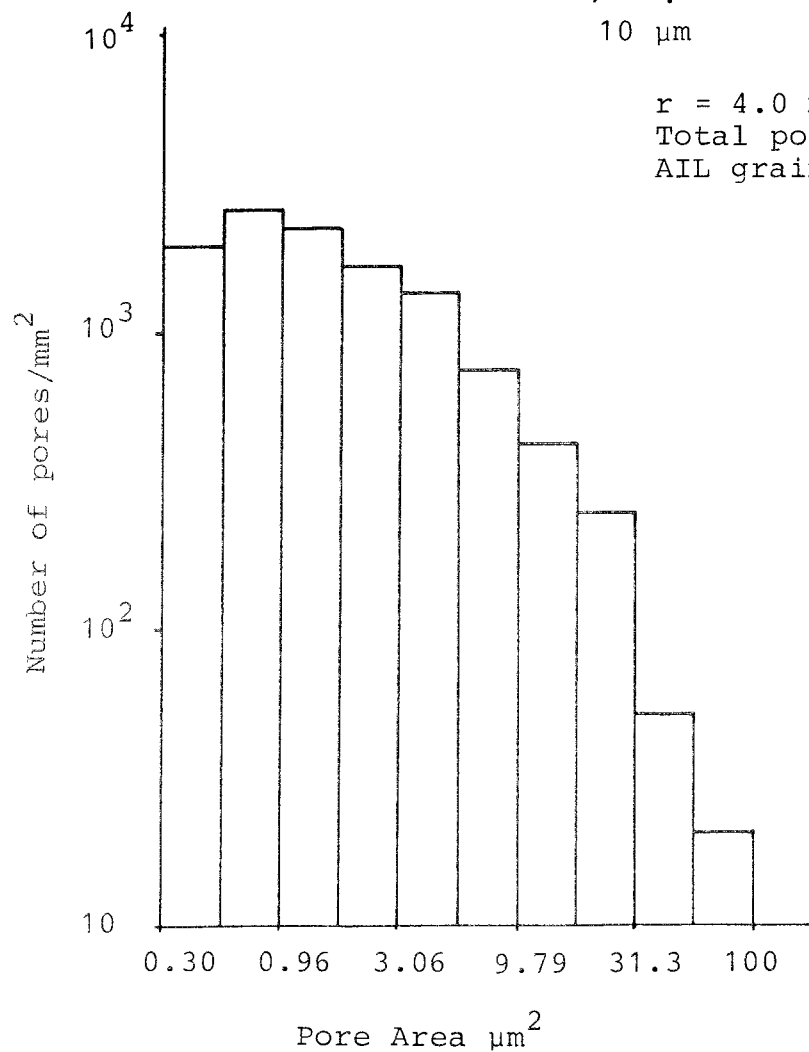
Table 1. Metallic fission product particles

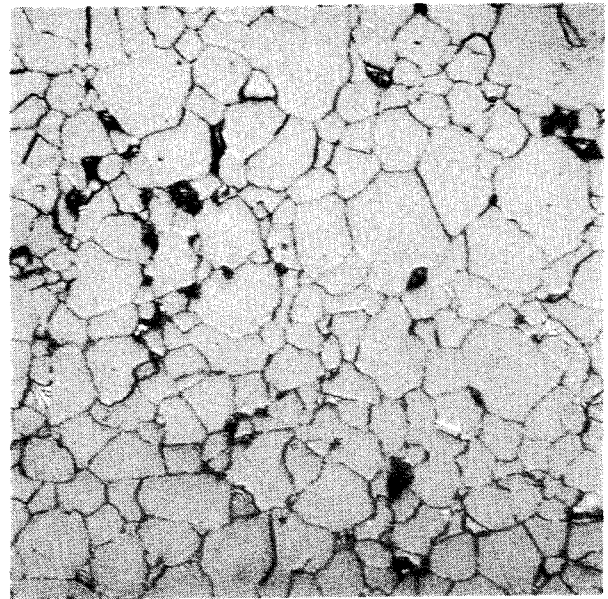
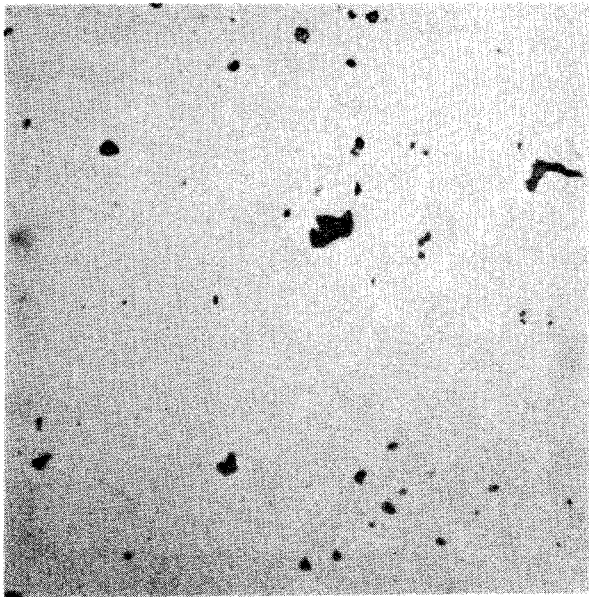
Radius mm	Total N_A mm^{-2}	$N_A > 0.3 \mu\text{m}^2$ mm^{-2}	Volume Fraction %
3.0	535	154	0.0183
2.0	1287	236	0.0291
1.0	2075	355	0.0410
0 (centre)	1976	498	0.0455



10 μ m

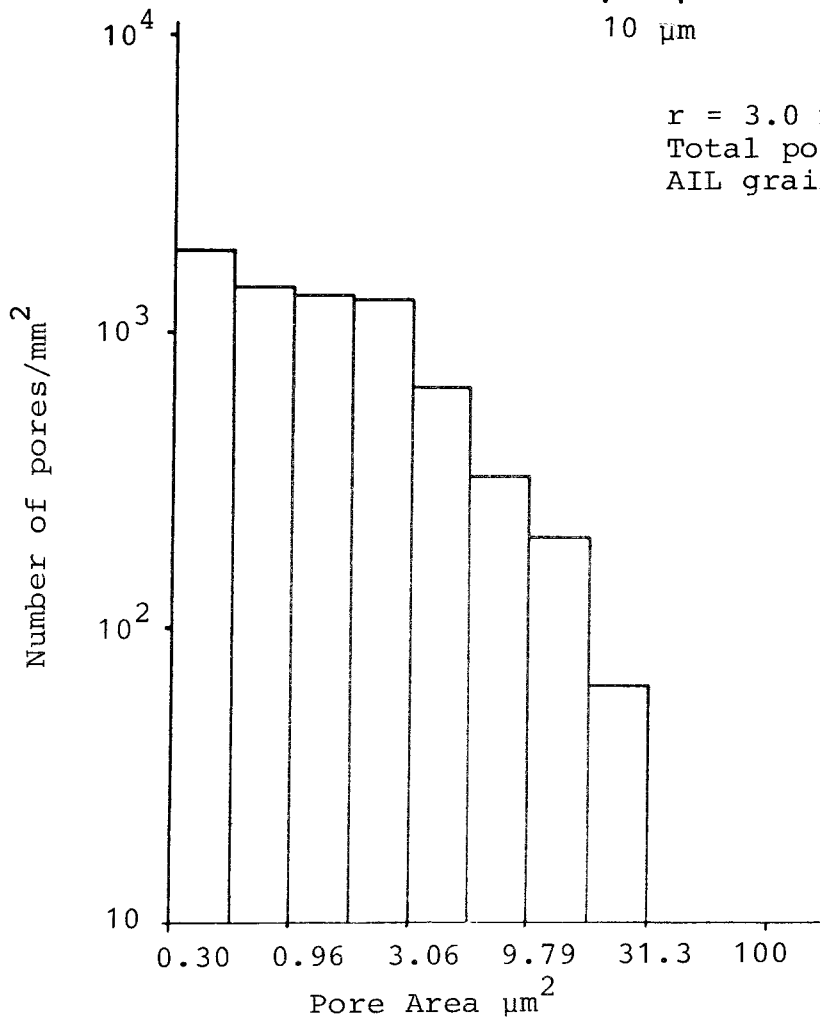
$r = 4.0$ mm (0.5 mm from periphery)
Total porosity = 3.4 %
AIL grain size = 4.3 ± 0.1 μ m

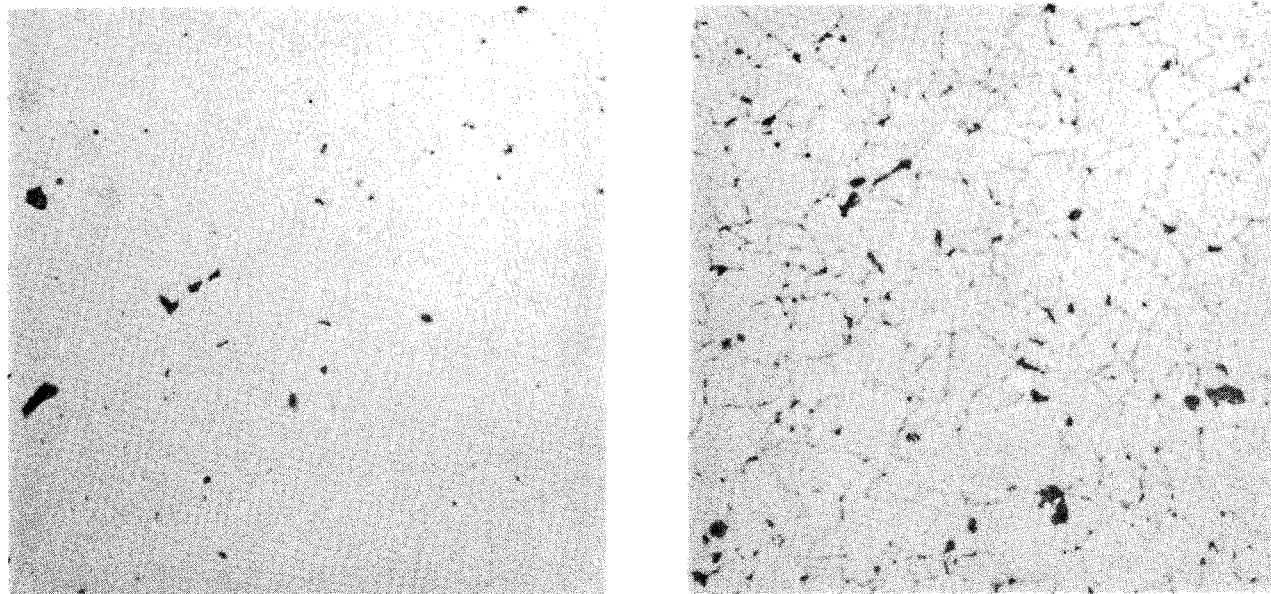




10 μm

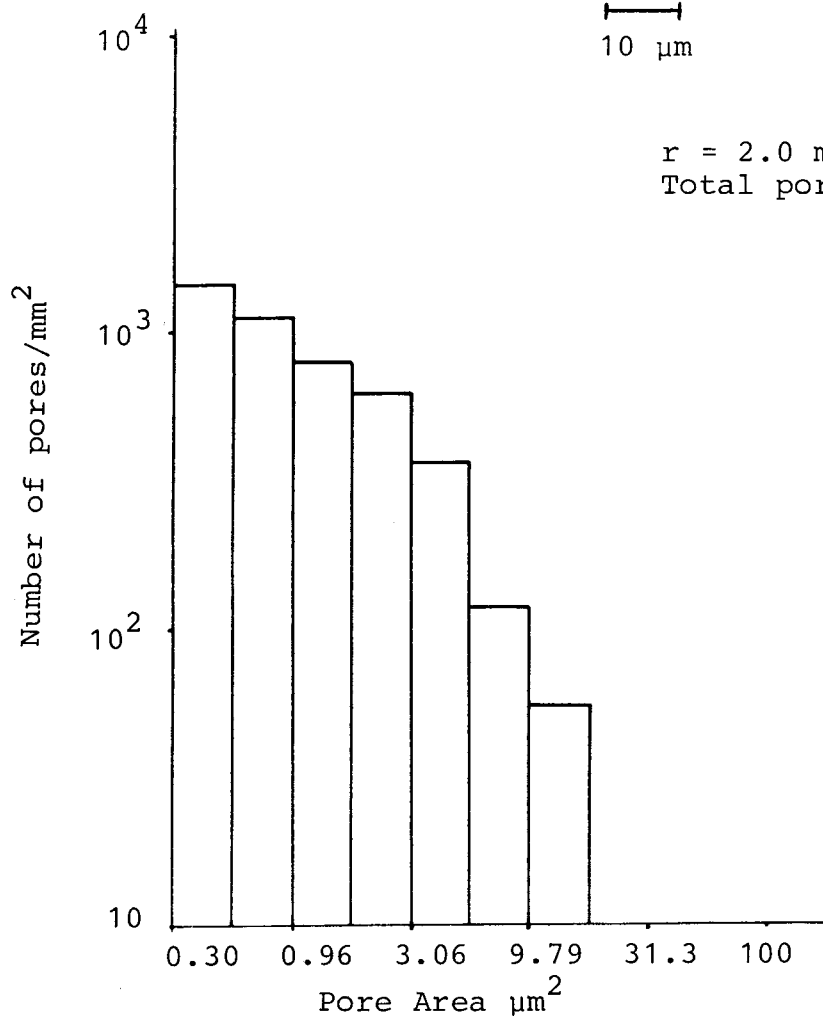
$r = 3.0 \text{ mm}$
Total porosity = 1.6 %
AIL grain size = $4.5 \pm 0.1 \text{ μm}$

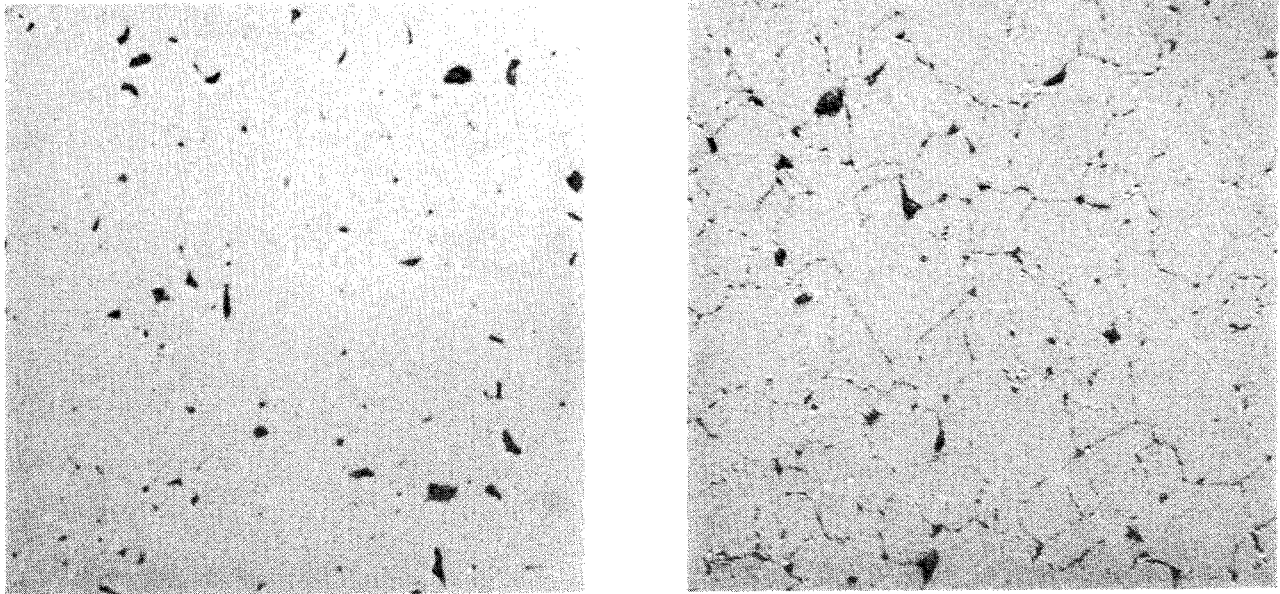




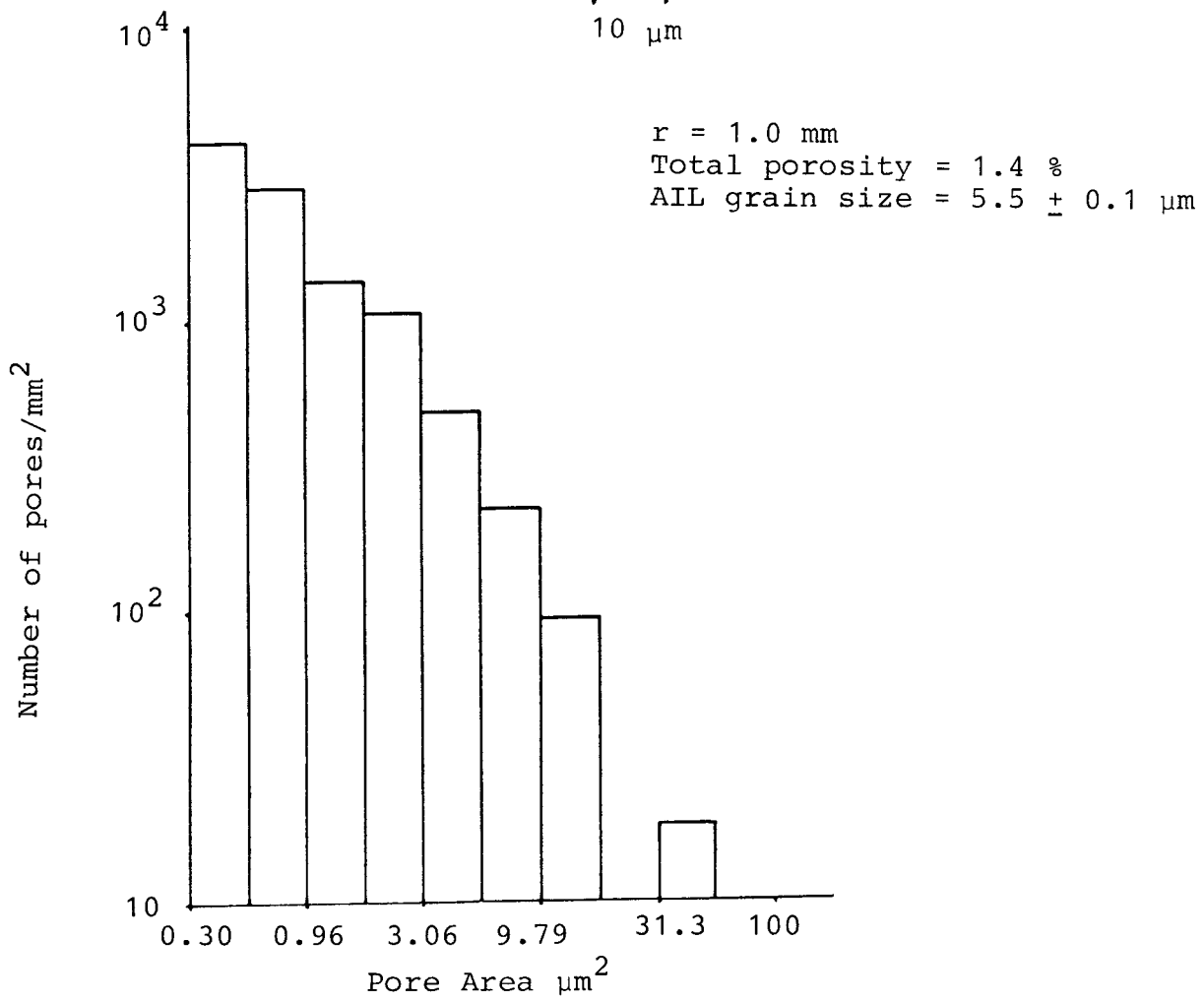
10 μm

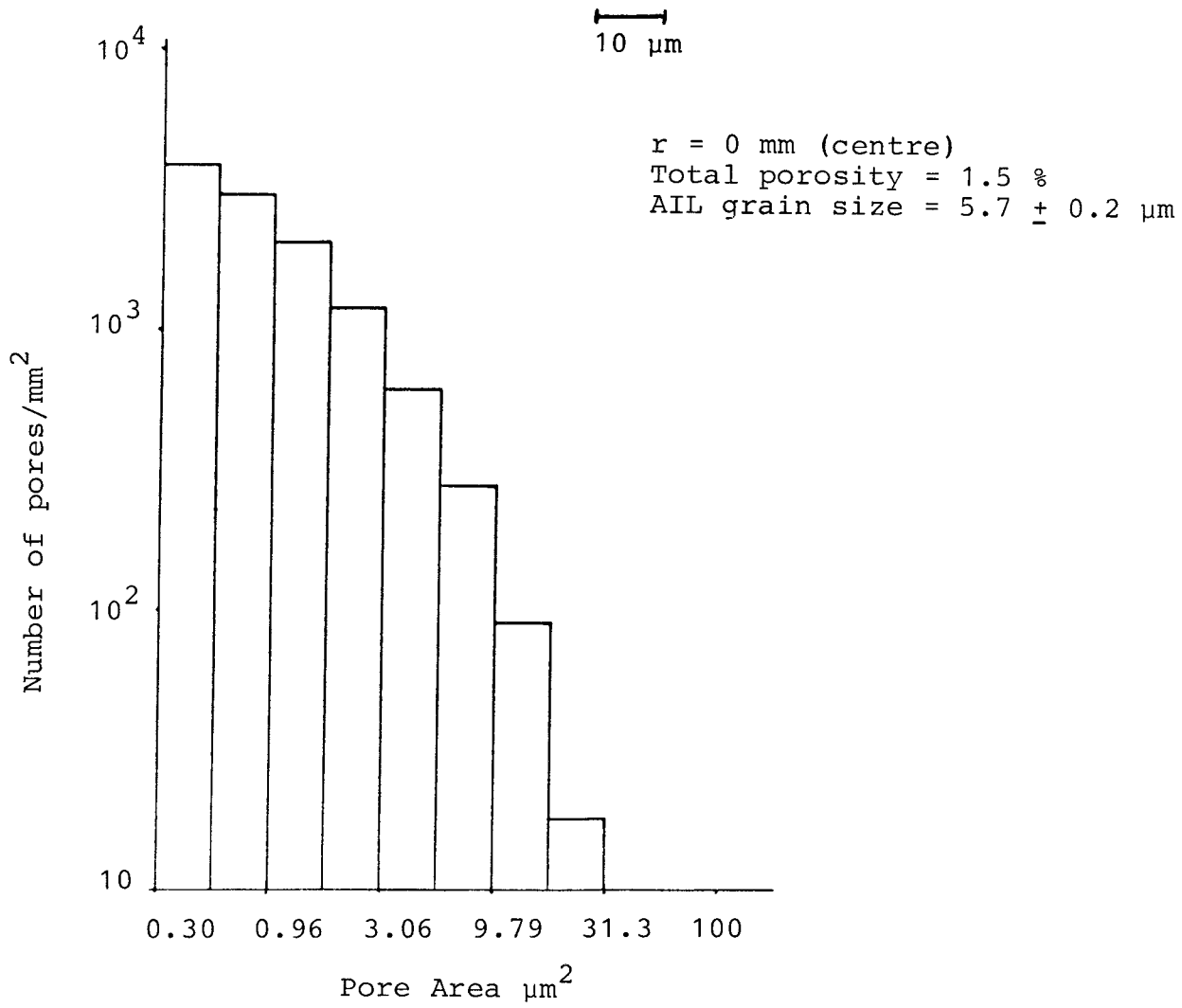
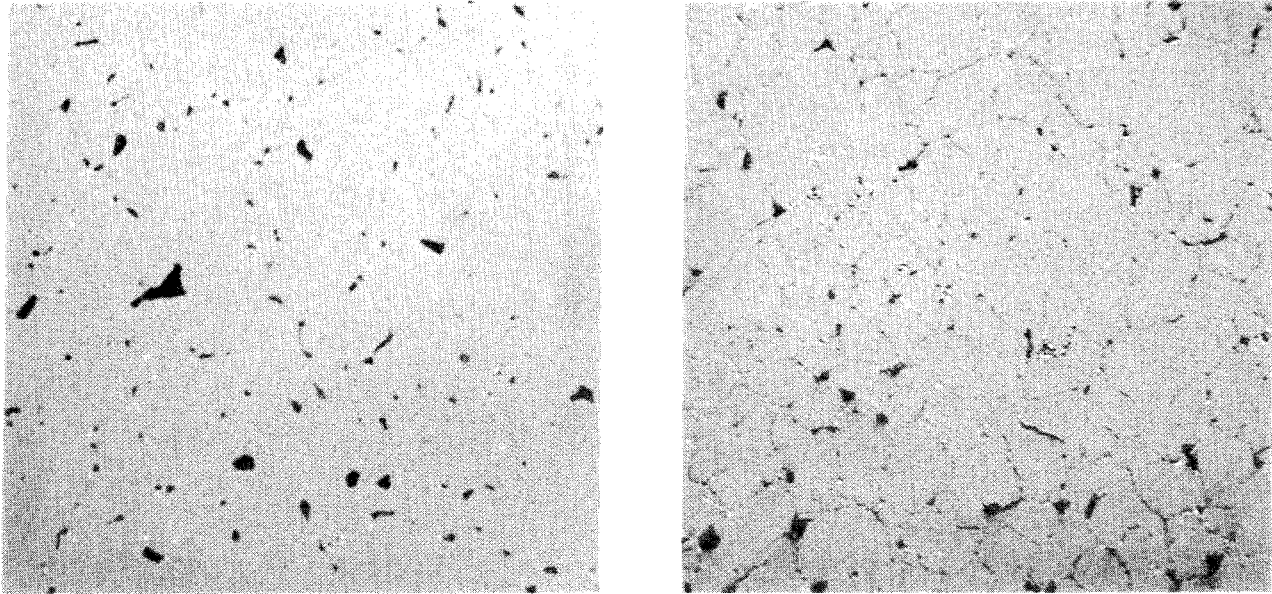
$r = 2.0 \text{ mm}$
Total porosity = 0.75 %

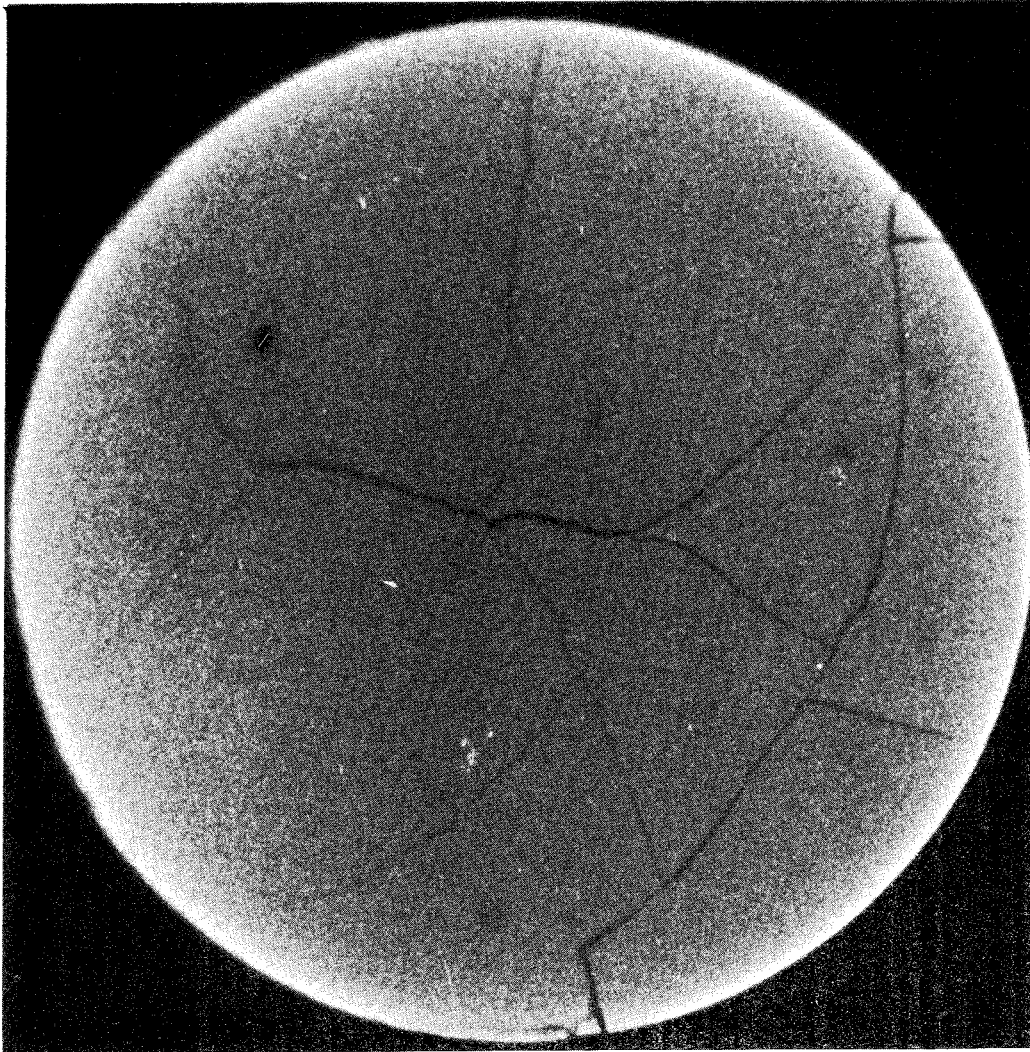




10 μm



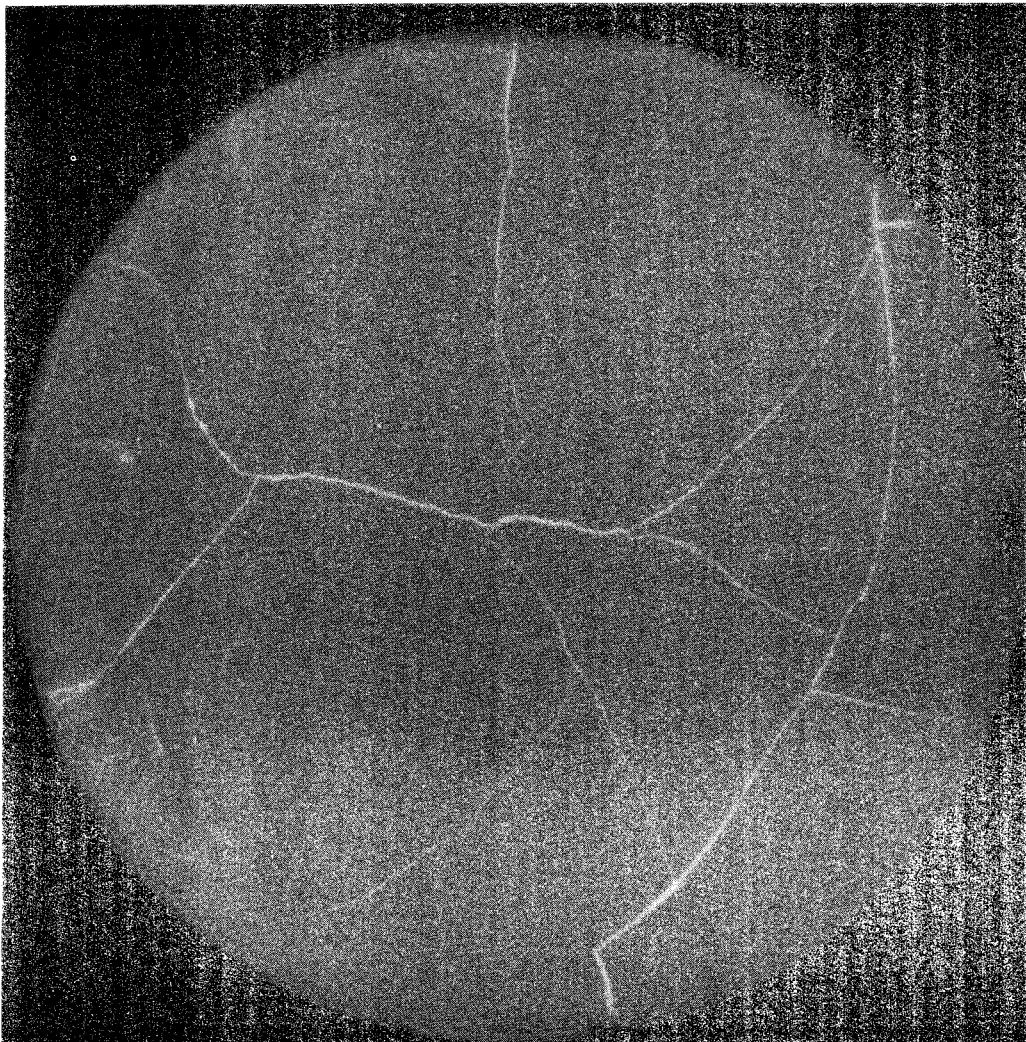




Sample 1265


α
Autoradiograph

—|—|—
1 mm



β - γ
Autoradiograph

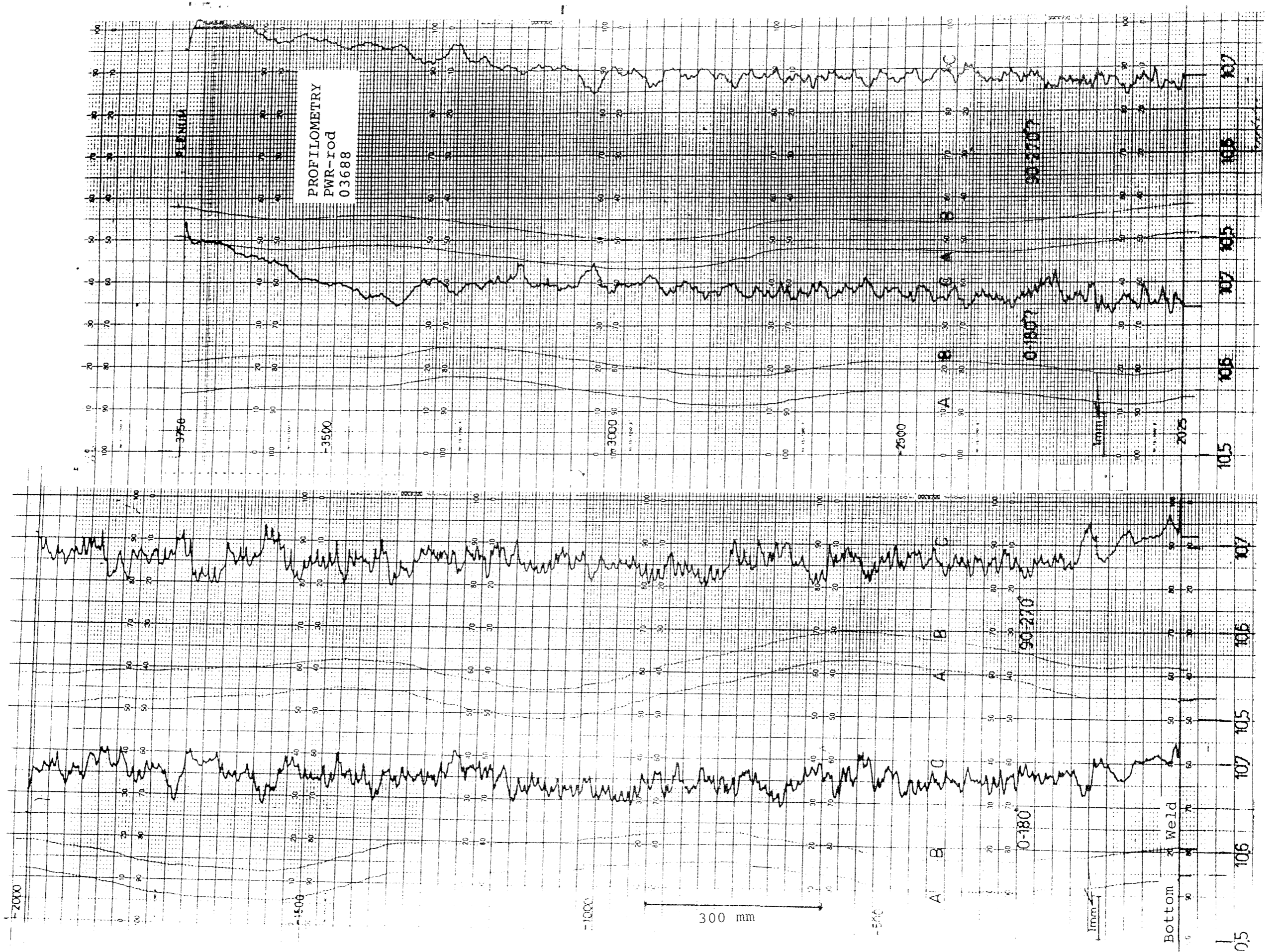
Studsvik Arbetsrapport - Technical Note

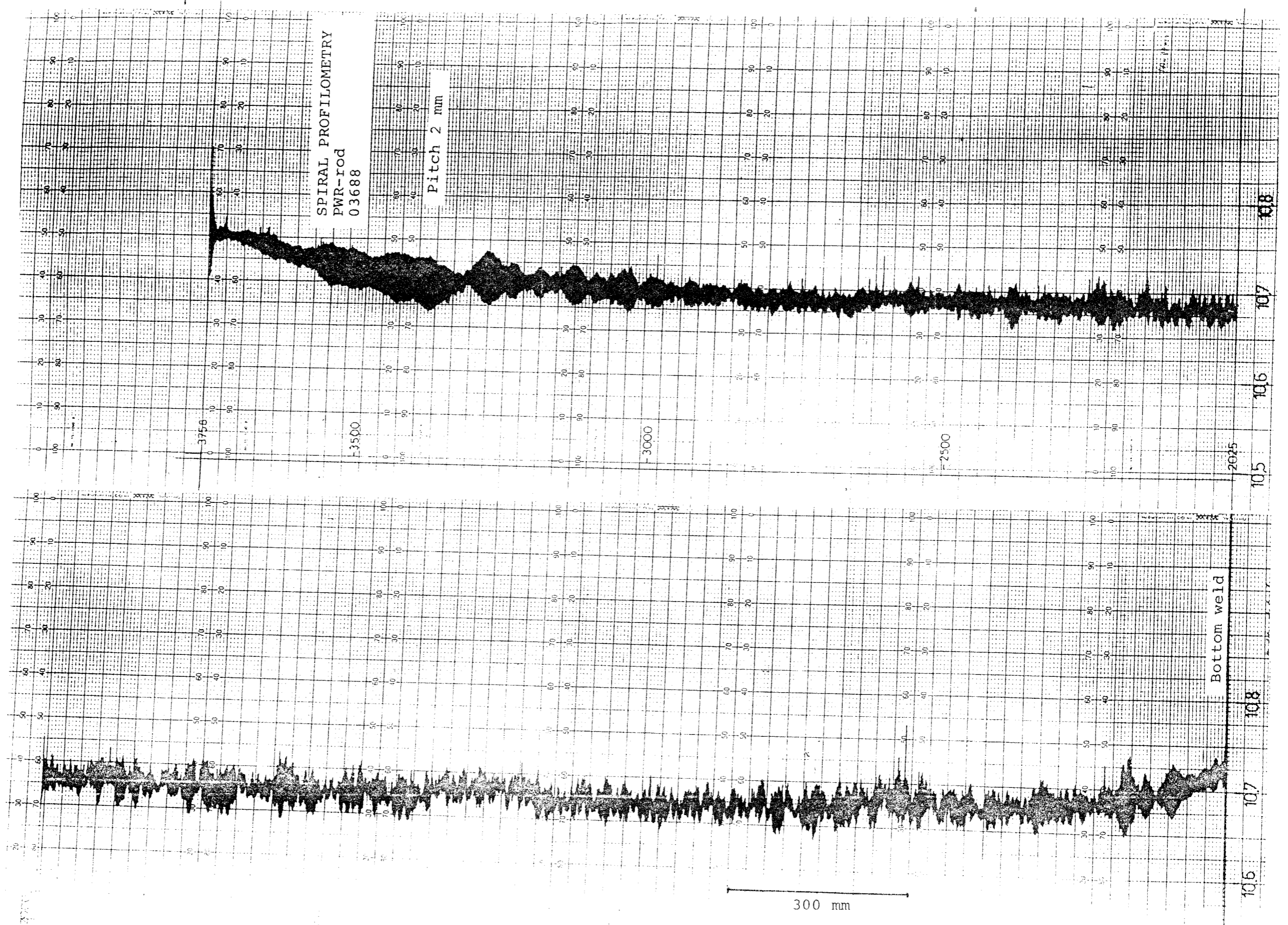
Projektidentifikation – Project identification		Datum – Date	Rapport nr – Report No.
SKB/STUDSVIK UO ₂ corrosion program		86-11-26	NF(P)-86/48
Titel och författare – Title and author			
Radial gamma measurements on a cross section from the PWR fuel rod number 03688 from Ringhals 2.			
Gunnar Lysell			
Distribution			
<input checked="" type="checkbox"/> Begränsad distribution – Restricted distribution		<input checked="" type="checkbox"/> Rapporten skall ej förhandsviseras – Internal note	
Godkänd av – Approved by		Kontonr – Internal note	Antal ex – No. of copies
		6228B	
ABSTRACT			
A fuel cross section 1675 mm from the fuel column bottom in the PWR rod 03688 from Ringhals 2 was radially gamma scanned. The measurements show that negligible thermal Cs-release has occurred.			
NF154/BEm			

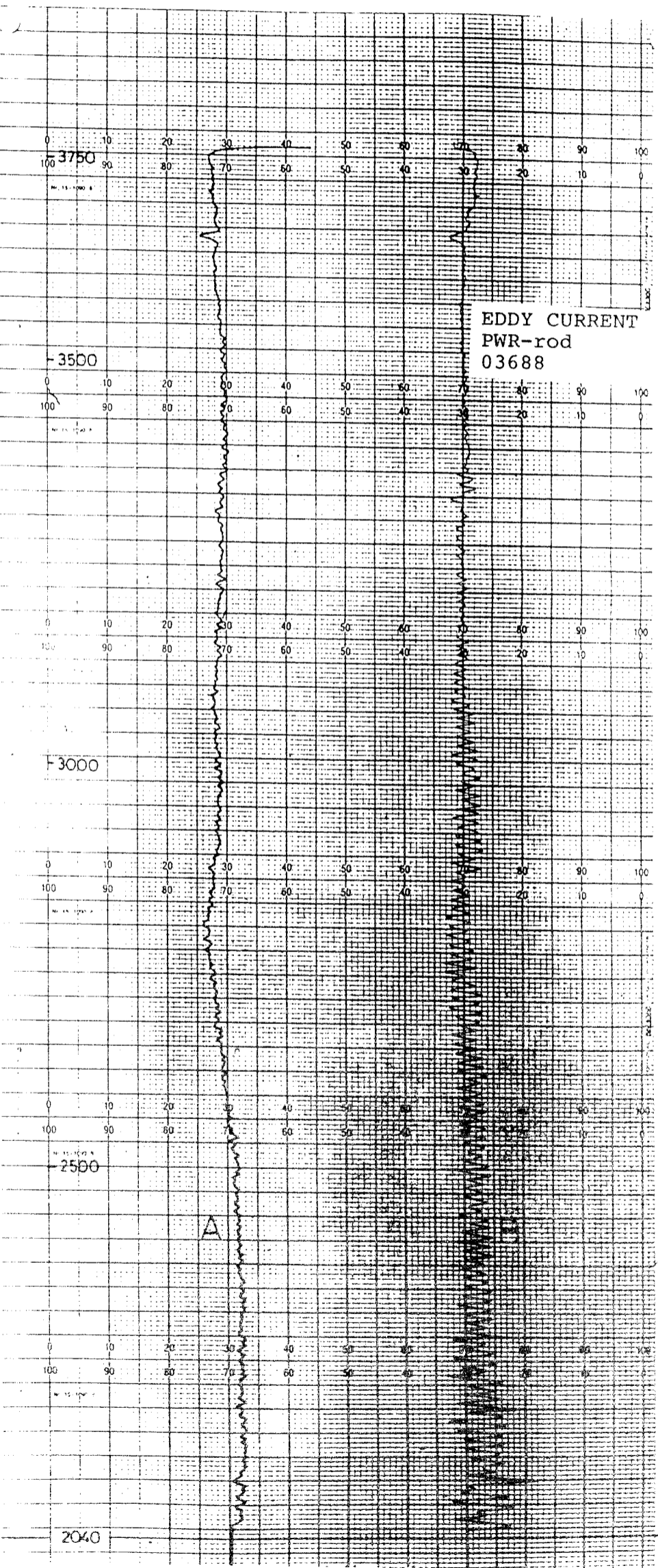
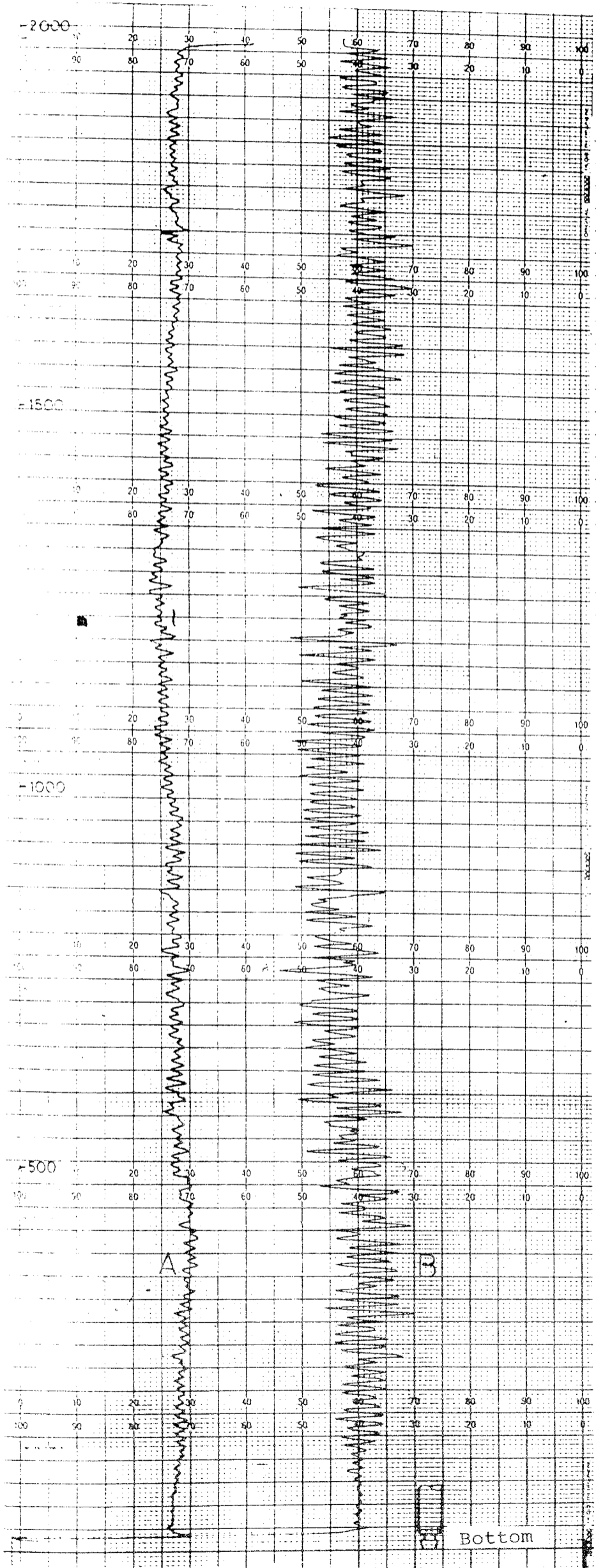
I.209042/I.209043 (Ej repr) 85-04

CONTENTS

	<u>Page</u>
1. INTRODUCTION	1
2. MEASUREMENTS	2
3. ANALYSIS	4
REFERENCE	5
Figures 1 - 16	
APPENDIX A	







1. INTRODUCTION

This work is part of a program for the study of the corrosion of spent reactor fuel in granitic groundwater.

The radial measurements were mainly done to quantify any significant release or redistribution of fission products in the fuel.

2. MEASUREMENTS

The fuel cross section, taken 1675 mm from the fuel stack bottom, was prepared as a ceramographic specimen with a thickness of 2 mm. The sample was ground in "white spirit" to avoid Cs-leaching.

The measurements were performed using our detector nr 178 and a collimator with a rectangular cross section of 1x2 mm.

The measurements were performed over the whole sample diameter with the normal to the long side of the collimator cross section in the direction of movement.

One series of measurements was made in each direction over the diameter of the specimen using a step length of 0.25 mm.

Over the edges of the sample two series of measurements with a step length of 0.1 mm were also performed. In all cases the measurement time at each point was 1000 s. All measurements were performed between 21st and 27th of May 1986.

The following nuclides and gamma peaks were analysed.

Nuclide	Energy (keV)	$T_{1/2}$ (years)	Abundance (photons/dis-integr.)	Relative detector efficiency (%)	μ (UO ₂) (cm ² /g)	$\frac{1}{\mu\rho}$ (UO ₂)	Escape Probability
						(cm)	
Ce-144	133	0.779	0.108	100	3	0.032	0.16
Cs-134	604	2.06	0.976	8.75	0.128	0.744	0.877
Ru-106	622	1.01	0.098	8.3	0.123	0.774	0.881
Cs-137	662	30.2	0.851	7.5	0.114	0.835	0.889
Cs-134	796	2.06	0.854	4.9	0.094	1.01	0.907
Eu-154	1274	16	0.336	2.6	0.055	1.73	0.944

The measurement data are shown in Figures 1 to 4. In some cases it is seen that the Eu-154 peak value is 0; this is due to drift in the electronics during the measurements so that the peak has moved outside the interval in which the computer seeks the peak.

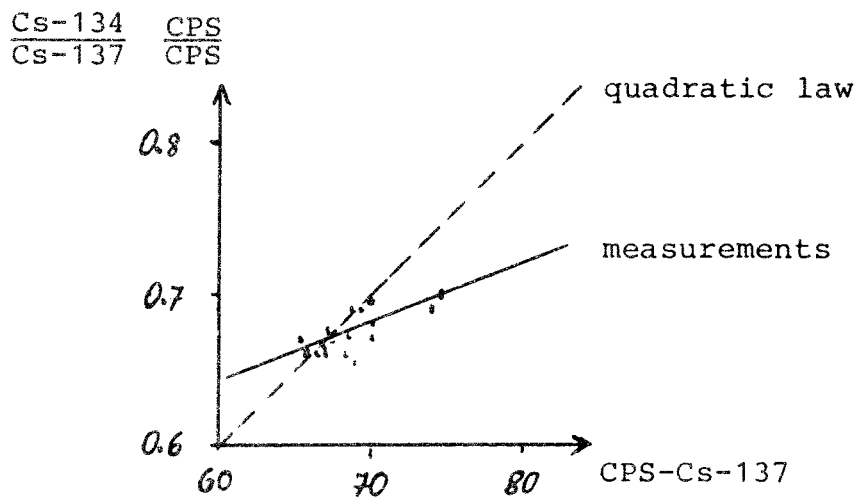
3. ANALYSIS

To obtain a better geometrical resolution than the direct measurements can give, a one-dimensional tomographic method has been applied. (See Appendix A.)

Plots of the collimator corrected curves are seen in Figures 5 to 16. It is apparent that the curves are peaking sharply near the periphery. This is due to the Pu buildup and consequent higher burnup at the periphery. The most pronounced peaking is seen for Ru-106 which has a fission yield of 0.4 per cent for U-235 in thermal neutrons. The Ru-106 fission yield for Pu-239 in thermal spectrum is ten times higher and therefore the Ru curve is dominated by the Pu fissions during the last year of irradiation, especially taking into account the rather short (1y) halflife of Ru-106.

The Cs-137 curves represent the local burnup distribution across the pellet. The Cs-134 curves are more representative of the square of the burnup since the Cs-134 is formed by neutron capture in the stable fission product Cs-133. However, at this high burnup (50 MWd/kg U) when the depletion of the U-235 is almost complete, a higher neutron fluence is needed for each unit of burnup increase and therefore the amount of Cs-134 formed will be higher than that given by the quadratic law. This is especially true in the pellet centre where the Pu buildup does not counteract the U-235 depletion as much as at the periphery. The phenomenon is illustrated in the figure below where the quotient of the Cs-134

604 keV peak and the Cs-137 662 keV peak at different radii is plotted versus the Cs-137 counts.



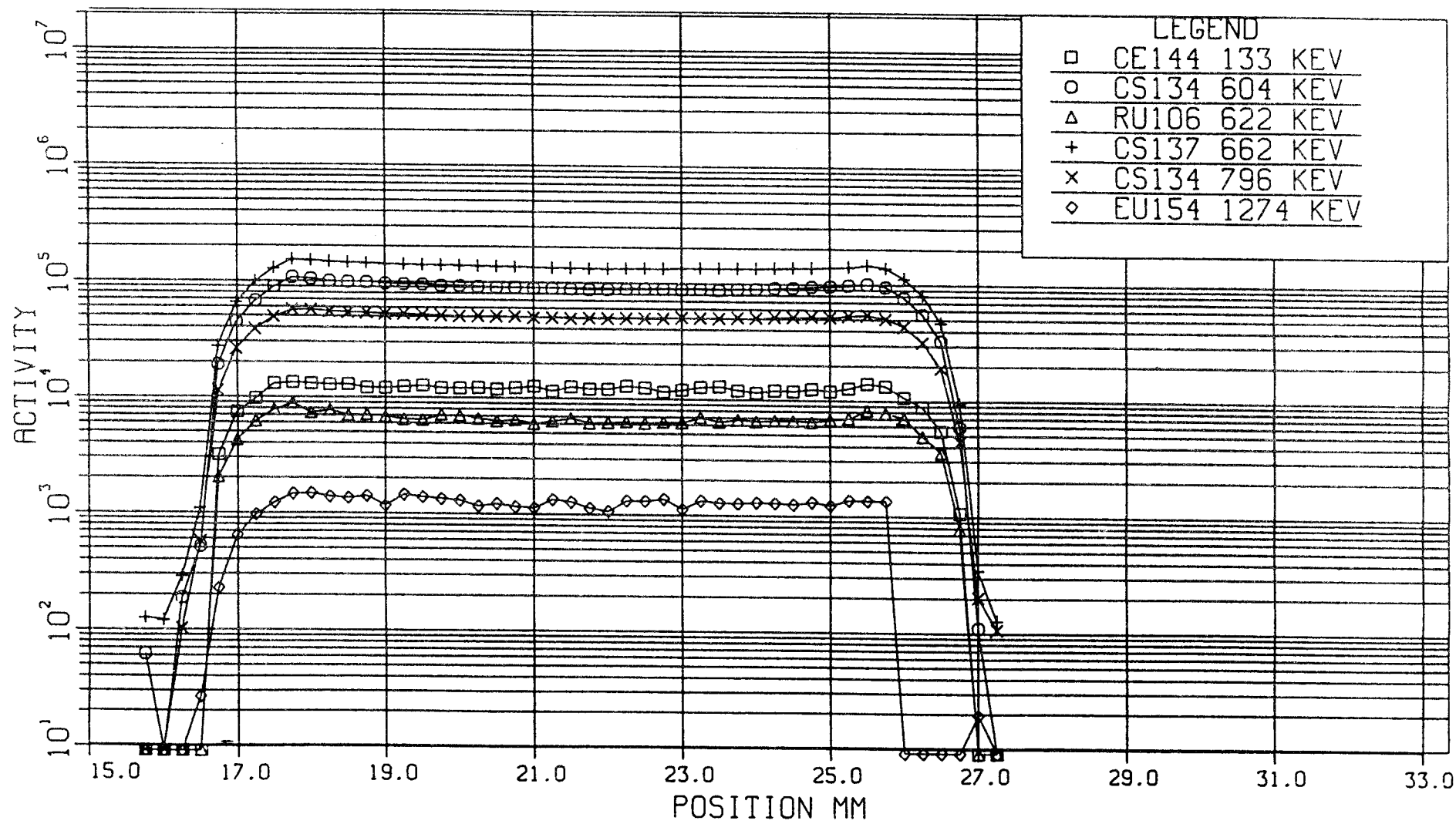
Taking an average of the Cs-134/Cs-137 cps ratio over the diameter gives a figure of 0.675. If this figure is transformed to a Bq ratio per 1st April 1985 one arrives at a value of 0.733 Bq Cs-134/Bq Cs-137 which is very close to the value 0.720 calculated from the figures for points 11 and 12 in Table 4 of ref 1 which deals with the point measurements on the rod.

REFERENCE

FORSYTH R. S. and BIVERED B.,
Axial gamma scanning of PWR fuel rod number 3688
from Ringhals 2.
NF(P)-85/19, 1985-03-27.

RADIAL GAMMA

ROD 3688 SPECIMEN 1265 RADIAL MEASUREMENT PWR1 8605



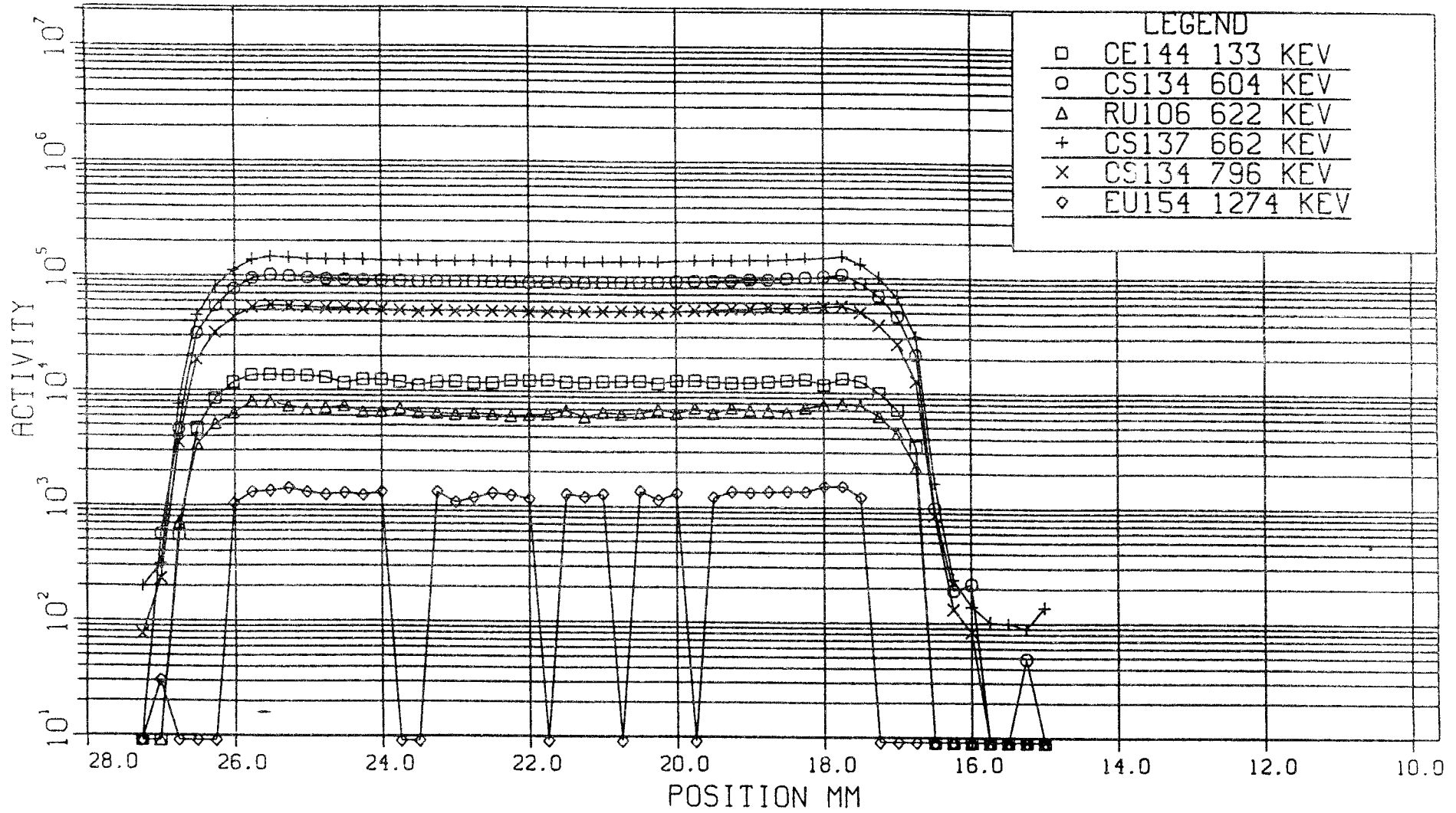
NF (P) -86/48
1986-11-26

Figure 1

STUDSVIK ENERGITEKNIK AB

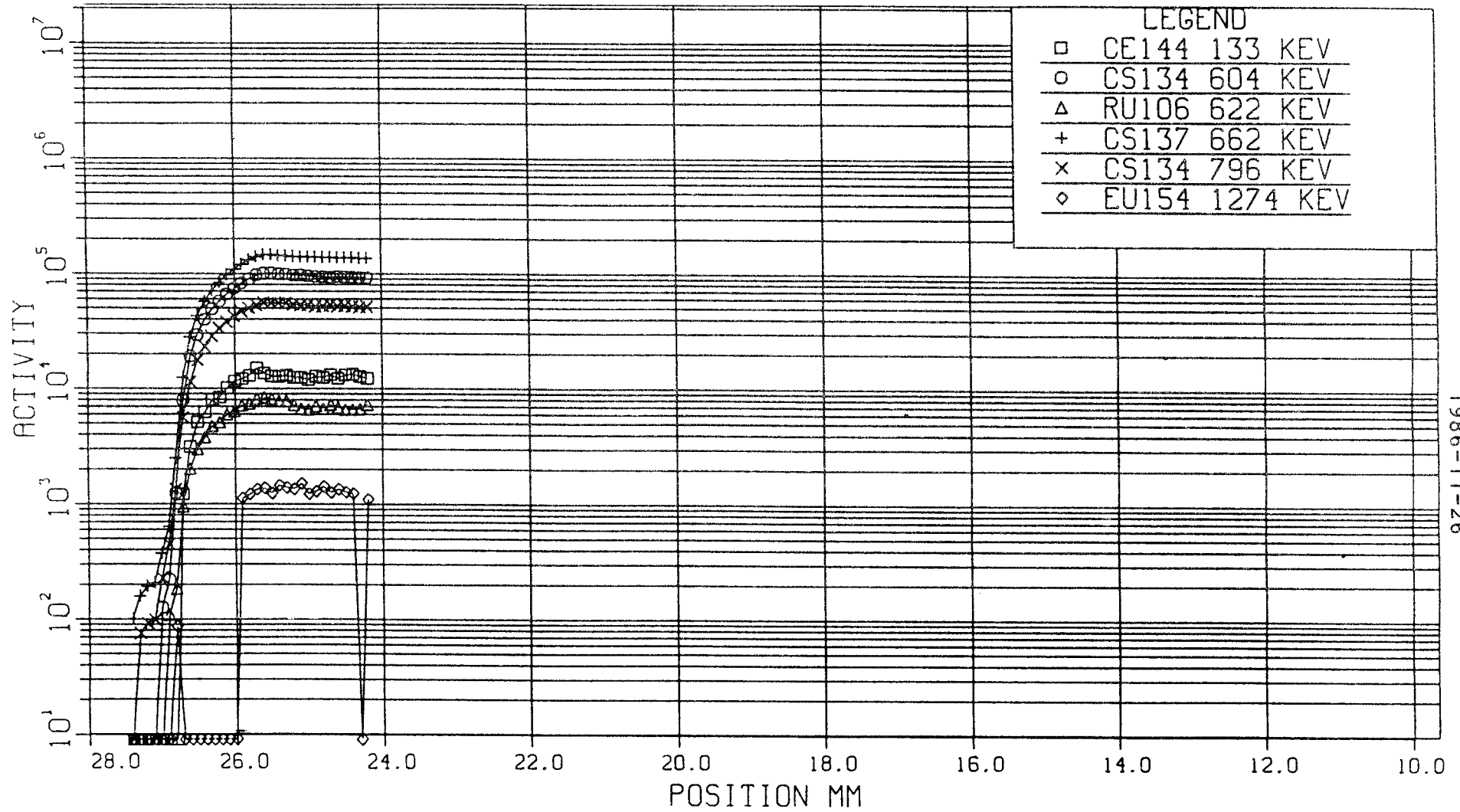
RADIAL GAMMA

ROD 3688 SPECIMEN 1265 RADIAL MEASUREMENT PWR3 8605



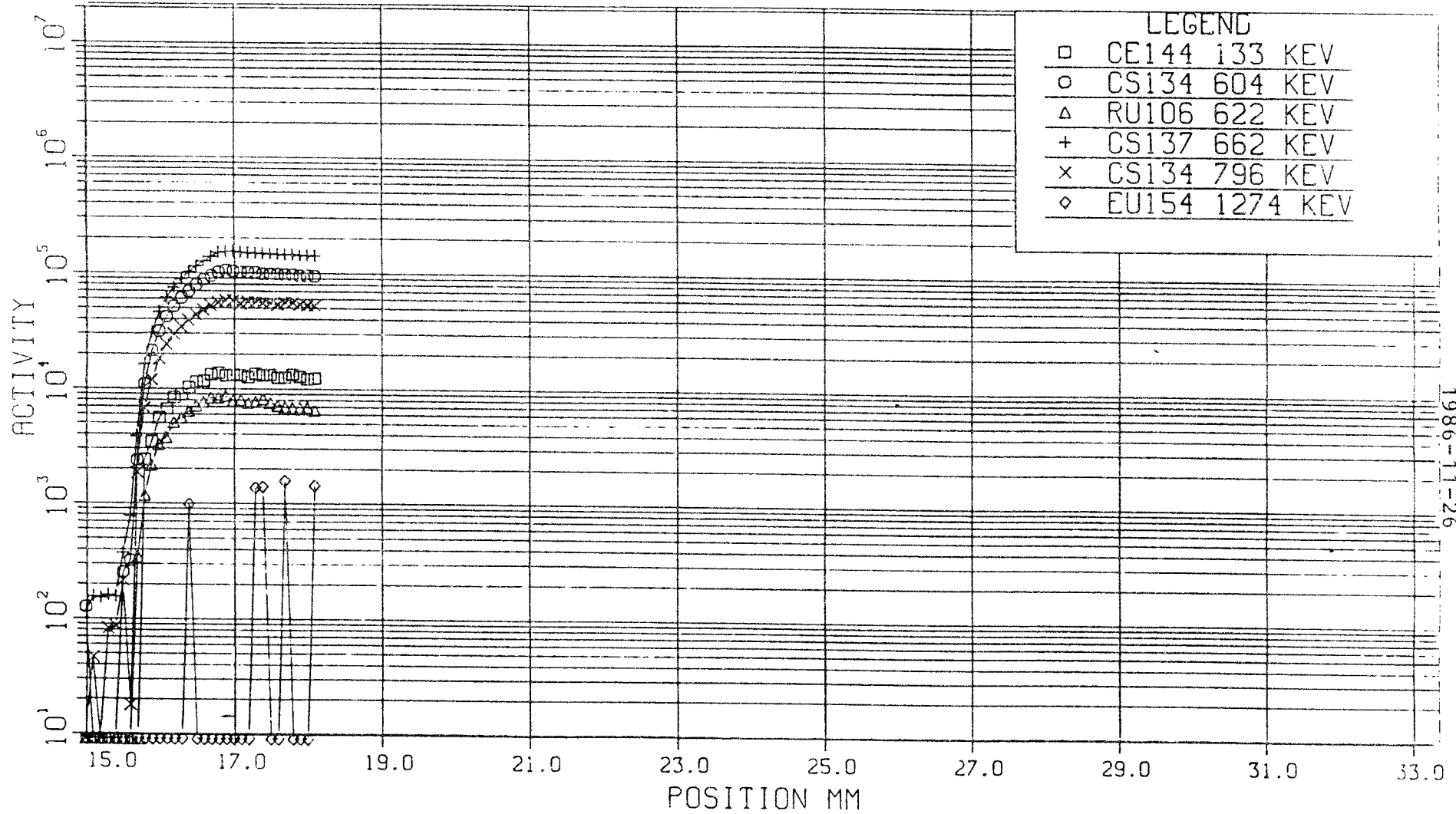
RADIAL GAMMA

ROD 3688 SPECIMEN 1265 RADIAL MEASUREMENT PWR2



RADIAL GAMMA

ROD 3688 SPECIMEN 1265 RADIAL MEASUREMENT PWR4 8605

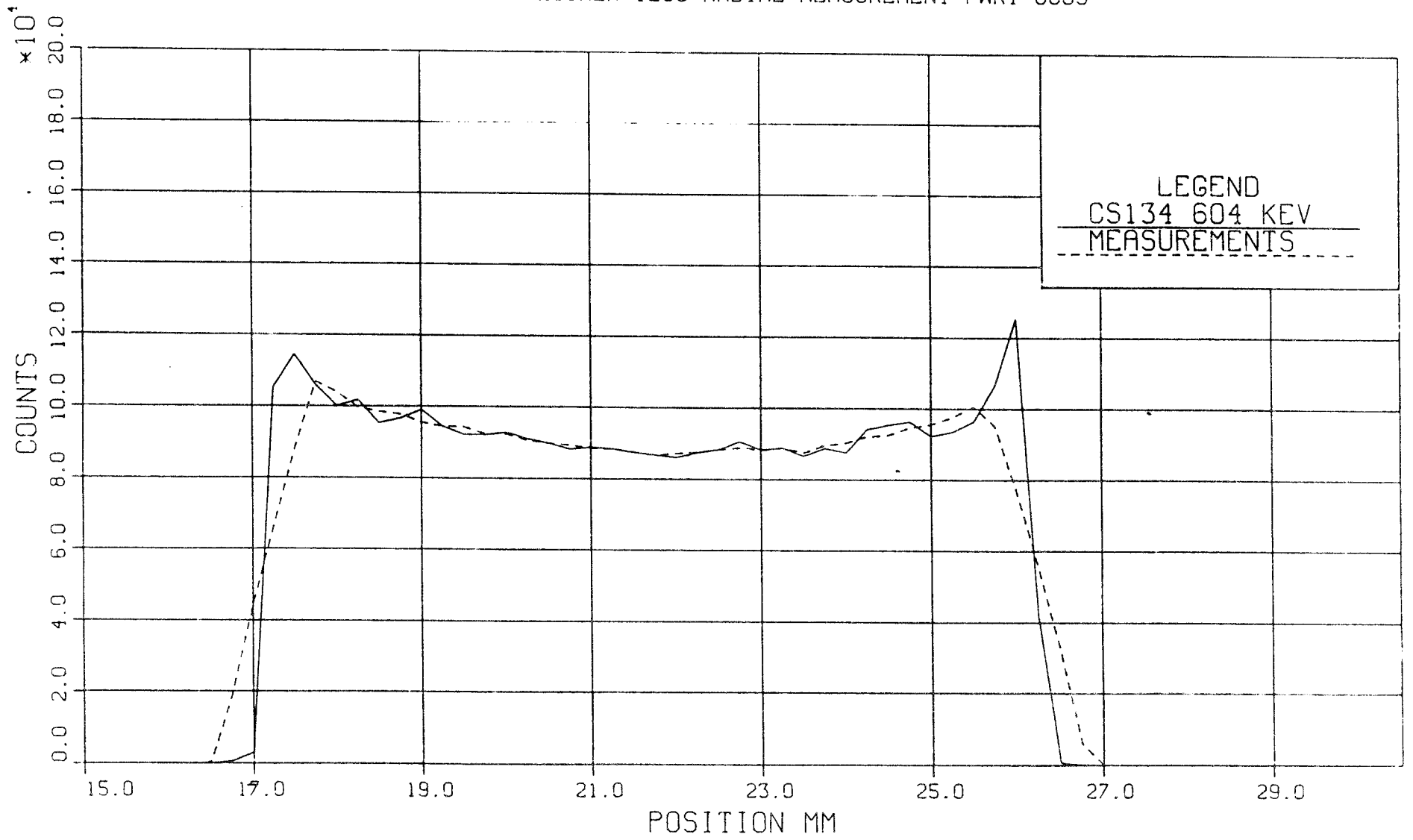


NF (P) -86/48
1986-11-26

Figure 4

RADIAL GAMMA - COLLIMATOR CORRECTED

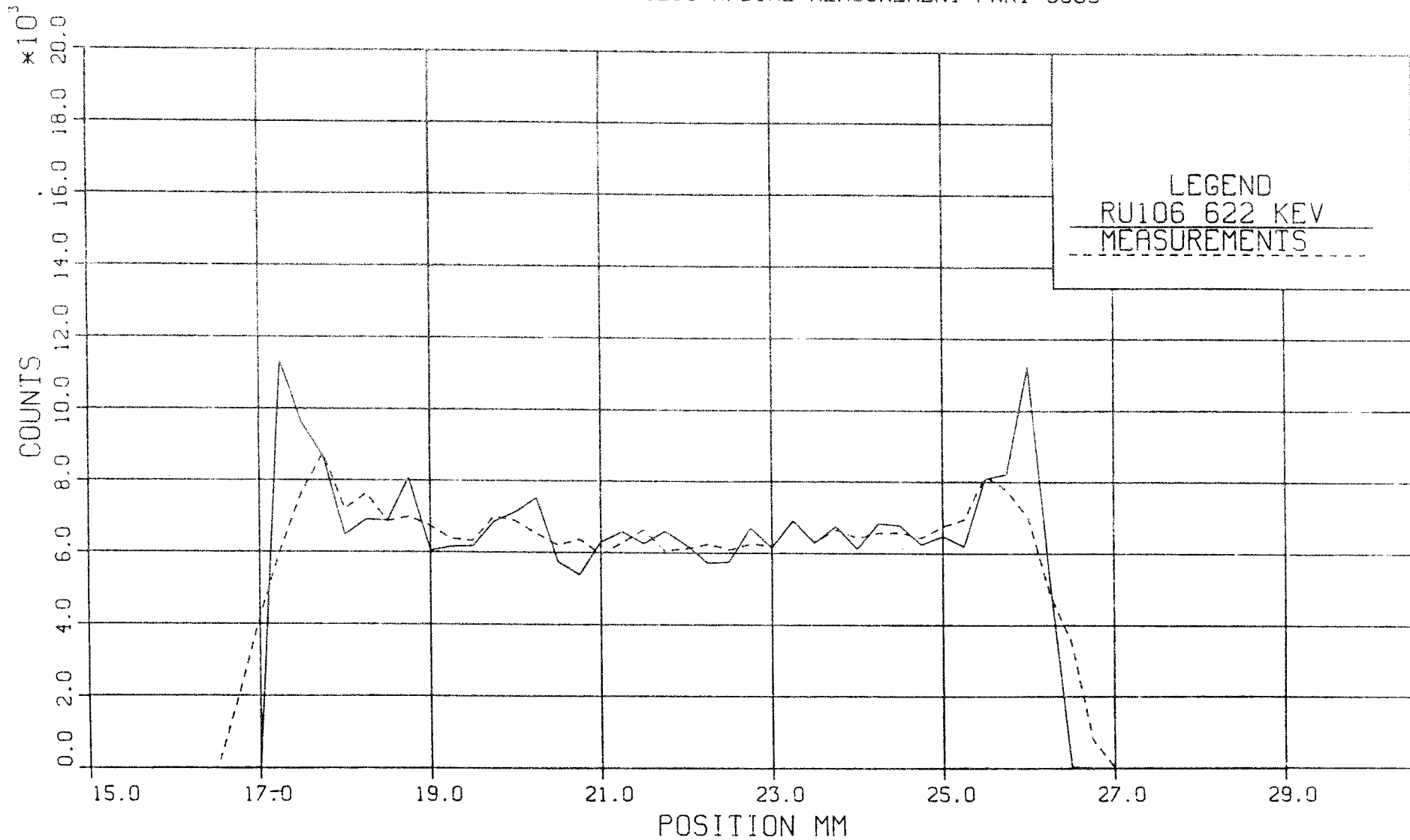
ROD 3688 SPECIMEN 1265 RADIAL MEASUREMENT PWR1 8605



08.17.97 WED 19 NOV 1986 08:17:29 STUDSVIK DATA DISPLA 9.0

RADIAL GAMMA - COLLIMATOR CORRECTED

ROD 3688 SPECIMEN 1265 RADIAL MEASUREMENT PWR1 8605



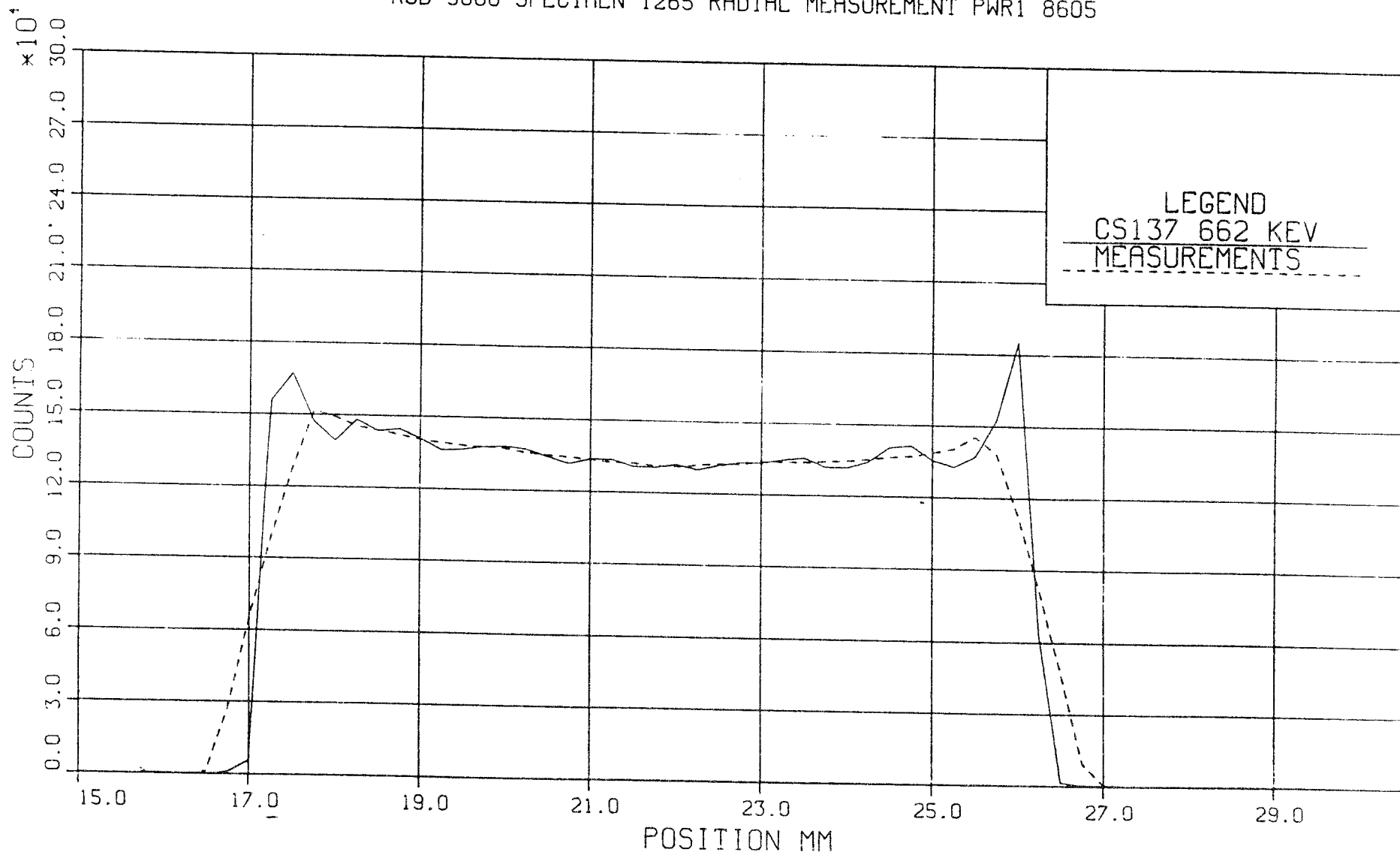
OR 18 05 MED 19 NOV 1986 JOB-CFZS STUDSVIK DATA DISPLAY 9.0

STUDSVIK ENERGITTEKNIK AB

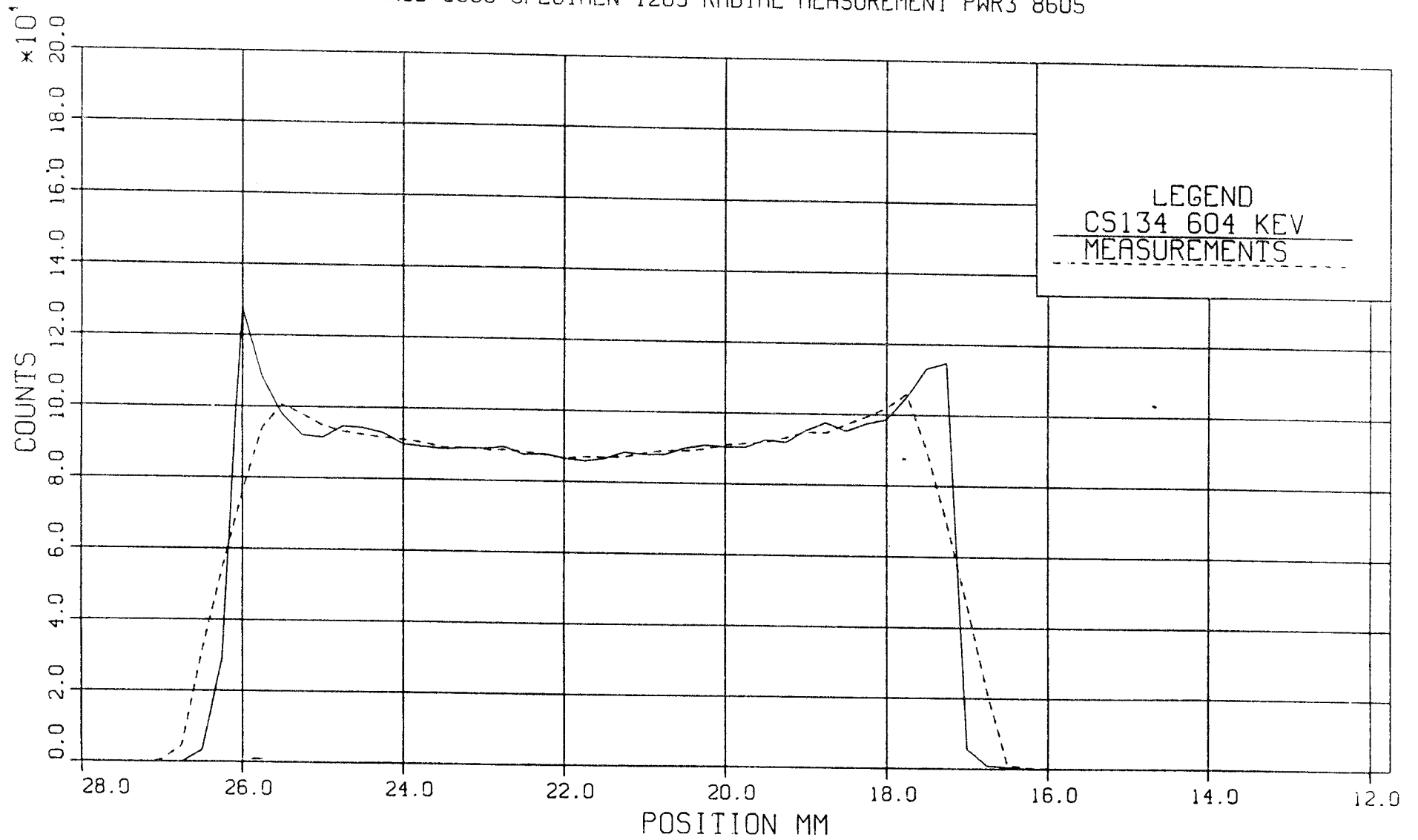
NF(P)-86/48
1986-11-26

Figure 6

RADIAL GAMMA - COLLIMATOR CORRECTED
ROD 3688 SPECIMEN 1265 RADIAL MEASUREMENT PWR1 8605

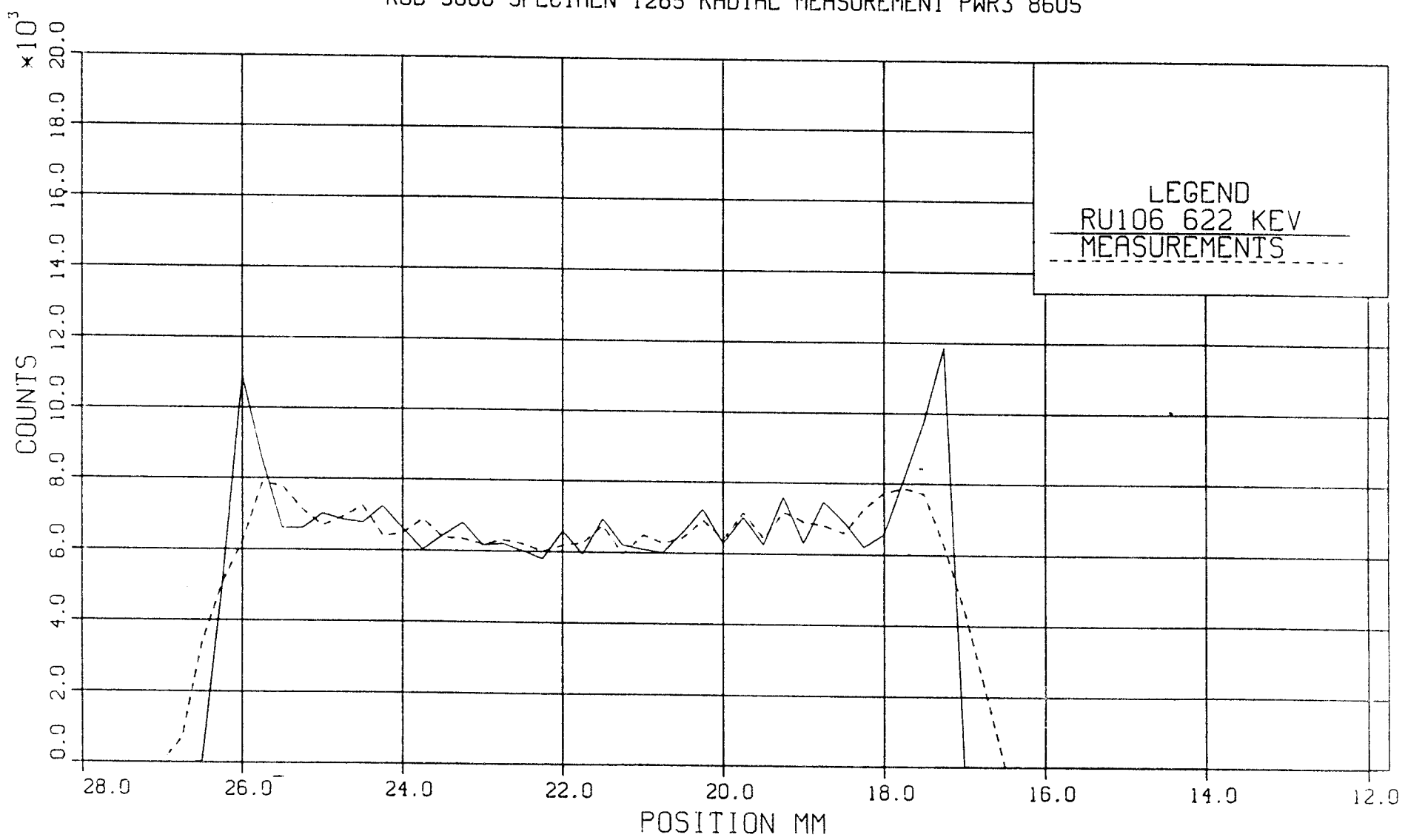


RADIAL GAMMA - COLLIMATOR CORRECTED
ROD 3688 SPECIMEN 1265 RADIAL MEASUREMENT PWR3 8605



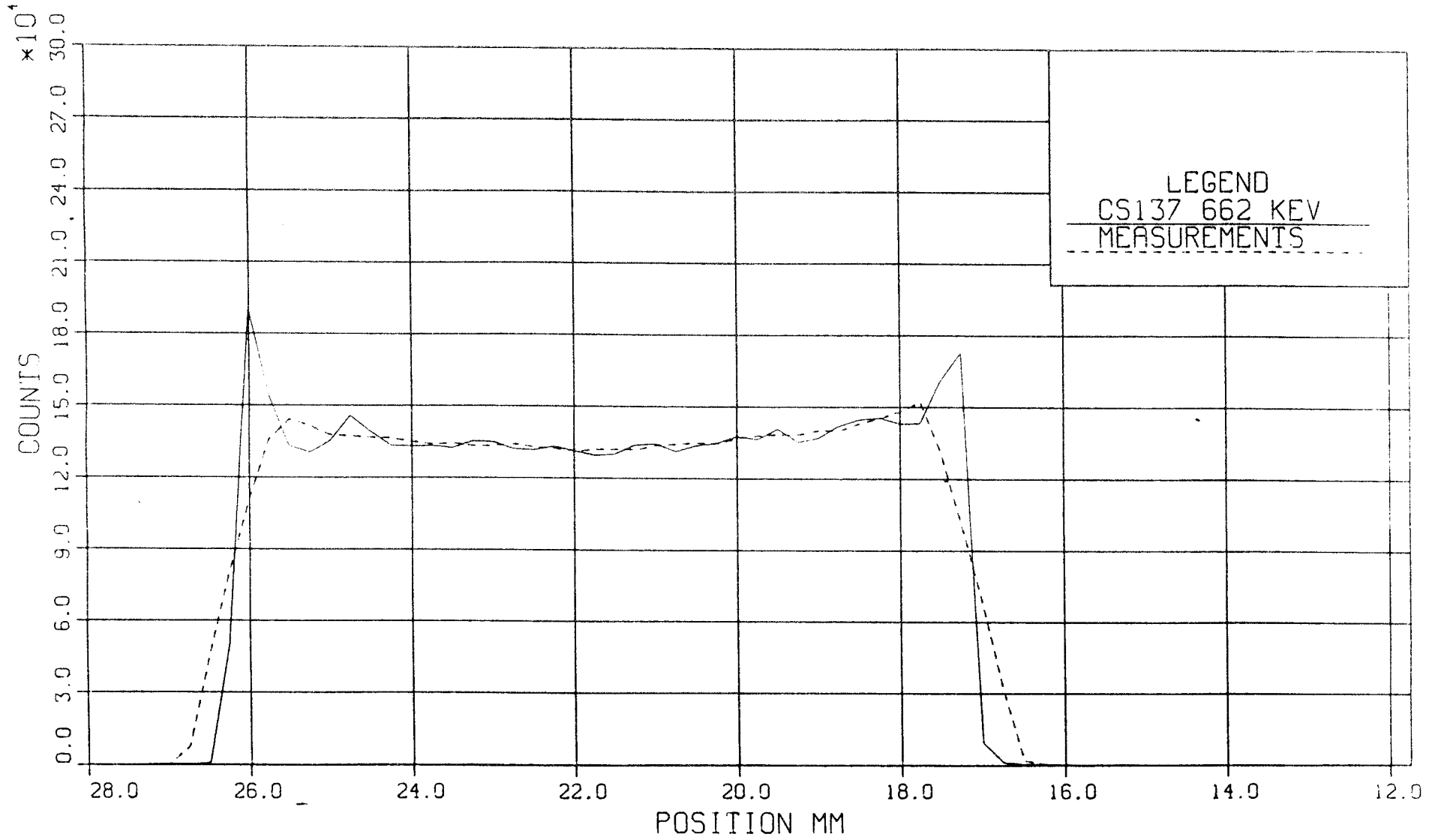
38.20.04 MFD 19 NOV 1986 JOB-CFZ5 STUDSVIK DATA DISPLA 9.0

RADIAL GAMMA - COLLIMATOR CORRECTED
ROD 3688 SPECIMEN 1265 RADIAL MEASUREMENT PWR3 8605

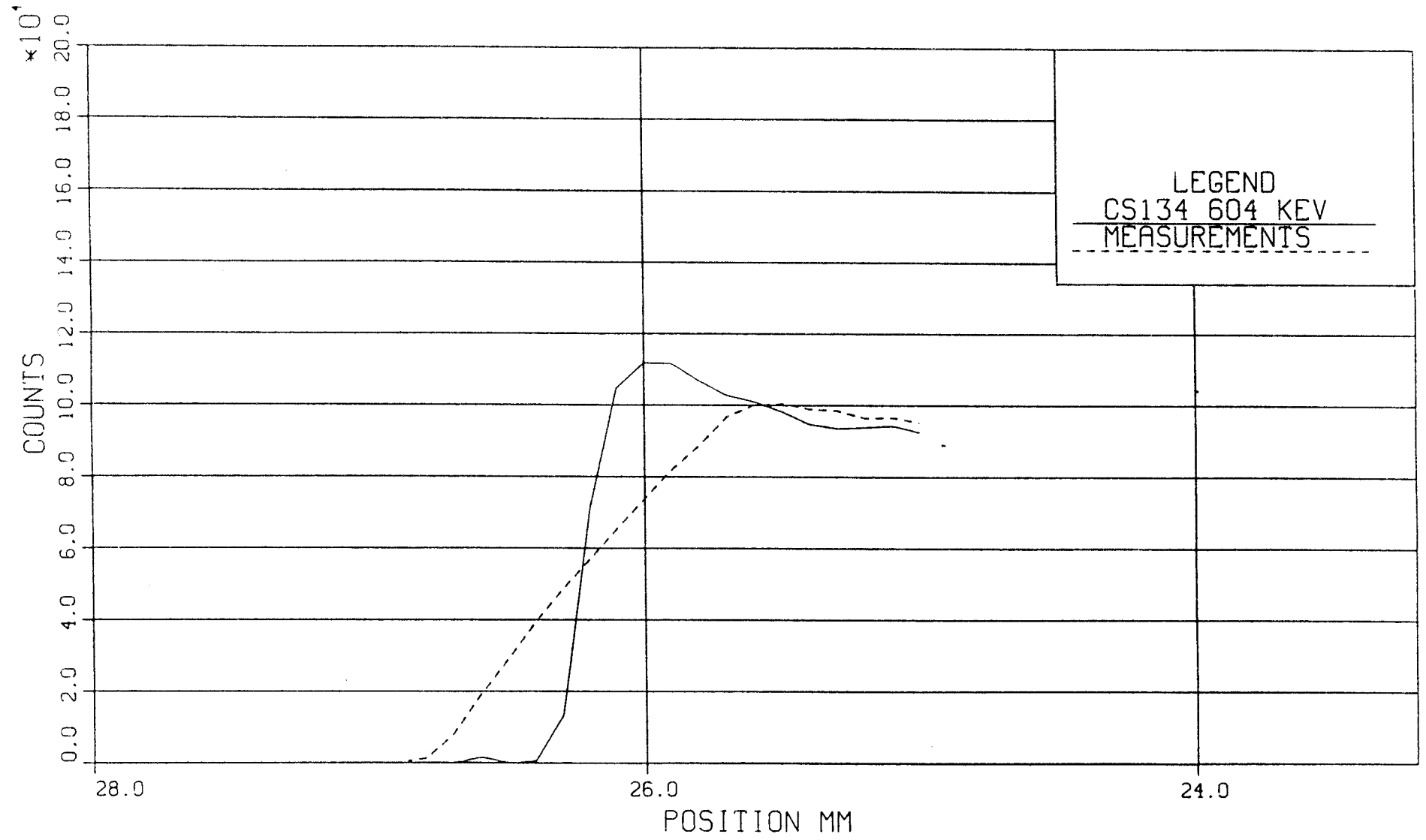


RADIAL GAMMA - COLLIMATOR CORRECTED

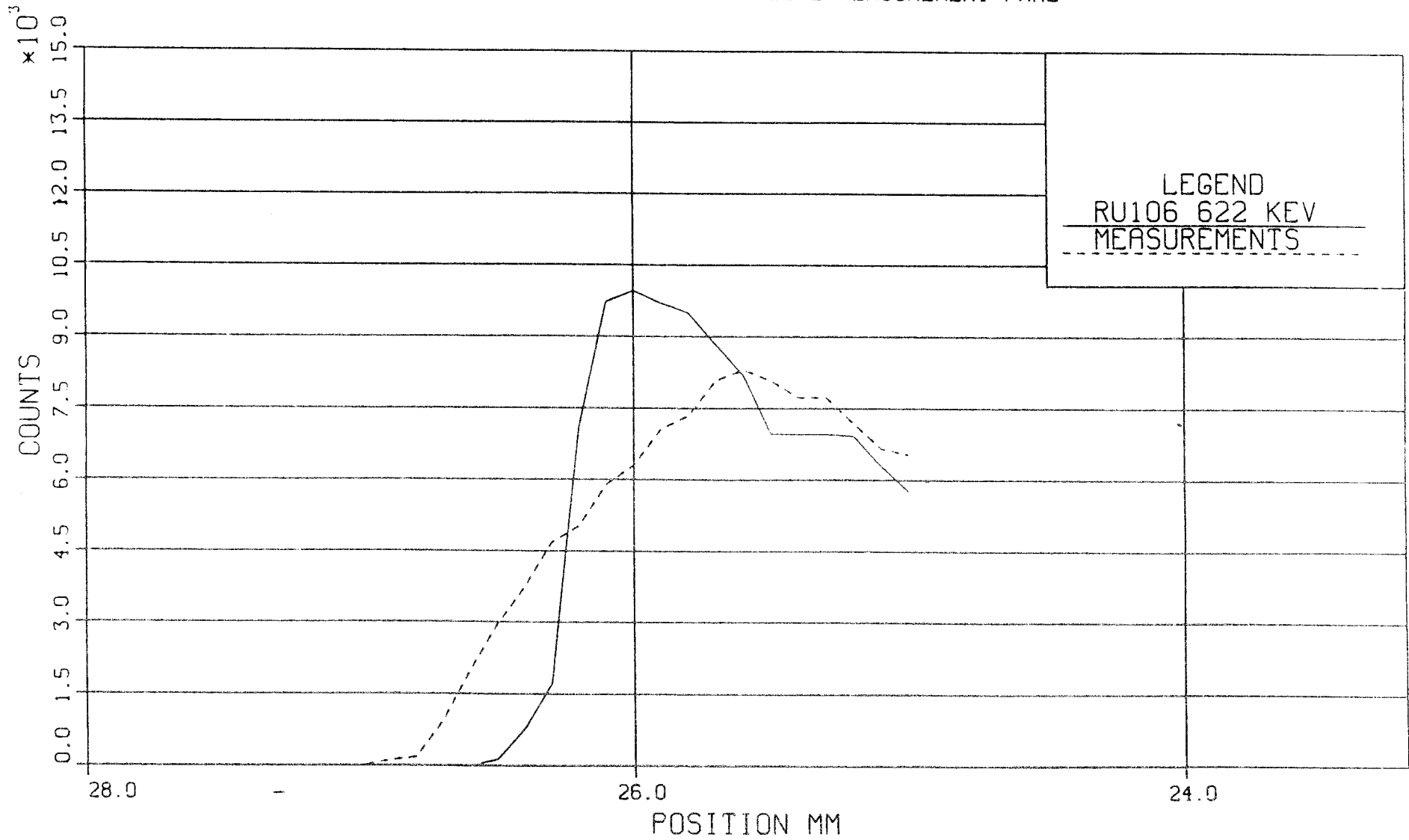
ROD 3688 SPECIMEN 1265 RADIAL MEASUREMENT PWR3 8605



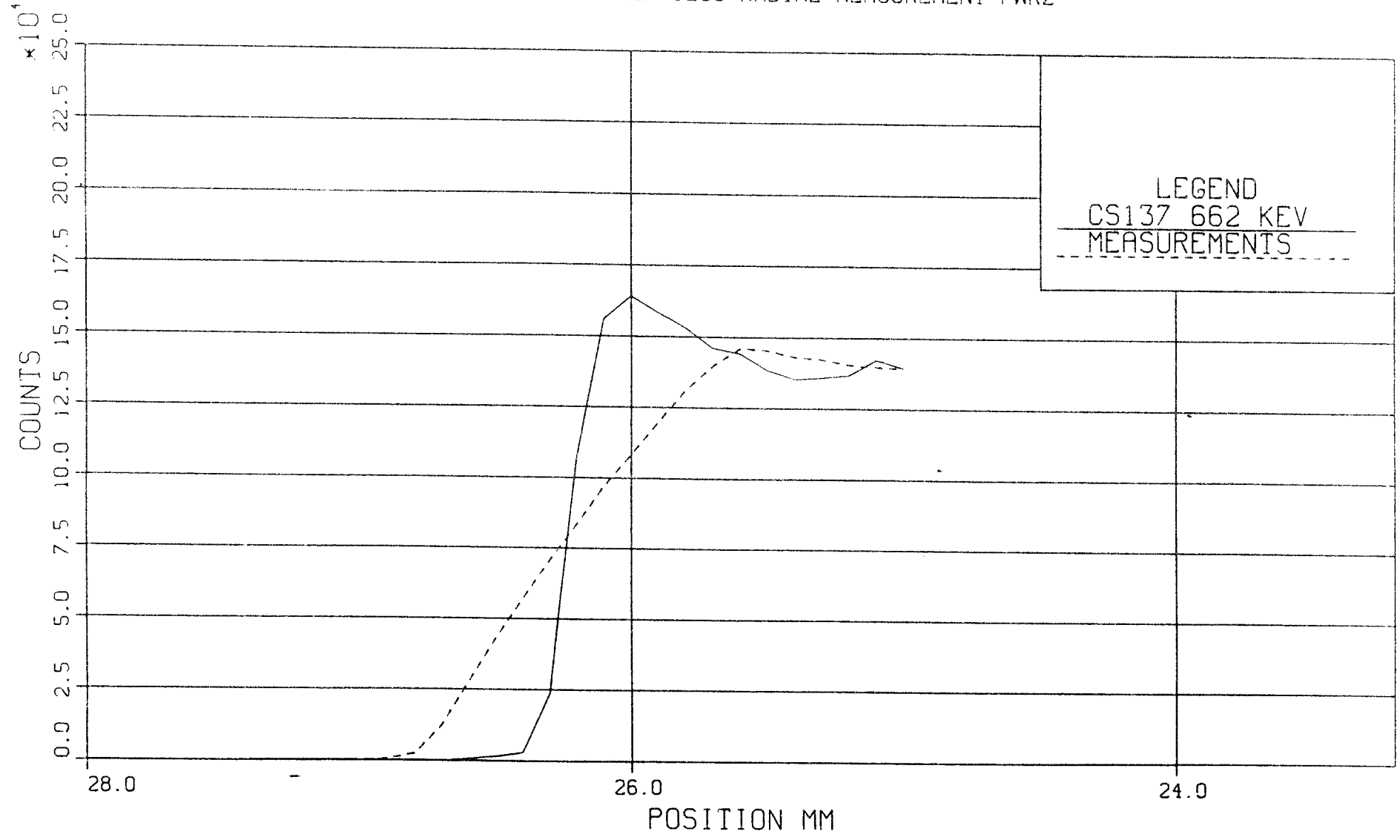
RADIAL GAMMA - COLLIMATOR CORRECTED
ROD 3688 SPECIMEN 1265 RADIAL MEASUREMENT PWR2



RADIAL GAMMA - COLLIMATOR CORRECTED
ROD 3688 SPECIMEN 1265 RADIAL MEASUREMENT PWR2

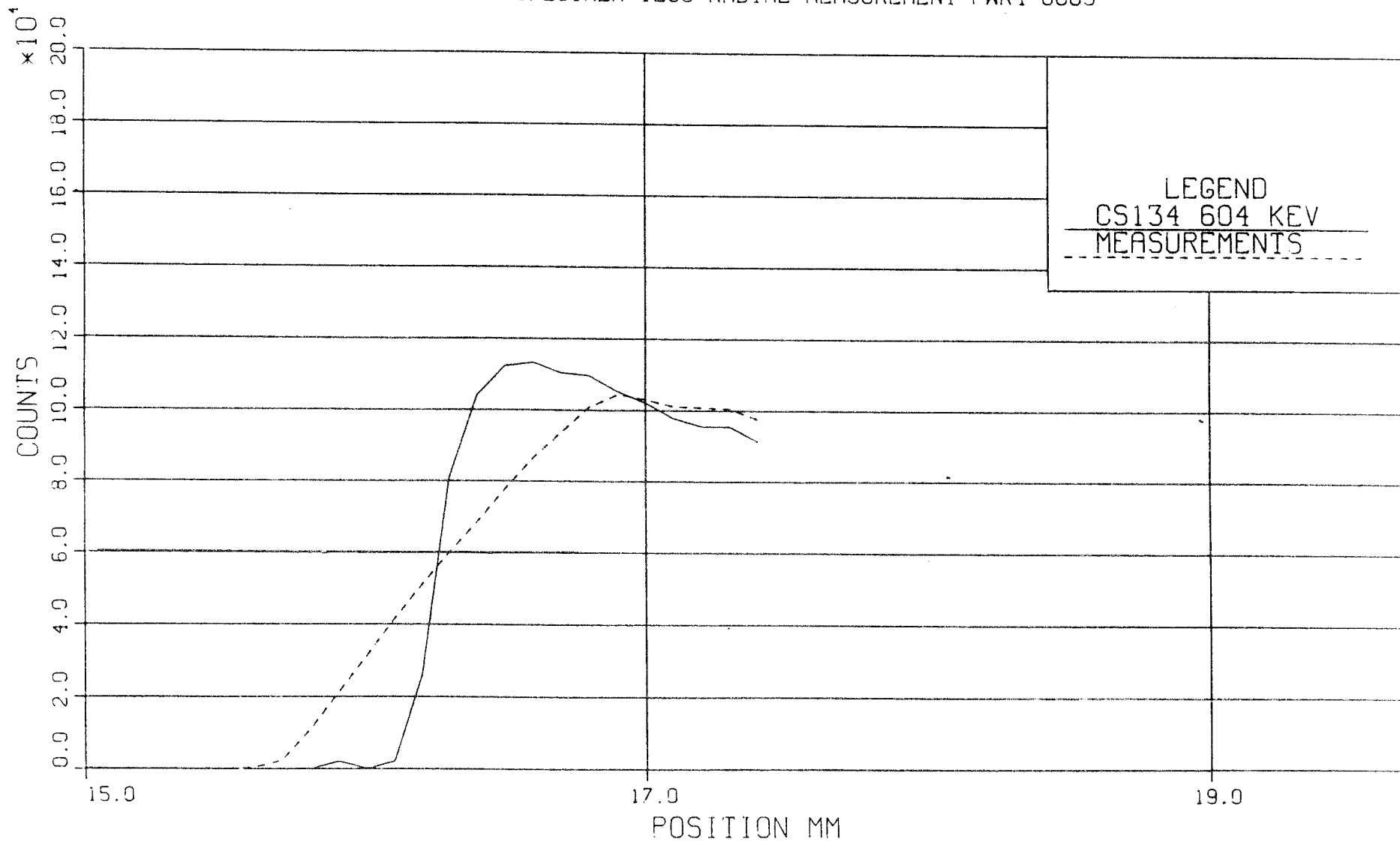


RADIAL GAMMA - COLLIMATOR CORRECTED
ROD 3688 SPECIMEN 1265 RADIAL MEASUREMENT PWR2

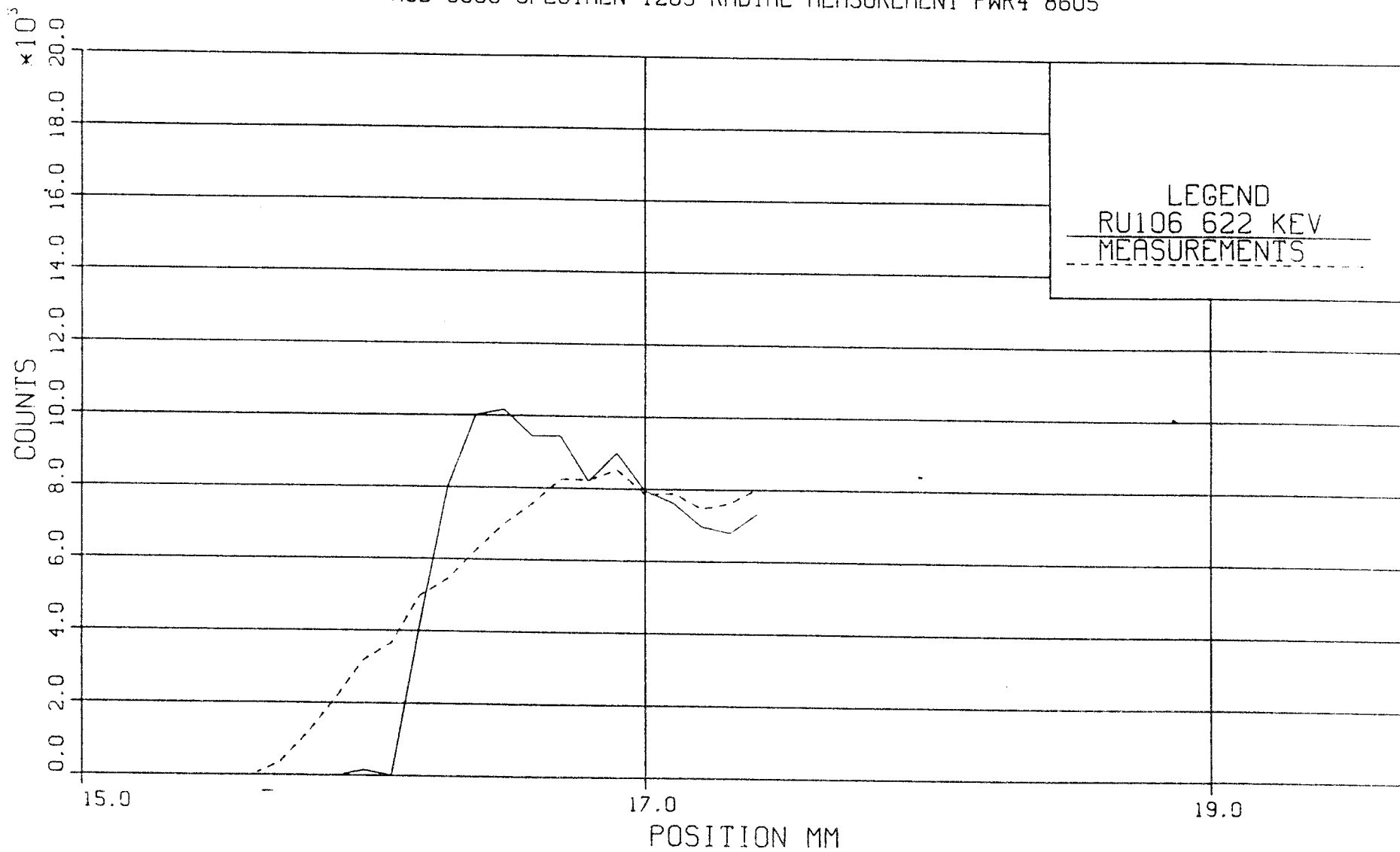


RADIAL GAMMA - COLLIMATOR CORRECTED

ROD 3688 SPECIMEN 1265 RADIAL MEASUREMENT PWR4 8605

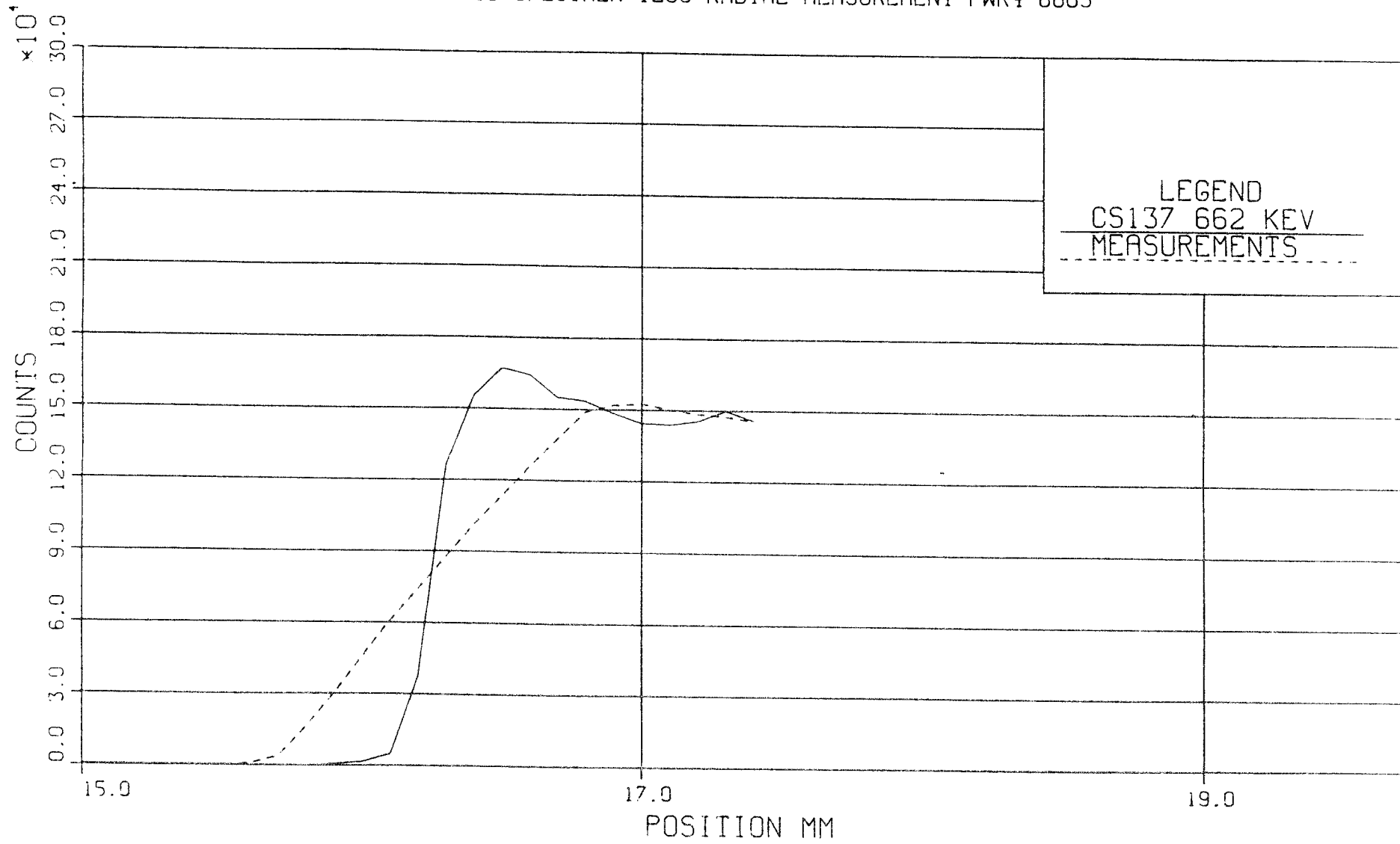


RADIAL GAMMA - COLLIMATOR CORRECTED
ROD 3688 SPECIMEN 1265 RADIAL MEASUREMENT PWR4 8605



RADIAL GAMMA - COLLIMATOR CORRECTED

ROD 3688 SPECIMEN 1265 RADIAL MEASUREMENT PWR4 8605



COLLIMATOR CORRECTION

The collimator was rectangular with a cross section of 1x2 mm . Since measurements were taken at 0.1 or 0.25 mm intervals each 0.1 or 0.25 mm wide fuel region is measured several times. This means that the resolution can be improved by image reconstruction. This is particularly important at the outer surface. It also shows to what extent other steep gradients have been smoothed out by the collimator.

The method used is the least-squares iterative technique with a damping factor also chosen in the least-squares sense (see e.g. (A1)).

The edge resolution is improved. The remaining uncertainty for the position of the edge is within 0.1 mm i.e. from one measurement point to the next. The activity seen in the 0.1 mm region covering the edge is correct but the fraction of the region which is fuel is not known. Concerning the distribution within the fuel the 1x2 mm collimator seems sufficiently small to resolve the gradients even without collimator correction.

REFERENCE

- (A1) BUDINGER T. F. and GULLBERG G. T.,
Three-dimensional reconstruction in
nuclear medicine emission imaging.
IEE Transactions on Nuclear Science,
Vol. NS-21, pp. 2-20, June 1974.

List of SKB reports

Annual Reports

1977-78

TR 121

KBS Technical Reports 1 – 120.

Summaries. Stockholm, May 1979.

1979

TR 79-28

The KBS Annual Report 1979.

KBS Technical Reports 79-01 – 79-27.

Summaries. Stockholm, March 1980.

1980

TR 80-26

The KBS Annual Report 1980.

KBS Technical Reports 80-01 – 80-25.

Summaries. Stockholm, March 1981.

1981

TR 81-17

The KBS Annual Report 1981.

KBS Technical Reports 81-01 – 81-16.

Summaries. Stockholm, April 1982.

1982

TR 82-28

The KBS Annual Report 1982.

KBS Technical Reports 82-01 – 82-27.

Summaries. Stockholm, July 1983.

1983

TR 83-77

The KBS Annual Report 1983.

KBS Technical Reports 83-01 – 83-76

Summaries. Stockholm, June 1984.

1984

TR 85-01

Annual Research and Development Report 1984

Including Summaries of Technical Reports Issued during 1984. (Technical Reports 84-01-84-19)
Stockholm June 1985.

1985

TR 85-20

Annual Research and Development Report 1985

Including Summaries of Technical Reports Issued during 1985. (Technical Reports 85-01-85-19)
Stockholm May 1986.

1986

TR86-31

SKB Annual Report 1986

Including Summaries of Technical Reports Issued during 1986
Stockholm, May 1987

Technical Reports

1987

TR 87-01

Radar measurements performed at the Klipperås study site

Seje Carlsten, Olle Olsson, Stefan Sehlstedt,
Leif Stenberg

Swedish Geological Co, Uppsala/Luleå

February 1987